Université de Montréal

Radiosynthesis of hexadecyl-4-[^{18}F]fluorobenzoate for labeling exosomes and chitosan hydrogels

Yanick Lee

Département de Pharmacologie et Physiologie, Faculté de Médecine

Mémoire présenté en vue de l'obtention du grade de M.Sc.A au programme Génie biomédical de l'Université de Montréal

Juillet 2017

Résumé

La tomographie par émission de positons (TEP) est une modalité d'imagerie nucléaire puissante, permettant des mesures fonctionnelles non-invasive dans les cellules, les animaux et les humains avec une haute sensibilité et résolution. Les exosomes sont des vésicules extracellulaires de 30 à 120 nm qui peuvent transférer leur contenu cytoplasmique entre cellules, mais comprendre leurs cheminements *in vivo* reste un défi. Les hydrogels thermosensibles à base de chitosane ont été développés et sont sous optimisation pour diverses applications telles que l'embolisation des vaisseaux sanguins, l'administration de médicaments, l''administration de lymphocytes et la réparation du cartilage et des disques intervertébraux. Il y a un besoin urgent de suivi *in vivo* à court terme pour évaluer la rétention des hydrogels et des exosomes. Le Hexadécyl-4- [^{18}F]-fluorobenzoate ([^{18}F]HFB) est un radiotraceur lipophile à longue chaîne qui est retenu dans les membranes cellulaires et les biomatériaux. Le but de ce travail était d'automatiser la radiosynthèse de [^{18}F]HFB pour marquer des exosomes et des hydrogels. La radiosynthèse et la purification de [^{18}F]HFB ont été réalisées en utilisant le synthétiseur de chimie commercial IBA Synthera®. [^{18}F]HFB a été préparé *via* substitution du précurseur d'ammonium quaternaire par [^{18}F]F-. Après une première purification *via* une cartouche C18, [^{18}F]HFB a été élué avec de l'acétonitrile et purifié par HPLC. [^{18}F]HFB a ensuite été reformulé dans une solution de DMSO (10%) après élimination du solvant HPLC sous azote, filtré et dilué dans une solution saline stérile. [^{18}F]HFB a été obtenu en rendement radiochimique allant de 15 à 45% (corrigé pour désintégration), en haute pureté radiochimique et chimique, et dans un temps de synthèse total de 60 minutes. Les exosomes n'ont pas été marqués avec succès. Cependant, les hydrogels de chitosane ont démontré un marquage élevé, avec une stabilité du complexe >90%, même après 8 heures d'incubation en solution saline. La TEP avec [^{18}F]HFB d'exosomes et de biomatériaux présente une approche novatrice pour déterminer leur distribution *in vivo*.

Mots clés : F-18, fluor-18, radiosynthèse, automatisé, exosome, nanovésicules, biomatériaux, hydrogels à base de chitosan, marquage, tomographie par émission de positons, TEP

Abstract

Positron emission tomography (PET) is a powerful nuclear imaging modality allowing for non-invasive functional measures in cells, animals and humans with high sensitivity. Exosomes are 30-120 nm extracellular vesicles that can transfer their cytoplasmic contents between cells, however, understanding where exosomes traffic in the body remains a challenge. Chitosan-based thermosensitive hydrogels have been developed and are currently under optimization for various applications such as blood vessel embolization, drug delivery, lymphocyte delivery systems, and cartilage and intervertebral disc repair. There is an urgent need for *in vivo*, short term follow-up of such procedures to assess the retention of hydrogels and exosomes at the site of injection. Hexadecyl-4-[^{18}F]fluorobenzoate ([^{18}F]HFB) is a long chain lipophilic radiotracer that has been reported to be retained within cell membranes or biomaterials. The aim of this work was to automate the radiosynthesis of [^{18}F]HFB for labeling exosomes and chitosan-based hydrogels. The radiosynthesis and purification of [^{18}F]HFB was done using the commercial IBA Synthera® chemistry synthesiser with the R&D IFP-cassette and HPLC module. As previously reported, [^{18}F]HFB was prepared by [^{18}F]F^{-} substitution of the trimethyl ammonium triflate precursor in DMSO. After removal of unreacted [^{18}F]F^{-} and DMSO *via* a C18 light cartridge, [^{18}F]HFB was eluted with acetonitrile and purified by semi-prep C18 HPLC. [^{18}F]HFB was then reformulated in DMSO (10%) solution after removal of the HPLC solvent from the radioactive product peak under nitrogen, filtered, and diluted in sterile saline. [^{18}F]HFB was obtained in radiochemical yield (isolated after HPLC and evaporation) ranging from 15 – 45% (decay-corrected), high radiochemical and chemical purities, and within a total synthesis time of 60 mins. Exosomes were not successfully labeled. However, high labeling efficiency was observed with the chitosan hydrogels displaying a stability >90%, even after 8 hours incubation in saline. PET imaging with [^{18}F]HFB of exosomes and biomaterials presents a novel approach to determining their *in vivo* distribution.

Keywords: F-18, fluorine 18, automated, radiosynthesis, exosomes, nanovesicles, biomaterials, chitosan hydrogels, radiolabeling, positron emission tomography, PET.

Statement of originality

Portions of the work discussed in this thesis were presented at the 22nd International Symposium on Radiopharmaceutical Sciences (ISRS) in Dresden Germany (May 2017) and at the journée scientifique 2017 of the Centre Recherche du Centre Hospitalier de l'Université de Montréal (CRCHUM) (May 2017).

Acknowledgements

I would first like to thank my supervisor Dr. Jean DaSilva, for the introduction to the field of radiochemistry and PET imaging back when we first met during my undergraduate studies. I am incredibly grateful for the opportunity Dr. DaSilva gave me to join his new laboratory at the CRCHUM and for his countless guidance throughout graduate school. I would also like to thank the PhD candidates in the DaSilva lab: Valentin, Luis-Michel and Aida, as well as Marc (Post-Doctoral Fellow) and Anne-Flore Plane (stagière) for their support, help and guidance. I am also very appreciative of the work Yasaman Alinejad (Post-Doctoral Fellow) completed for our collaboration on radiolabeling hydrogels and the guidance Dr. Sophie Lerouge provided for this project as well. I am forever grateful to our laboratory technicians: Keegan, Luis-Miguel, Nabil, Mehdi and Cecile for all the work they contributed to my project. Furthermore, I would like to thank Dr. Derrick Gibbings for his help and collaboration with our exosome project. Finally, I would like to express my most sincere gratitude to my friends and family for being there to help me through the whole process, including the many frustrations inherent to research. A special mention is owed to Dr. Lojan Sivakumaren for always being there for me - inside and outside of the lab and for providing me with enough daily caffeine and energy drinks to get through it all.

I would also like to express my gratitude to our sources of funding including CIHR and for the various scholarships and awards I received from the University of Montréal and the CRCHUM.

Table of Contents

List of Figures

List of Tables

List of abbreviations

[^{18}F]DOPA	^{18}F-dihydroxyphenylalanine
[^{18}F]FDG	^{18}F-fluorodeoxyglucose
[^{18}F]FLT	^{18}F-fluorothymidine
[^{18}F]FMISO	^{18}F-Fluoromisonidazole
[^{18}F]HFB	Hexadecyl-4-[^{18}F]fluorobenzoate
[^{99m}Tc]-HMPAO	^{99m}Tc-hexamethylpropyleneamineoxime
AF	Ammonium formate
AUC	Area under curve
BBB	Blood brain barrier
BGP	ß-glycerophosphate disodium salt hydrate
BSA	Bovine serum albumin
$CDCL_3$	Deuterated chloroform
CH	Chitosan
CPCs	Circulating progenitor cells
DCM	Dichloromethane
DMF	Dimethylformamide
DMSO	Dimehtyl sulfoxide
EOB	End of beam
EtOH	Ethanol
GA	Gelation agent
HPLC	High pressure liquid chromatography
IFP	Integrated fluidic processor
ILVs	Intraluminal vesicles
ITLC	Instant thin layer chromatography
LOR	Line of response
MA	Molar activity

MeCN	Acetonitrile
MeOH	Methanol
MS	Mass spectrometry
MSCs	Mesenchymal stem cells
MVBs	Multivesicular bodies
NaOH	Sodium hydroxide
NMR	Nuclear magnetic resonance
PBS	Phosphate buffered saline
PD	Parkinson's disease
PET	Positron emission tomography
PHA	Pulse height analyzer
PM	Photomultiplier tube
Ppm	Parts per million
QC	Quality control
Qat	Quaternary ammonium
GC	Gas chromatography
RCY	Radiochemical yield
R&D	Research and development
Rf	Retention factor
RISC	RNA interfering-induced silencing complex
Rt	Retention time
SDS	Sodium dodecyl sulfate
SHC	Sodium hydrogen carbonate
siRNA	Small interfering RNA
S_N2	Substitution nucleophilic bimolecular
S_NAr	substitution nucleophilic aromatic
SPD	Sodium phosphate dibasic
SPECT	Single photon emission computed tomography

SPM	Sodium phosphate monobasic
TLC	Thin layer chromatography
TOF	Time of flight
VEGF	Vascular endothelial growth factor
µPET	microPET

Introduction

Chapter 1: Positron Emission Tomography and Radiochemistry

1. Nuclear Imaging

Nuclear imaging is a branch of nuclear medicine that deals with the application and detection of decaying radioisotopes. Typically, a radiopharmaceutical is injected, inhaled or swallowed by a patient and the detection of the radioactive decay is done through either positron emission tomography (PET) or single photon emission computed tomography (SPECT) [6]. In clinical nuclear medicine, roughly 95% of radiopharmaceuticals are used for diagnostic purposes, with the remaining 5% employed for therapy [7]. Radiopharmaceuticals usually contain a radioisotope linked to a small amount of active ingredient, with the main purpose of obtaining an image or a measure of biological activity/biodistribution. Radiopharmaceuticals do not usually have any pharmacological activity as they are administered in extremely small concentrations and therefore do not display any dose-response relationships. PET and SPECT have the advantage of being highly sensitive imaging modalities with the total mass of tracer needed to create an image being in the nanogram range[8]. However, PET and SPECT offer lower spatial resolution, the minimum distance between two points in an image that can be detected by a scanner, as compared to X-ray, CT and MRI (**Table 1.1)**. The lower resolution makes it difficult to visualize small details and limits the size of structures that can be accurately imaged [9], although the radiation exposure that results from a clinical FDG PET scan of a human is approximately half that for a whole-body diagnostic x-ray CT image [10]. Finally, compared to optical fluorescence and echography imaging, PET and SPECT have higher sensitivity [9]. Our discussion will focus on PET and the various aspects involved with PET imaging including radiochemistry, PET tracer design and applications in translational research.

1.1 Introduction to the PET concept

PET is a nuclear imaging modality that has become the most powerful molecular imaging technique currently available for clinical and basic scientific use. In recent years, PET has seen an increase in clinical applications due to advances in instrumentation and synthetic chemistry, resulting in the development of high sensitivity PET scanners and a broad range of PET tracers [11]. PET allows for the quantitative assessment of numerous biological processes including perfusion, metabolism, protein expression and enzyme activity, *in vivo,* in a non-invasive manner [12]. PET works through the detection of gamma ray photons resulting from the annihilation between a positron emitted from a decaying radionuclide and an electron to construct a three-dimensional image. PET tracers are predominantly developed through combining radionuclides (radioactive isotopes) with biologically active molecules to produce a radiolabeled probe that can image a biochemical pathway or receptor. The radionuclide undergoes beta-decay through the emission of a positron, which travels a short distance and undergoes an annihilation event with an electron. This produces two high-energy 511 keV photons that travel in opposite directions that are detected as a coincidence event (**Figure 1.1**) [6]. This allows for the quantification of radioisotope concentration and the construction of an image based on radiotracer distribution throughout the body [13]**.**

The variety of available PET tracers combined with advanced analytical methods supports the application of PET for the assessment of normal biological processes, changes in biological processes associated with disease formation and progression, and the ability to longitudinally monitor the response of healthy and diseased tissues to therapeutic intervention [12]. Furthermore, PET also sees applications throughout the drug discovery process to assess novel drug biodistribution, drug occupancy at specific biological targets and biological response

to drug exposure [8]. The ability for PET to image biodistribution will be of high importance for this work and will be discussed in more detail in chapters 2 (exosomes/biomaterials).

1.2 Introduction to Radioactivity

Radionuclides are most commonly produced artificially in a cyclotron or reactor (for PET) although some exist naturally. Radionuclides are unstable as they have excess energy due to an unsuitable ratio of neutrons to protons [6]. To become stable, this excess energy can be emitted from the nucleus as gamma radiation or through the emission of particles such as α particles, $ß^-$ particles, $ß^+$ particles, electron capture and isomeric transition. Through the emission of energy or various particles, the unstable nuclide is said to have undergone a decay event, resulting in the production of a different nuclide which may be stable or remain unstable [6].

Positron decay occurs when a radionuclide is proton rich and neutron poor. The process involves the conversion of a proton into a neutron with the emission of a positron ($ß^+$) and a neutrino (ν). Positron decay leads to nuclear transmutation, whereby an atom of one chemical element is transformed into an atom of an element with an atomic number that is less by one unit. This is seen in **Figure 1.2** where radioactive fluorine-18 ($[^{18}F]$) undergoes decay primarily through positron emission (96.86%) and the remainder electron capture (the nucleus captures a nearby orbital electron) to form stable oxygen-18. In this case, the atomic number decreased by 1 (9 to 8), whereas the mass number remained the same (18) [6]. PET makes use of positrons through the resultant process that occurs after decay. As the positron is emitted, it begins to lose kinetic energy by interaction with matter, and then with electrons of absorber atoms where it combines with an electron [7]. At this moment, both particles (electron and positron) are annihilated due to a matter-antimatter interaction, producing two 511-keV photons emitted in

opposite directions (~ 180˚). The detection of the two opposite 511-keV photons in coincidence by detectors is the basis of PET [6].

1.3 PET Imaging

PET tracers are made up of a biologically active molecule and a short-lived positron-emitting isotope. The most common radioisotopes utilized in PET are ^{15}O, ^{13}N, ^{11}C and ^{18}F, with ^{18}F having the longest half-life of 109.6 minutes (**Table 1.2**). The advantage of a longer half-life allows for more complex synthesis procedures, long PET imaging protocols, shipment of the PET tracer to offsite facilities without the infrastructure to produce PET isotopes and the ability to perform multiple patient scans from one production of tracer [7]. To produce PET tracers, a laboratory must be able to manufacture radioisotopes and combine these with precursor molecules to produce a final radiolabeled tracer under automated conditions.

PET radioisotopes are produced in a cyclotron; a cylinder-shaped high-vacuum chamber that combines a magnetic field and a radio-frequency system to produce an alternating electric field which is applied to accelerate particles to very high energies. These accelerated particles can in turn be utilized as projectiles to bombard stable elements loaded in a target to induce different types of nuclear reactions that lead to the production of radioactive elements [7]. Most medical cyclotrons are negative ion cyclotrons and accelerate negative hydrogen atoms (H^-). These H^- ions are accelerated in a circular path with increasing kinetic energy until they are stripped of two electrons to produce positive ions (protons) which are used to bombard a target. The proton is absorbed by the target nucleus causing a nuclear transformation which produces an unstable radioactive isotope (**Table 1.2)**. For example, to produce $[^{18}F]F^-$, ^{18}O enriched water is bombarded with 11 MeV protons, according to the nuclear reaction ^{18}O (p, n)^{18}F [6]:

$$^{18}_{8}O + {}^{1}_{1}H \rightarrow {}^{18}_{9}F + {}^{1}_{0}n$$

After radioisotope production, the radioisotope is transferred to a shielded hot cell to an automated synthesis module. Here, the radioisotope undergoes a chemical reaction with a precursor molecule to produce a PET tracer.

To detect annihilation photons, PET scanners utilize a circular ring of pairs of gamma ray detectors that works off the basis of coincidence detection of gamma photons. The detection of the gamma rays determines a line of response (LOR) along which the annihilation took place (**Figure 1.3)**. A true coincidence event is determined by imposing an acceptance window on the time difference between detection of the two events (a few nanoseconds wide) which helps to filter out scattered or random coincidences [14]. The time of flight (TOF) PET technique is based off the measurement of time differences in the arrival of the two photons at the detectors and provides the probability the event occurred at a specific location along the LOR.

Block detectors are the most common type of detectors and they consist of a solid scintillation detectors coupled to a photomultiplier tube (PM), a linear amplifier, and a pulse height analyzer (PHA) [6]. A scintillation detector is employed to absorb the gamma ray and convert this into lower energy light photons. The light photons are then converted into an electrical pulse by the PM, amplified and analyzed by the PHA. A PHA is a device that sorts out photons of different energies and in the case of PET systems, the PHA is centered at 511 keV [6]. If the annihilation photons are registered as a coincidence event, mathematical tomographic image reconstruction algorithms transform the signal into an image that represents a slice through the object in the plane of the detector ring. Some image reconstruction algorithms that are currently in use with PET scanners include: filtered backprojections, expectation maximization, ordered subset expectation maximization, and maximum aposteriori [12]**.**

Modern PET scanners are often coupled with other imaging modalities such as CT or MRI. This helps physicians to compare the higher resolution CT or MRI images to the low-resolution PET images to determine precise localization of anatomical structures before administering therapy. Furthermore, by combining PET and CT, it is possible to perform a CT transmission scan that can be implemented for attenuation correction for PET images, resulting in a more accurate image [6]. The CT scan creates a density map of the body that can be used to correct for the different absorption of photons through various tissues of the body. Another factor that helps to increase the quality of the images is to correct for the partial volume effect. The partial volume effect leads to a smearing of activity over a larger area than it occupies in a reconstructed image and this is due to the limitation in the spatial resolution of PET scans. A correction needs to be applied for overestimation or underestimation of activities in small structures to obtain better quality images [6].

Many research efforts have been focused on maximizing the performance of PET scanners, which becomes more complicated when dealing with small animal imaging [12]. Small animal imaging (μPET) provides many advantages for completing translational research for understanding human diseases, however, size differences in organs and tissues between humans and small animals creates many challenges for μPET imaging. The human/mouse and human/rat mass ratios fall in the range of 2,500 to 3,750 and 250 to 375, respectively [12], which results in an approximate 10 times smaller volume in these small animals. Consequentially, to obtain the same quality of images in small animals as humans, the spatial resolution of μPET scanners would need to be improved by a factor of 10. Current PET scanners have a spatial resolution of approximately 6-8 mm and μPET scanners around 1-2.5 mm [15]. Furthermore, an important factor to consider when completing small animal studies is the concentration of tracer being

administered. In human studies, the amount of tracer being injected does not perturb any biological systems, however, this may not always be true for small animals due to their significantly smaller body weight.

1.4 PET Tracers

In theory, any biological molecule can be labeled with a radioisotope by direct substitution of a nonradioactive isotope, leading to a labeled compound with virtually identical biochemical properties to the native compound that can trace the target of interest without disturbing the system [8]. The range of targets available for PET imaging are essentially limitless, and can include, but is not limited to: specific receptors, second messenger systems, enzymes, proteins, metabolic pathways and perfusion. Once the target has been identified, there is the option of developing a new compound or opting to work with a known pharmaceutical. The advantages of working with an established pharmaceutical are that the pharmacological profile and toxicology are already known, which facilitates the approval process for human use by regulatory agencies such as Health Canada. Regardless of which radioisotope is utilized, it is important that the labeled compound maintain the biological and chemical properties of the native compound.

Many factors need to be met for a PET tracer to succeed and this also depends on whether the target is saturable or nonsaturable. In general, the radiotracer should be present in a very low concentration so that it does not disturb the biological process under study and ideally only interact with one specific receptor or binding site, therefore minimizing non-specific binding. The radiotracer should also have a high target-to-background ratio, a fast clearance from plasma and resistance to metabolism for quantitative studies. If the radiotracer is metabolized by the body, this can lead to radiolabeled metabolites that can greatly interfere with interpretation of

the results as the signal coming from the native molecule and the labeled metabolite could have different pharmacological binding profiles [12].

From a radiochemists standpoint, the radiosynthesis should be simple, fast, reproducible, high-yielding, easy to purify and automate with a synthesizer. Automated synthesizer units (ASUs) are controlled by microprocessors and software programs to carry out the sequential physical and chemical steps to accomplish the entire synthesis of a radiotracer (synthesis and purification) [6]. These ASUs have reagent vials filled with solvents and precursor molecules connected to a reactor through various valves that can be programed to perform actions at a given time point. Today, there are commercially available kits that can be prepared and loaded on to ASUs to produce radiotracers routinely, examples of these include ^{18}F-fluorodeoxyglucose ([^{18}F]FDG), ^{18}F-fluorothymidine ([^{18}F]FLT) and ^{18}F-dihydroxyphenylalanine ([^{18}F]DOPA). The synthesizer that was utilized to complete this work is the IBA Synthera®, which is a kit-based ASU allowing for automated processes including reformulation of the final tracer.

The concept of molar activity (MA) needs to be taken into consideration when dealing with receptors that are saturable, present in low densities or if there as a competing ligand for the binding site. The MA of a radiotracer is defined as the radioactivity per unit mass of a labeled compound and is usually reported in Ci/μmole. The lower the density of the receptor, the higher MA is needed due to competition for the binding site between the labeled and unlabeled compounds [6]. Many factors can affect the MA of a radiotracer, including: tubing, reagents or gases that contain nonradioactive isotopes of the ones being used (eg. ^{19}F in Teflon tubing) and any contamination that may be present in the cyclotron target. MA is not important when dealing with sites that are non-saturable such as perfusion or glucose metabolism studies.

1.5 Fluorine-18

Fluorine-18 has many advantages over the other PET radioisotopes due to its ease of production in high quantities, longer half-life (109 mins), its positron decay (97%) and positron weak energy. Out of the available positron emitters for clinical use, ^{18}F has the lowest mean positron emission energy of 0.64 meV and an average range of 0.83 mm in soft tissue (**Table 1.3**) which has several important consequences. The dose of radiation received by the patient will be lower and the distance between disintegration of the radionuclide and the annihilation site (positron and electron) is reduced, which results in higher resolution PET images [7]. The challenge of working with F-18 is that it is not common in biological molecules. [4]. Fluorine can act as a bioisostere for hydrogen and oxygen as they have similar radii, and substituting a hydrogen/oxygen atom for a fluorine atom does not usually result in substantial steric differences between both molecules [7]. However, the electronegativity difference that comes with fluorine can change the physicochemical properties of the molecule (reactivity, hydrogen bonding, interaction with receptors, metabolism) which means that the biological activity of the fluorinated analog must be assessed.

There are many constraints imposed on radiosyntheses such as: radiation protection, working in hot-cells with ASUs, fast reaction times and the need for obtaining the radiotracer with high MA, chemical purity and radiochemical purity. The total synthesis time including synthesis, final purification (usually through high pressure liquid chromatography (HPLC)), formulation and the quality control (QC) must be completed as quickly as possible with the incorporation of the radioactive isotope as late as possible in the reaction scheme [4]. It is important to note that high yielding reactions are not necessarily the goal of radiochemistry processes due to the high sensitivity of PET scanners and the small amount of tracer needed to

obtain an image. Rather, the purity and reliability of the radiotracer production is desired and optimized by the radiochemists.

1.6 Radiolabeling with F-18

In order to incorporate ^{18}F into a molecule, this requires either electrophilic fluorination starting from molecular fluorine $[^{18}F]F_2$, or nucleophilic substitution starting from the fluoride ion $[^{18}F]F^-$ [4]. These variants of ^{18}F depend on the target material being bombarded in the cyclotron. When the target is ^{18}O enriched water, an aqueous solution of $[^{18}F]F^-$ is obtained and when the target is $^{18}O_2$ gas, $[^{18}F]F_2$ gas is obtained. The advantage of working with nucleophilic $[^{18}F]F^-$ is that the reaction is much more efficient giving higher amounts of radioactivity and MA than electrophilic ^{18}F production [2]. In the case of $[^{18}F]F^-$ production, the $[^{18}F]F^-$ anion is obtained and trapped on an anion exchange cartridge, and then generally eluted with a solution containing: potassium carbonate dissolved in a minimum of water and cryptand (Kryptofix-222) mixed with acetonitrile (MeCN), which increases the nucleophilicity of the $[^{18}F]F^-$ by complexing with the potassium cation eventually trapped within the cryptand. The water is then dried through azeotropic evaporation with MeCN allowing the$[^{18}F]F^-$ to react with a precursor [4]. For $[^{18}F]F_2$, a carrier (^{19}F-F_2) gas is sometimes added to extract the $[^{18}F]F_2$ from the target which in turn reduces the MA and the theoretical radiochemical yield of electrophilic fluorination reactions. This has led to the majority of radiopharmaceuticals being prepared with nucleophilic $[^{18}F]F^-$ methods [2].

For nucleophilic fluorination, $[^{18}F]F^-$ can be introduced into aliphatic positions through S_N2 reactions or into aromatic molecules via nucleophilic aromatic substitutions (S_NAr). Nucleophilic substitutions are carried out in polar aprotic solvents such as dimethyl sulfoxide (DMSO), *N,N*-dimethylformamide (DMF) or acetonitrile (MeCN) under heating temperatures of

100 – 150˚C. Nucleophilic substitutions require precursors with good leaving groups, with the reactivity of leaving groups as follows: Cl < Br < I < tosylate < mesylate < nosylate < triflate [2]. The better the leaving group, the less likely you are to form undesired by-products through competitive side reactions. Depending on the stability of the precursor and other functional groups on the molecule, it may be necessary to complete the fluorination in the first step followed by the removal of a protecting group or conversion of an intermediate into the final product in a second step [2]. Examples of radiopharmaceuticals prepared by S_N2 reactions include: [^{18}F]FDG, [^{18}F]FLT, ^{18}F-Fluoromisonidazole ([^{18}F]FMISO) and [^{18}F]Fluoroethylflumazenil **(Figure 1.4)**. S_NAr substitutions are more favorable for activated phenyl rings *via* the presence of electron withdrawing groups (eg. -CN, -CF_3, carbonyl) located either *ortho* or *para* to the leaving group, although S_NAr substitutions are still possible without activation through recently developed methods including boronic esters and iodonum ylides [17A,17B]. Activated phenyl groups limit the availability of molecules that can be labeled *via* S_NAr substitutions, however, there are still several radiopharmaceuticals prepared by this technique, such as: 6-[^{18}F]fluorodopamine, (-)6-[^{18}F]fluoronorepinepherine, and [^{18}F]Fluoro-Setoperone **(Figure 1.4)** [2, 16].

Recently, there has been an interest in labeling bioactive molecules such as peptides, proteins and oligonucleotides because of their specificity *in vivo*. The challenge in radiolabeling these molecules lies in the fact that they are not stable under radio-fluorination conditions and often do not have easily accessible labeling sites [17]. Therefore, two methods have been developed to meet the need for labeling bioactive molecules. The first method is direct labeling and it involves [^{18}F]F^- substitution directly on the biomolecule that may have undergone modifications to facilitate radiolabeling. This method has been reported in the literature,

however, could suffer from poor MA due to difficulties in separating the modified precursor (eg Br- or Cl-analogs) from the desired ^{18}F-labeled product [17]. Furthermore, the harsh reaction conditions, (pH, temperature) may cause hydrolysis of the biomolecule. The second approach for labeling biomolecules is the indirect method involving radiolabeling of a small prosthetic group as a first step, followed by attachment of the prosthetic group to the biomolecule *via* amine or thiol reactions, alkylation, amidation, imidation or click chemistry [2]. Choosing a prosthetic group and the labeling site on the biomolecule is critical because this can affect the physical and physiological characteristics of the labeled molecule [18]. A typical ^{18}F-labeled prosthetic group synthesis involves multiple steps with a purification step in between the conjugation with the biomolecule to remove fluorination reagents and other by-products that can be produced. The short half-life of ^{18}F remains a challenge when designing an indirect radiosynthesis [2].

1.7 Hexadecyl-4-[^{18}F]fluorobenzoate

Hexadecyl-4-[^{18}F]fluorobenzoate ([^{18}F]HFB) is a long chain fluorinated PET tracer that was first developed by Ma *et al* in 2005 [19]. [^{18}F]HFB was prepared in a one-step synthesis by S_NAr substitution of [^{18}F]F^- on hexadecyl-4-(*N,N,N*-trimethylamino)benzoate triflate (**Figure 1.5**). Quaternary ammonium (Qat) analogs, with a triflate as a counter-ion, have been shown to be good leaving groups on aryl derivatives for S_NAr fluorination, when combined with an electron withdrawing carbonyl at the *para/ortho* position (**Figure 1.6)**. This results in electron density being pulled away from the Qat, making it susceptible to nucleophilic substitution by [^{18}F]F^-. [^{18}F]HFB was employed to label rat mesenchymal stem cells (MSCs). Due to its high lipophilicity, [^{18}F]HFB was efficiently and quickly absorbed into the cellular membranes of the MSCs in a similar fashion to fluorescent dyes used for cell labeling. The injected [^{18}F]HFB-

labeled MSCs were then imaged in a rat *via* μPET imaging allowing for short term in vivo tracking of the biodistribution of the labeled stem cells [19].

[^{18}F]HFB was then utilized by Zhang *et al* [20] to label human circulating progenitor cells (CPCs) to evaluate cell tracking in a rat myocardial infarction model and this was compared to CPC labeling with [^{18}F]FDG. It was determined that [^{18}F]HFB cell labeling efficiency and stability was superior to that of [^{18}F]FDG, whereas neither labeling approach significantly altered cell viability, phenotype or migration potential up to 24 h post-labeling [20]. The [^{18}F]HFB-CPC signal in the target area was greater than that of [^{18}F]FDG-CPCs, however, only 16-37% of the initial injection dose was retained in the injection site at 10 min post-delivery. It was concluded that compared to [^{18}F]FDG labeling, human CPCs labeled with [^{18}F]HFB provided a more efficient, stable, and accurate method to quantify the distribution of transplanted cells and that PET imaging can be applied to enhance understanding of early retention, homing, and engraftment with cardiac cell therapy [20].

[^{18}F]HFB proved to be a versatile radiotracer when it was implemented to label an injectable collagen based biomaterial to evaluate the retention and distribution after injection. [^{18}F]HFB and Qdot labeling were used to evaluate collagen matrix delivery in a mouse model of myocardial infarction *via* PET or fluorescence imaging, respectively. [^{18}F]HFB was non-covalently linked to the collagen matrix and demonstrated an 82% labeling efficiency, compared to 96% for covalently bound Qdots [21]. The study conducted by Ahmadi *et al* concluded that [^{18}F]HFB labeling along with PET imaging as a promising modality for assessing the biodistribution of injectable biomaterials for applications in the heart [21].

Taken together, the work using [^{18}F]HFB proved that this radiotracer has the potential to study both biodistribution, and trafficking of cells and biomaterials/matrices *in vivo.* In this work,

we describe the automated kit-based synthesis of [^{18}F]HFB using the Synthera® to produce large amounts of radioactivity in high concentrations that can be utilized for long term biodistribution studies. Two of the studies cited looked at only the heart, however, [^{18}F]HFB has many possible applications outside of cardiology, as we will see in the following chapter.

Chapter 2: Applications of [^{18}F]HFB

2.1 Drug Delivery Nanovesicles

Many research efforts have been dedicated to developing alternatives to traditional drug delivery methods to increase the bioavailability, therapeutic index and enhance the activity of drugs as well as decrease the degradation of other biologically active drugs. To this end, nanoparticles have been employed as drug delivery vectors and have been loaded with small molecules, peptides, proteins, DNA or siRNA [22]. Due to their structure (1 to 100 nm), nanoparticles have many unique properties, such as being able to efficiently cross barriers such as the blood-brain barrier (BBB) [23] and can be transported transdermally [24]. Furthermore, nanoparticles go through a process known as passive targeting to get to their targets. To enter tissues, nanoparticles must circulate through the blood stream. Macrophages and neutrophils that line the liver and spleen engulf large sized particles (250 – 1000 nm), whereas small particles flow through endothelial gaps [22]. Therefore, nanoparticles need to be small enough to avoid being eliminated through phagocytosis, but must be above a certain size to prevent absorption in the blood. Through various experiments, it was concluded that particles approximately 20 – 100 nm in diameter are the ideal size for efficient delivery to target tissues [25].

2.2 Exosomes as natural nanoparticles

Exosomes are 30 – 150 nm membranous vesicles that are endogenously produced by most cell types. Exosomes were initially believed to be a means to dispose of cellular waste, however, further research concluded that exosomes have important physiological and therapeutic

impacts [3]. Exosomes contain the critical nanoparticle characteristics required for drug delivery and possess additional unique characteristics such as targeting specificity as well as their intrinsic biological effects on the targeted cells due to the exosome cellular origin [22].

Exosomes are believed to originate from endosomes (or multivesicular bodies (MVBs) as intraluminal vesicles (ILVs). Early endosomes mature into late endosomes and during this process, they accumulate ILVs in their lumen. The ILVs that are formed by inward budding of the early endosomal membrane sequester proteins, lipids, and cytosol that are specifically sorted [3]. Once the ILVs are formed, the MVB can fuse to a lysosome and be degraded by lysosomal hydrolases or fuse to the plasma membrane and release the newly formed exosomes [26] **(Figure 2.1)**. To fuse to the plasma membrane, exosomes have been shown to require specific Rab proteins for docking and fusing of the MVB to the plasma membrane, although this is dependent on the cell type [27].

Due to their unique biogenesis mechanism, exosomes have plasma membrane-derived receptors on their surface and cytoplasmic contents inside. The lipid composition of the exosome lipid bilayer includes cholesterols, ceramides, lipid rafts, and sphingomyelin, and surface protein markers such as Alix, TSF101, CD63, CD9, CD81 and HSP70 [26]. Exosomes can be isolated from a variety of fluids and tissues, including but not limited to: blood, urine, breast milk, liver cells, bone cells, and saliva. The content of exosomes varies based on the cell type they are obtained from, although in general, exosomes contain DNA, miRNA, cytoskeletal and heatshock proteins, MHC class I and II molecules, and peptides [28]

2.3 Exosomes and drug delivery

Recent research demonstrates that exosomes play a critical role in intracellular communication through the horizontal transfer of cellular cargoes including DNA, mRNA,

miRNAs, peptides and proteins [26]. It was shown that exosomes promote tumor invasion and exosomes derived from tumor cells can transfer their contents to distant sites in mice and induce tumors. It was suggested that preventing the production of tumor-derived exosomes could block tumor invasion and this was accomplished through studies using knockdowns of Rab27a, which led to a decrease in primary tumor growth [29]. Furthermore, it was demonstrated that exosomes could reach the central nervous system via intranasal administration of exosomes leading to the efficient delivery of curcumin and an anti-Stat3 inhibitor to the brain [30]. Exosomes are not cytotoxic in the brain, and are more efficient than synthetic nanoparticles in the delivery of agents to the brain, making them a delivery vehicle of choice [22]. Exosomes were also recently tested as drug delivery vehicles for Parkinson's disease (PD) therapy by a group at the University of North Carolina. Exosomes were loaded *ex vivo* with a potent antioxidant (catalase) used to treat PD and these were evaluated in a mouse model of PD. The catalase loaded exosomes provided significant neuroprotective effects *in vitro* and *in vivo* models and provided evidence that exosomes can represent a strategy to treat inflammatory and neurodegenerative disorders [31]. Therefore, there is increasing evidence of the benefit of gaining a better understanding of exosomes for their roles in clinical therapeutics.

2.4 SiRNA as a drug

The 2006 Nobel Prize in medicine was awarded for the discovery of a new type of drug: small interfering RNA (siRNA). siRNAs 20-25 base pairs of double stranded RNA molecules that can specifically silence any gene. siRNAs are incorporated into the RNA interfering-induced silencing complex (RISC), which mediates mRNA sequence specific binding and cleavage [32]. In other words, siRNA interferes with the expression of specific genes with a complementary sequence to itself through degrading mRNA after transcription.

siRNA has the potential to treat virtually any disease, however, there are many current limitations to using siRNA therapeutically. The major extracellular limitations to siRNA delivery include: siRNA degradation, aggregation of siRNA nanoparticles in serum, and targeting [32]. In the body, siRNAs are easily degraded by RNAses and free siRNAs have a half-life of only several minutes to an hour [33]. Chemical modifications can be made to the siRNA structure to stabilize the siRNA in serum, however, this does not solve the problem of targeting. Nanoparticles have been developed using monoclonal antibodies or ligands to specifically target antigens or cell surface receptors [32]. Successful results were obtained including a monoclonal antibody-protamine fusion protein to selectively target leukocytes containing lymphocyte function associated antigen-1 integrins [34] and N-acetylgalactosamine modified nanoparticles to target hepatocytes [35]. The internalization of the nanoparticles inside the cells was observed to be a problem as well as the aggregation of the nanoparticles due to the surface charge of siRNA loaded nanoparticles (net positive) [32]. In the human body, siRNAs are produced and transported using exosomes. This provides both protection and specific targeting for the siRNA. Utilizing exosomes for the delivery of specific siRNA sequences could unlock a whole new therapeutic approach to treating many diseases. This approach was recently applied to deliver siRNA loaded, lamp2b modified exosomes to a mouse brain *via* systemic injection. The siRNA resulted in the knockdown of *BACE1*, a therapeutic target in Alzheimer's disease, without non-specific uptake in other tissues [36].

Taken together, these studies demonstrate that exosomes are excellent candidates for the targeted delivery of small molecules, proteins, peptides, miRNAs, siRNAs and other important molecules that would normally be degraded by the cell [26]. This would help overcome the major challenge of delivering these drugs to their targets, which has been a major obstacle for the

treatment of many diseases. To accomplish this, more work is needed in understanding how exosomes function and traffic *in vivo*.

2.5 Challenges with Exosomes and drug delivery

The unique biogenesis of exosomes produces exosomes with receptors on their surface that cause them to interact with specific cells in a highly selective fashion. To utilize the cell to cell communication system that exosomes possess for the therapeutic application of exosomes as drug delivery vehicles, it is necessary to gain a better understanding of where exosomes traffic in the body. Many technical challenges have led to difficulties in studying exosome trafficking and no robust studies of exosome trafficking have been published. Exosomes are extremely small and therefore difficult to strongly label without altering their biological functions. An imaging probe must be introduced in a way that maintains the physiological and structural integrity of the system/cell in question [37]. Furthermore, it is very expensive and demanding to produce exosomes, with typical studies to inject a single mouse requiring purifying exosomes from 200 mL – 1 L of cell culture [3]. Current approaches to follow exosome trafficking *in vivo* have used fluorescent hydrophobic dyes (DiR). These dyes require large amounts of exosomes for trafficking studies and they have also been shown to form micelles that co-purify with exosomes or surround exosomes. This results in inconclusive results related to the trafficking of exosomes. Therefore, there is an urgent need for a highly sensitive technique to follow exosome trafficking in animals. PET imaging of exosomes could solve the key issue in the studies of exosome physiology and allow for a comprehensive study of their trafficking *in vivo.*

2.6 Radiolabeling Exosomes

As previously mentioned, PET has been implemented during the drug development process for biodistribution purposes and a similar approach can be used for exosome tracking. To

date, the only paper published on radiolabeled exosomes to study their trafficking was completed by a group in South Korea [5]. The approach utilized exosome-mimetic nanovesicles derived from macrophages labeled with ^{99m}Tc-hexamethylpropyleneamineoxime (HMPAO) combined with SPECT/CT to monitor the *in vivo* distribution of the exosomes in mice. ^{99m}Tc-HMPAO is an uncharged, highly lipophilic radiotracer that has been utilized for cell labeling. Intracellular glutathione converts ^{99m}Tc-HMPAO to its hydrophilic form, trapping it inside the cell [5]. The exosome-mimetic nanovesicles were incubated with ^{99m}Tc-HMPAO for 1 hour, followed by a purification to remove free ^{99m}Tc-HMPAO and analysis *via* instant layer thin chromatography (ITLC). The expression of the exosome specific protein CD63 did not change after radiolabeling and the labeled vesicles showed high serum stability (90%). The SPECT/CT images of the mice injected with ^{99m}Tc-HMPAO exhibited high uptake in the liver and no retention in the brain, whereas mice injected with ^{99m}Tc-HMPAO only displayed high brain uptake (**Figure 2.2)** [5].

Taking this approach one step further with PET imaging would allow for an even more robust study of exosome trafficking. Exosomes have never been labeled with an ^{18}F-based radiotracer and [^{18}F]HFB has potential for success. [^{18}F]HFB is highly lipophilic and resembles the lipids found in the bi-layer of the exosome membrane. Based on previous studies using [^{18}F]HFB to label cells, it is quickly absorbed within cell membranes and it should not disrupt the cell function. SPECT provides lower-resolution images that are prone to artifacts and attenuation, as compared to PET images. Furthermore, in the study using ^{99m}Tc-HMPAO, exosome-mimetic vesicles were used due to ease of purification and the larger mass of mimetic vesicles obtained as compared to true exosomes. The trafficking of exosomes obtained from different cell types has never been reported, therefore, understanding exactly where exosomes

from different cell types traffic to in the body will be key in the therapeutic application of exosomes as drug delivery vehicles.

2.7 Injectable Biomaterials

Another promising application of radiotracers is for radiolabeling injectable biomaterials. With the increasing use of cells and injectable biomaterials for the treatment of disease and regeneration of tissues, there is a clear need for imaging methods that allow to follow their injection and possible migration within the body. Hydrogels are highly biocompatible, three-dimensional hydrophilic polymer networks, capable of absorbing large amounts of water or biological fluids [38]. Their high-water content and soft consistency makes hydrogels similar to natural tissues. Hydrogels can be made from various materials including protein-based polymers (collagen, fibrin and gelatin), carbohydrate-based polymers (cellulose derivatives, agarose, alginate, hyaluronate and chitosan) and fully synthetic polymers (polylactic acid and polyglycolic acid) [38]. Recently, Dr. Sophie Lerouge's group at the CRCHUM has developed chitosan-based thermosensitive hydrogels for the treatment of disease and regeneration of tissues. Chitosan is a natural hetero-polymer chain with ß(1-4) linked D-glucosamine and N-acetyl-D-glucosamine residues, obtained by alkaline deacetylation of chitin, one of the most abundant polysaccharides obtained from crustaceans [39] (**Figure 2.3)**. The chitosan hydrogels are obtained by mixing an acidic solution of chitosan with a mixture of weak bases, namely sodium hydrogen carbonate (SHC) with phosphate buffer (PB) or beta-glycerophosphate (BGP) as gelling agents (GA). These hydrogels are thermosensitive and quickly gel *in vivo* in a non-reversible manner. Their iso-osmolality, physiological pH and macroporisity are suitable for cell encapsulation [39A]. The hydrogels are currently under optimization for various applications

such as blood vessel embolization, drug delivery, lymphocyte delivery systems and cartilage and intervertebral disc repair [38-40].

When working with biomaterials, an important factor to consider is the mechanical properties of the hydrogels as well as the gelation kinetics (rheological properties). The secant modulus of elasticity refers to the ratio of stress to strain at any point on the curve of a stress-strain diagram (the slope of a line from the origin to any point on a stress-strain curve) whereas the storage modulus is an indicator of the ability to store deformation energy in an elastic manner [39]. Furthermore, the gelation kinetics refers to the time it takes for the hydrogel to fully gel and can change depending on the formulation of the hydrogel. These properties are unique to a given biomaterial and must be considered/measured when making changes to the formulation of a biomaterial as we will see when radiolabeling hydrogels.

2.8 Radiolabeling Hydrogels

The safety and efficacy of minimally invasive procedures, (hydrogels), is determined by the behavior of the injectable scaffolds and cells *in vivo*. Therefore, there is an urgent need for *in vivo*, short term follow up of such procedures to assess the retention of the hydrogel and cells at the site of injection. The high sensitivity of PET, combined with its non-invasive imaging capabilities make it an ideal candidate for the study of hydrogels. Vascular endothelial growth factor (VEGF) loaded chitosan hydrogels were previously labeled by Kim *et al* using I-131 and analyzed *via* autoradiography in rat myocardial infarct models [41]. I-131 is better suited for long term studies due to its long half-life of 8 days, however for short term distribution studies, ^{18}F is the radioisotope of choice for PET studies. [^{18}F]HFB was previously employed by Ahmadi *et al* for the non-covalent labeling of a collagen based biomaterial. The group saw high retention (82%) of [^{18}F]HFB after two hours in the biomaterial and a similar approach will be completed

here to assess the *in vivo* distribution of chitosan-based hydrogels. Chitosan hydrogels have never been labeled with an ^{18}F-based radiotracer for PET imaging. Radiolabeling of chitosan hydrogels with [^{18}F]HFB would allow to determine their retention and possible migration at the site of administration *in vivo* in small animals. Understanding the biological mechanisms and local effects of transplanted cells remains mostly restricted to postmortem histological assessment, whereas PET provides an effective alternative to this. This method will allow for the determination of the localization *in vivo* and efficacy of injectable hydrogels that have the potential for numerous clinical applications.

Table 1.1. Common imaging modalities and their characteristics (Adapted from: [9]).

Imaging Modality	Form of energy	Spatial resolution	Sensitivity (mol/L)	Amount of probe used
PET	Annihilation photons	1-2 mm	10^{-11} - 10^{-12}	Nano grams
SPECT	Gamma Rays	1-2 mm	10^{-10} – 10^{-11}	Nano grams
MRI	Radio frequency waves	25-100 µm	10^{-3} – 10^{-5}	Micrograms to milligrams
Ultrasound	High frequency sound waves	50 – 500 µm	not well characterized	Micrograms to milligrams
CT	X-rays	50 – 200 µm	not well characterized	N/A
Optical fluorescence imaging	Visible light or near-infrared	10 nm	~ 10^{-9} – 10^{-12}	Micrograms to milligrams

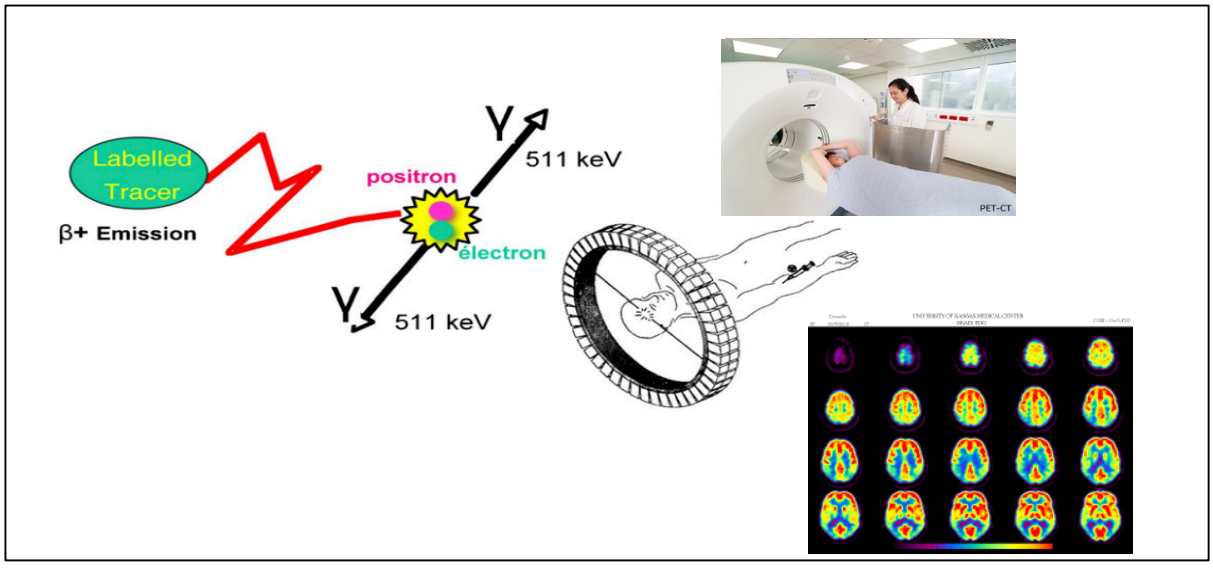

Figure 1.1. The PET concept. A radiolabeled tracer is injected into a patient, a positron is emitted from the tracer through beta decay. The positron produces an annihilation event with an electron resulting in the production of two 511 keV photons at ~ 180˚ which are detected by the PET scanner. Figure adapted from: [4].

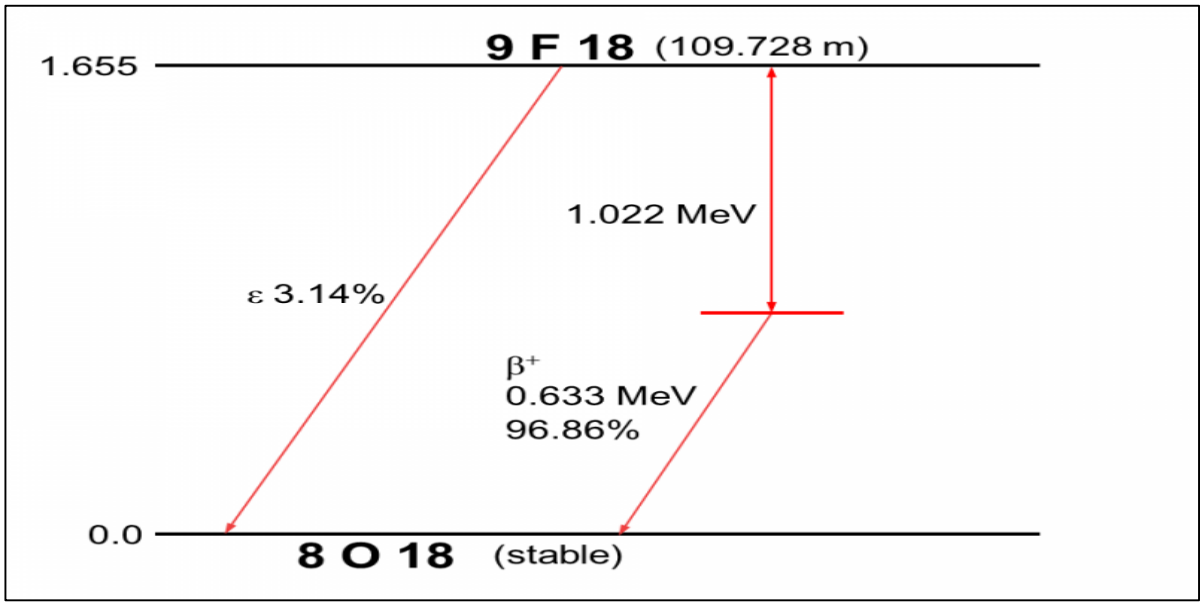

Figure 1.2. Decay scheme for fluorine-18. Unstable, high-energy fluorine 18 decays, primarily by positron decay (96.86%) to produce stable oxygen-18 via the emission of a positron and a neutrino.

Table 1.2. Physical characteristics of the most commonly utilized positron emitters for clinical use.

Isotope	**$T_{1/2}$ (min)**	**% (Beta decay)**	**Common nuclear reaction for production in cyclotron**
^{11}C	20.4	99.7	$^{14}N(p,\alpha)^{11}C$
^{13}N	9.9	99.8	$^{16}O(p,\alpha)^{13}N$
^{15}O	2.0	99.9	$^{14}N(d,n)^{15}O$
^{18}F	109.6	96.7	$^{18}O(p,n)^{18}F$

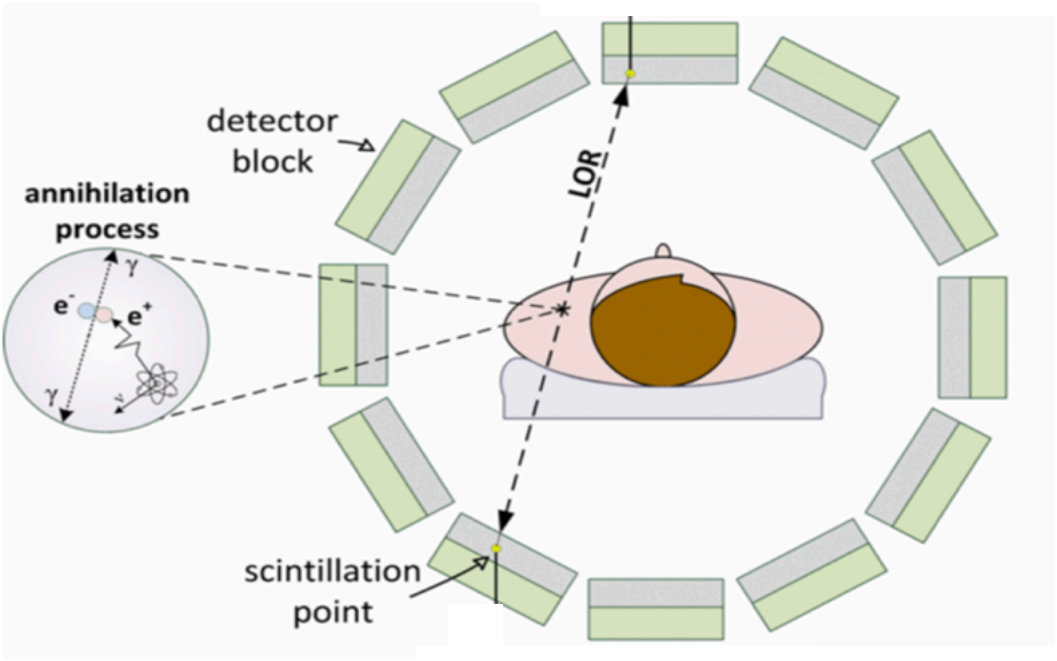

Figure 1.3. PET coincidence detection along the LOR. The circular arrangement of block detectors and an annihilation even corresponding to an LOR during a scan.

Table 1.3. Positron-emitter average energy and positron range in soft tissue.

Radionuclide	**^{11}C**	**^{13}N**	**^{15}O**	**^{18}F**
Energy$_{avg}$ (MeV)	0.386	0.492	0.737	0.250
Range$_{avg}$ (mm)	1.52	2.05	3.28	0.83

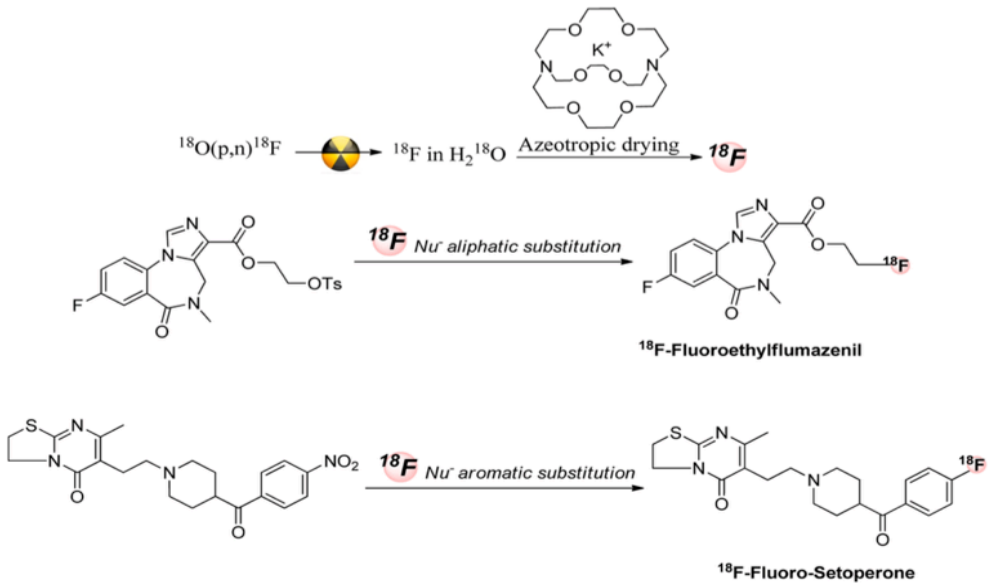

Figure 1.4. Various [18F] radiosynthetic reactions. [^{18}F] drying after cyclotron production and nucleophilic aliphatic and aromatic [^{18}F] substitution reactions. Figure adapted from [2]**.**

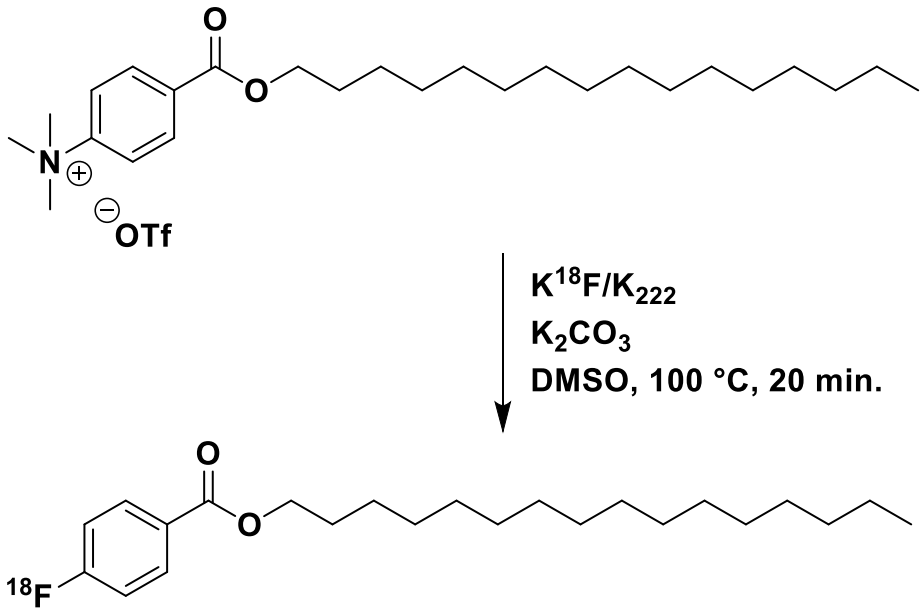

Figure 1.5. Synthesis of Hexadecyl-4-[^{18}F]fluorobenzoate ([^{18}F]HFB) from the precursor: hexadecyl-4-(N,N,N-trimethylamino)benzoate triflate.

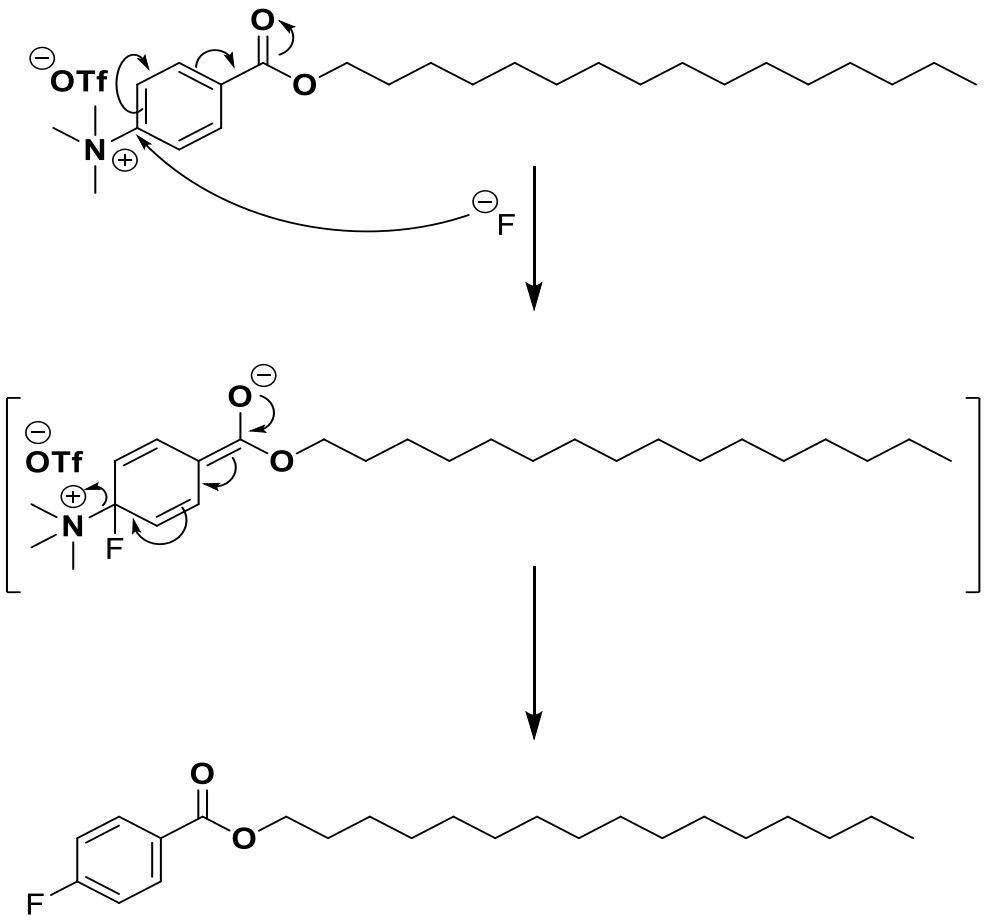

Figure 1.6. Reaction mechanism and resonance through activation of the phenyl ring by the carbonyl group on the precursor: hexadecyl-4-(N,N,N-trimethylamino)benzoate triflate.

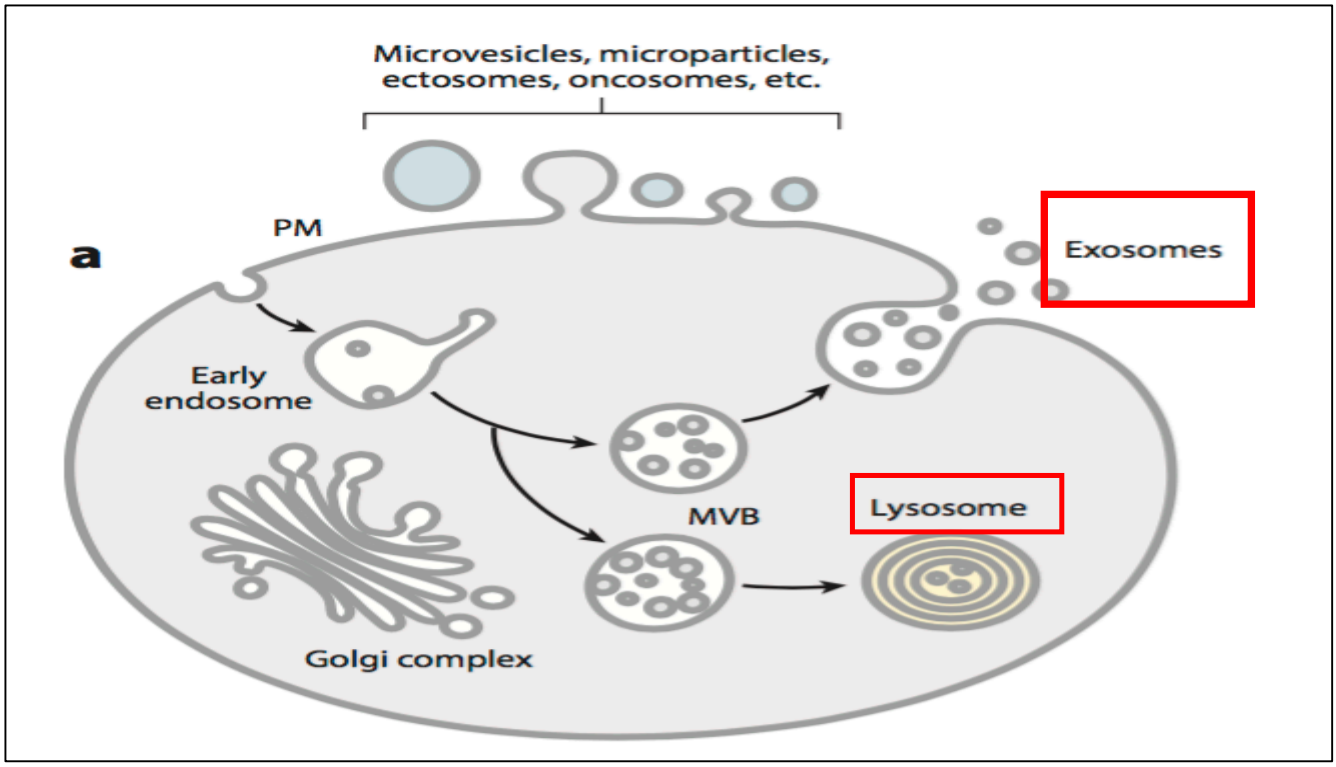

Figure 2.1. The biogenesis of exosomes. Once the MVB is formed, it can fuse to a lysosome and be degraded or fuse to the plasma membrane to release the newly formed exosomes (as highlighted above). Figure adapted from [3].

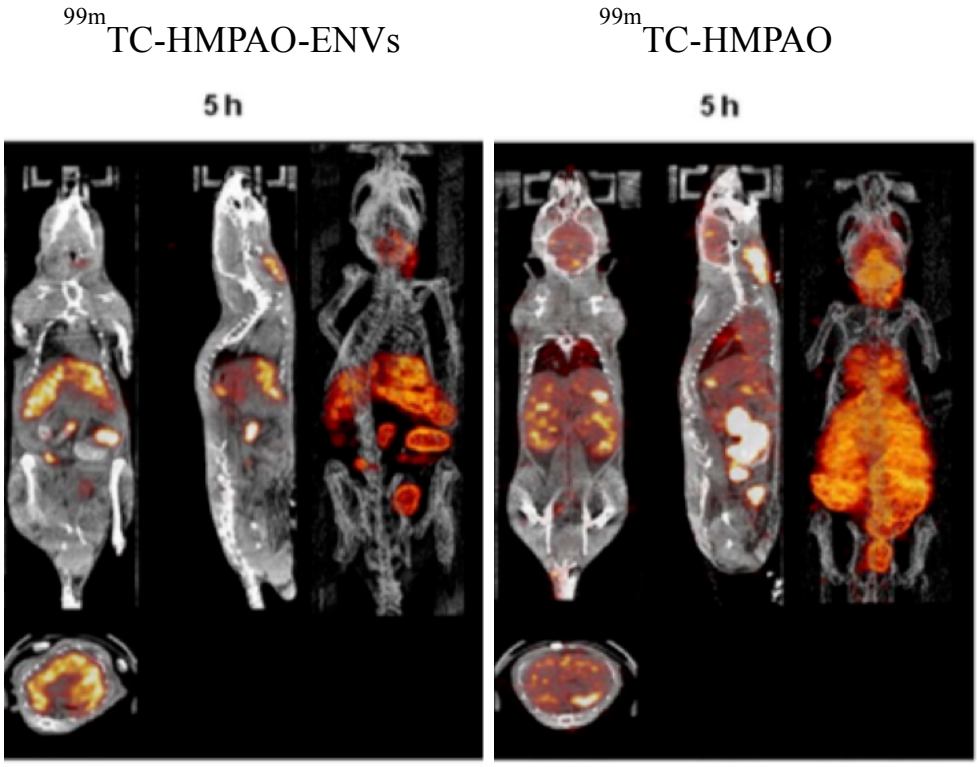

Figure 2.2. SPECT/CT images of mice injected with 99mTc-HMPAO labeled exosome-mimetic vesicles and free 99mTc-HMPAO. After 5h, the labeled exosome-mimetic vesicles showed higher uptake in the liver, whereas the free ^{99m}Tc-HMPAO sowed higher brain uptake. Figure adapted from [5].

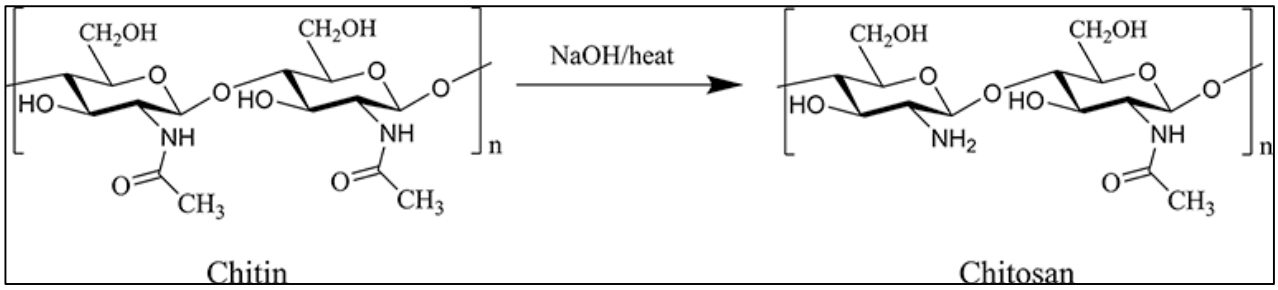

Figure 2.3. Deacetylation of chitin under basic conditions to produce chitosan [1].

Thesis Overview

2.1 Hypothesis

The radiosynthesis of [^{18}F]HFB can be automated in high purity to label exosomes and chitosan-based hydrogels for *in vivo* distribution studies using PET imaging.

2.2 Objectives

1. The [^{18}F]HFB precursor (hexadecyl-4-(*N,N,N*-trimethylamino)benzoate triflate) and non-radioactive HFB will be produced as standards.
2. Synthesize [^{18}F]HFB in high chemical and radiochemical purity (>95%), in a reproducible manner using the cassette-based Synthera® ASU module.
3. Produce [^{18}F]HFB with a final formulation that will have the appropriate solvent composition and pH for working with exosomes and living cells.
4. Use [^{18}F]HFB to radiolabel exosomes and chitosan-based hydrogels.
    4.1 The radiolabeling of exosomes should not alter their structure and/or trafficking *in vivo*.
    4.2 The radiolabeling of the hydrogels should not have any adverse effects on their mechanical properties, gelation kinetics and should have high labeling stability.

Materials and Methods

3.1 Chemistry

3.1.1 Materials

All reagents and solvents were purchased from Sigma-Aldrich, classified as 98% purity (or greater) or HPLC grade, and used without further purification or manipulation. All reactions were performed in oven-dried glass round-bottom flasks equipped with magnetic stir bars. Analytical thin layer chromatography (TLC) was performed on silica gel 60 F254 plates from EMD. Purification of reaction products was carried out by flash column chromatography using silica gel. A Phenomenex Luna C18(2) column (250 x 4.6 mm, 10 μm) or a Shimadzu C18 (50x4.6 mm, 5 μm) were used for all analytical HPLC in combination with either a Shimadzu LC-20AB/SPD-20A HPLC system or a Waters 1525/ 2489 HPLC system.

^{1}H-Nuclear magnetic resonance (NMR) was performed at the Université de Québec à Montréal department of chemistry using a Bruker 300 MHz at ambient temperature. Proton chemical shifts are reported in parts per million (ppm) using residual solvent as the internal standard ($CDCL_3$ at 7.26 ppm), coupling constants (*J)* are reported in Hertz (Hz). Multiplicity is defined by s (singlet), br (broad), d (doublet), t (triplet), q (quartet), qn (quintet), sx (sextet), or m (multiplet). High-resolution mass spectrometry (MS) was performed by technicians at the CRCHUM in positive or negative ion mode using a Thermo Scientific Q-Exactive Plus Orbitrap Mass Spectrometer *via* direct injection with no chromatograph. Melting point measurements were completed using a Mel-Temp® melting point apparatus.

3.1.2 Experimental

All compounds were prepared as per the literature [19] (**Figure 3.1** and **Figure 3.2).**

Synthesis of *N*-hexadecyl-4-(*N,N*-dimethylamino)benzoate

Hexadecyl-4-(*N,N*-dimethylamino) benzoate was synthesized from 4-(*N,N*-dimethylamino)benzoyl chloride (0.500 g, 2.72 mmol) and 1-hexadecanol (0.792 g, 3.26 mmol) in the presence of triethylamine (0.76 ml, 5.4 mmol) and dichloromethane (DCM) (10 mL). The reaction mixture was stirred at room temperature for 4 h and monitored via TLC. Once no starting material remained, the reaction mixture was extracted with water and DCM. The organic phase was dried over magnesium sulfate, filtered, concentrated and purified by column chromatography (9/1 dichloromethane/methanol (MeOH)). The product was recrystallized using a minimum of hot ethyl acetate to give pure *N*-hexadecyl-4-(*N,N*-dimethylamino)benzoate.

Synthesis of hexadecyl-4-(*N,N,N*-trimethylamino)benzoate triflate (Triflate Precursor)

A mixture of *N*-hexadecyl-4-(*N,N*-dimethylamino)benzoate (0.2 g, 0.51 mmol) and methyl triflate (0.10 g, 0.61 mmol) in DCM (3 mL) was stirred overnight at room temperature under argon. The reaction mixture was monitored via TLC until no more starting material remained. The solvent was evaporated and the product was crystallized using hexanes/DCM. Analytical HPLC analysis was completed on the precursor (Shimadzu C18 (50x4.6 mm, 5 μm), 95/5 (MeCN/AF (0.1M), 1.5 mL/min).

Synthesis of hexadecyl-4-fluorobenzoate (HFB Standard).

1-Hexadecanol (0.183 g, 0.75 mmol) was dissolved in DCM (3 mL) and to this was added 0.175 mL (1.2 mmol) of triethylamine and 4-fluorobenzoyl chloride (0.1 g, 0.63 mmol). The reaction mixture was stirred at room temperature for 3 h and the progress of the reaction was monitored via TLC. Once no starting material remained, the reaction mixture was extracted with water and DCM. The organic phase was dried over magnesium sulfate, filtered, concentrated and purified by column chromatography (96/4 hexanes/ethyl acetate). Analytical HPLC analysis was completed on the HFB standard. (Shimadzu C18 (50x4.6 mm, 5 μm), 95/5 (MeCN/AF (0.1M), 1.5 mL/min).

3.2 Radiochemistry

3.2.1 Materials

[^{18}F]Fluoride was produced in our IBA Cyclone® 18 MeV cyclotron from proton irradiation of 97% [^{18}O]H_2O-enriched water *via* the $^{18}O(p,n)^{18}F$ nuclear reaction. Target water was delivered through polyethylene tubing and collected in a 10-mL vial in the dispensing cell. The radioactivity was transferred to the Synthera® once ready.

The Synthera® ASU was purchased from IBA® (**Figure 3.3**), including two synthesis modules and one HPLC purification module (UV detector, radiation detector and HPLC pump). An automated syringe driver system was installed between the synthesis modules and the HPLC module. This was done to minimize the loss of product when transferring from the reactor in the synthesis module to the HPLC loop, as the previous system pushed the product directly to the HPLC loop using air. This can often result in losses through overshooting the HPLC loop, therefore, the HPLC loading was accomplished *via* a syringe driver system **(Figure 3.4)**. Research and development (R&D) integrated fluidic processor (IFP) cartridges

were purchased from ABX and used for a maximum of 5 runs each (cleaned in between each run). The IFP's were slightly modified to accommodate larger reagent vials; positions 3 and 4 on the IFP (**Figure 3.5)** were connected to external 30 mL and 10 mL vials, respectively. Phenomenex Luna C8(2) and C18 (2) columns (250 x 10 mm, 10 μm) were used for semi-preparative HPLC with a mobile phase consisting of 95/5 MeCN/ammonium formate (AF) (0.1 M in water). The buffer was filtered through a 0.2 μm filter paper prior to use.

Sep-Pak Light Waters Accell Plus QMA cartridges (Waters) were utilized to trap F-18 from the target water. These QMA cartridges were conditioned by passing 5 mL of an 8.4% sodium bicarbonate solution, followed by 10 mL of water and drying. The C18 light (Waters) cartridges were conditioned by passing 5 mL of ethanol (EtOH) or MeOH followed by 10 mL of water. F-18 eluent was ordered from ABX and contained per vial: 22.6 mg Kryptofix2.2.2, 4.2 mg potassium carbonate, 0.3 mL anhydrous acetonitrile and 0.3 mL water for injection. A heating block set at 120˚C was implemented post purification to evaporate the HPLC solvent. The final product was reformulated using sterile DMSO and/or saline/1x phosphate buffered saline (PBS).

3.2.2 [^{18}F]HFB

3.2.2.1 Experimental

For every [^{18}F]HFB run, either a new R&D IFP was used or a previously used IFP was cleaned and dried using a pre-programmed cleaning recipe with the reagent vials containing acetonitrile, EtOH and water (1 mL each). A minimum of 12 hours was given before opening the hot cell to allow for decay. Several different reaction conditions (fluorination temperatures of 80˚C, 100˚C and 140˚C and times 20 min and 30 min) were tested to optimize the reaction conditions through minimizing production of side products while

maximizing yield of [^{18}F]HFB. [^{18}F]HFB was prepared *via* nucleophilic displacement of a Qat leaving group by [^{18}F]fluoride ion (**Figure 1.5**).

To remove any unreacted [^{18}F]fluoride, other salts and dimethyl sulfoxide (DMSO) prior to going to semi-prep HPLC purification (to prevent damage to the column), the reaction mixture was passed through an activated C18 Seppak light cartridge. The elution conditions of HFB from a C18 light cartridge were tested by dissolving 0.5 mg of cold HFB in 600 μL of DMSO and passing this through a conditioned C18 light cartridge. The cartridge was then rinsed with 20 mL of water to remove the DMSO, and either MeCN or EtOH to elute HFB in 0.5 mL fractions. These fractions were then analyzed *via* analytical HPLC to determine how much solvent was needed to completely remove HFB from the C18 light cartridge.

A checklist was developed for the radiosynthesis of [^{18}F]HFB in order to minimize human error prior to the synthesis. The first step in the radiosynthesis of [^{18}F]HFB was to ensure that the HPLC solvent bottles (A and B) were full of solvent (1 L). Solvent bottle A contained 95/5 (MeCN/0.1M ammonium formate) and bottle B used for cleaning contained 70/30 (MeCN/H_2O). The HPLC procedure was then started which involved a loop and column cleaning with solvent B, followed by a column conditioning with solvent A. While this was running, slight modifications were made to the IFP to connect larger vials to positions 3 and 4 (**Figure 3.5)**. This involved removing the tubing from the normal inlet to the reagent vials and connecting these to external 30 mL and 10 mL vials, respectively. The kit was then placed onto the synthera A module and the reagents were prepared as follows: vial 1: Cryptand solution, vial 2: hexadecyl-4-(*N,N,N*-trimethylamino)benzoate triflate precursor (3 mg/600 uL DMSO), vial 3: Sterile Water (20 mL), and vial 4: Acetonitrile (4

mL). Furthermore, the QMA light cartridge and C18 light cartridges were conditioned and placed in Sep-Pak positions 1 and 2 on the IFP (**Figure 3.5**).

Before transferring [^{18}F]F$^-$ to the synthera, the pre-synthesis HPLC conditioning and IFP tests were completed. The IFP tests involved pressurizing the reactor and reagent vials along with pushing air and turning the valves to ensure no lines were leaking, obstructed or vials malfunctioning. Once all the tests were passed, [^{18}F]F$^-$ was transferred from the dispening hot cell to the synthera *via* the vaccum pump on the synthera module.

3.2.2.2Radiosynthesis

[^{18}F]F$^-$ (1 – 1.2 Ci) was trapped on a Waters Sep-Pak QMA light catridge through vaccum suction into the synthera module while the O-18 water was collected in a designated vial. The [^{18}F]F was eluted into the reactor using 0.6 mL of cryptand solution. The eluate was azeotropically evaporated at 110˚C for 5 min under nitrogen gas flow, leaving potassium [^{18}F]fluoride complexed with Kryptofix 2.2.2. in the reactor. Next, 3 mg of precursor in 600 µl of DMSO was added to the reactor and fluorination was completed at 100˚C for 20 mins. Five mL of water was added to cool and dilute the reaction mixture, and this was passed through a C18 light cartridge, trapping [^{18}F]HFB and organic compounds, and disposing of unreacted [^{18}F]F$^-$ and salts. The cartridge was rinsed 3 times with 5 mL of water and then eluted using 4 mL of MeCN into an intermediate vial. An automated syringe driver system was used to transfer the eluate to semi-preparative HPLC purification using a C18 column. MeCN/0.1 M AF 95/5 at a flow of 10 mL/min was used as the mobile phase. The radioactive product peak (retention time ~ 20 min) was collected and transferred to the dispensing hot cell. The HPLC solvent was evaporated at 120˚C under nitrogen flow and vacuum aspiration. [^{18}F]HFB was then reformulated with 0.5 to 0.7 mL of DMSO, depending on the desired

final concentration/activity. The formulation was filtered through a 0.22 μm filter (DMSO resistant Acrodisc®) into 4.5 - 6.3 mL of sterile saline or PBS for a final tracer formulation of 10% DMSO/Saline. The total synthesis time including purification was approximately 60 mins.

3.2.3 Quality Control

Post-synthesis quality control (QC) was completed using analytical HPLC to confirm the product identity, purity and calculate the molar activity of [^{18}F]HFB. Analytical HPLC was completed using a Phenomenex Luna C18(2) column (250 x 4.6 mm, 10 μm) and a mobile phase of 99/1 (MeCN/AF (0.1M)). An aliquot of the final formulation of [^{18}F]HFB was co-injected with cold standard to confirm the product identity. Molar activity was calculated by injecting [^{18}F]HFB alone and comparing the area of the UV absorbance peak (254 nm) to that of a known amount of standard. Gas chromatography was completed with an Agilent 7890B GC system with a 7697A Headspace sampler. Instant TLC (ITLC) was analyzed using an Eckert & Ziegler TLC scanner (B-AR200-1). All radioactivity was measured using a Capintec CRC-55tW.

3.2.3.1Gas Chromatography Analysis

Gas chromatography (GC) analysis was completed to measure the amount of residual solvent that remained in the final formulation, after evaporation. Two approaches were tested to ensure full evaporation of the HPLC solvent. The first approach involved placing 15 mL of HPLC solvent (95/5 MeCN/AF (0.1M) in a 30-mL product vial, evaporating at 120˚C until no solvent remained and then adding an additional 2 minutes to ensure dryness. The second approach was similar; however, an additional 2.5 minutes were added to ensure complete

dryness. 5 mL of saline was then added to the vials and GC analysis was completed to test for residual: methanol, ethanol, acetone and acetonitrile.

3.2.3.2Calculating Molar Activity

A specific volume of standard of known concentration was injected onto analytical HPLC and the area under the curve (AUC) was recorded (254 nm). A sample of the final formulation of [^{18}F]HFB was then injected in a separate injection and the activity in the syringe was measured before and after injection. The AUC of the injected [^{18}F]HFB was recorded (254 nm) and the amount of cold mass in the product was determined by comparing the two AUCs with respect to the amount of standard injected.

3.3 Labeling exosomes and hydrogels with [^{18}F]HFB

3.3.1 Materials

Exosome exclusive spin columns (MW 3000) and instant thin layer chromatography (ITLC) paper was ordered from Thermo Fisher scientific and disposable PD10 (MW 5000) desalting columns were ordered from sigma Aldrich. Purified exosomes obtained from different sources (lung, liver, bone) were provided by Dr. Derrick Gibbing's lab at the University of Ottawa Faculty of Medicine. Centrifugation for exosome purification was completed using a TL-100 Ultracentrifuge (TLA 100.3 rotor). Following radiolabeling, removal of [^{18}F]HFB from labeled exosomes was completed using one of two centrifuges: a Thermoscientific Legend Micro21R or a Beckman Coulter Optima L-90K ultracentrifuge with a SW40TI rotor.

Chitosan (Chitoscience 95/100, DDA 92.6%) was purchased from Heppe Medical Chitosan (Germany), ß-glycerophosphate disodium salt pentahydrate (BGP) ($C_3H_7Na_2O_6P{\cdot}5H_2O$) was purchased from Sigma-Aldrich (Oakville, ON, Canada), sodium

hydrogen carbonate ($NaHCO_3$, hereafter SHC) was purchased from MP Biomedicals (Solon, OH, USA) and provided by Dr Sophie Lerouge's lab at the CRCHUM and used without further manipulation.

3.3.2 Experimental

3.3.2.1 Exosome Purification

Exosomes were purified and isolated by sequential centrifugation by members of the Gibbings lab. All the centrifuge tubes were balanced using PBS. Briefly, the supernatant media fluid from a cell culture dish was transferred into a 50-mL centrifuge tube and centrifuged at 300 x g at 4˚C for 10 min. The supernatant was then transferred into a new 50 mL centrifuge tube and centrifuged at 2000 x g at 4˚C for 10 min. The supernatant was then transferred into an ultracentrifuge tube and centrifuged at 10,000 x g at 4˚C for 30 minutes. The supernatant was then transferred to a new ultracentrifuge tube and centrifuged at 100,000 x g at 4˚C for 2 hours. The supernatant was then removed and the pellet resuspended in 1 mL PBS. The pellet solution was transferred to a 1.5 mL ultracentrifuge tube and centrifuged at 100,000 x g at 4˚C for 15 mins. The supernatant was removed and the exosome pellet was resuspended in a small volume of PBS (20-34 µL). The exosomes were then stored at 4˚C and shipped to the CRCHUM until used.

3.3.2.2 Exosome Radiolabeling using [^{18}F]HFB

3.3.2.2.1 Exosome labeling conditions

Several strategies were implemented to label exosomes, based on the radiolabeling of exosome-mimetic vesicles using ^{99m}Tc-HMPAO and labeling of exosomes using fluorescent dyes (unpublished work complete by the Gibbing's lab) (**Figures 3.6** and **3.7)**. The final formulation volume of [^{18}F]HFB varied from 5 to 7 mL (10% DMSO/pbs) depending on the

desired concentration/activity per incubation with exosomes. Three different incubation temperatures were tested: 4˚C, room temperature (RT) and 37˚C with an incubation time of 30 min. Each Eppendorf tube of purified exosomes obtained from the Gibbing's lab contained approximately 16 µg of exosomes dissolved in ~ 34 µL of PBS. An Eppendorf tube was either used completely or split into various aliquots. The incubation volumes, temperatures and times that were investigated along with centrifugation conditions are indicated in **Table 3.1.** For each labeling condition, a control was also completed without exosomes where the volume of the exosomes was replaced with PBS.

Table 3.1. Exosome labeling conditions.

Volume of Exosomes (µL)	Volume of [^{18}F]HFB (µL)	Volume of BSA (µL)	Total volume (µL)	Incubation conditions (˚C/min)	Centrifugation conditions	Rinse
5	495	--	500	4, RT, 37/30	12,000 rpm/1hr	PBS/DMSO
8	400	--	408	37/30	200,000 x g /1h, 2h, 4h,	---------
10	990	--	1000	4, RT, 37/30	21,000 rpm/1 hr	PBS
34	200	--	234	37/30	21,000 rpm/2 hr	PBS/DMSO
34	50	--	84	37/30	200,000 x g/ 4h	---------
34	50	50	134	37/30	200,000 xg/4h	---------

The effect of bovine serum albumin (BSA) on the radiolabeling of exosomes was also investigated through completing a 30 min incubation of BSA at 37˚C with [^{18}F]HFB prior to the addition of exosomes. Furthermore, normal Eppendorf tubes and low retention Eppendorf tubes were tested to see the effect of [^{18}F]HFB sticking.

3.3.2.2.2 Purification strategies

Various strategies were tested to remove free [^{18}F]HFB from labeled exosomes including exosome exclusive spin columns, PD10 size exclusion desalting columns and centrifugation. For the exosome exclusive spin columns, the columns were hydrated with 650 µL of 1x PBS for 15 min at RT. The spin column was then placed in a 2-mL collection tube and spun at 750 x g for 2 min at RT to remove excess interstitial fluid. The collection tube was discarded and the sample (maximum volume of 100 µL/column) was loaded directly onto the center of the gel bed. The column was then placed in a 1.5 mL elution tube and spun at 750 x g or 500 x g for 1 – 2 min at RT. The elution tube was collected and analyzed. A gravity protocol was used for the PD10 desalting columns, where the column was first equilibrated with 25 mL of 1x PBS or 25 mL of 1x PBS + 0.1% Tween, followed by sample application ([^{18}F]HFB reformulated in 10% DMSO/PBS, 5% DMSO/PBS or 10%DMSO/PBS + 0.1% Tween) and elution using 1x PBS or 1x PBS + 0.1% Tween. Fractions (0.5 mL) were collected. The force of centrifugation varied from 12,000 rpm – 21,000 rpm to 200,000 x g in the ultracentrifuge. Centrifugation times also varied from 1 to 4 hours, with a washing step completed using PBS or 10% DMSO/PBS (in select experiments). Due to the long-time constraints of the ultracentrifugation (up to four hours), and the loss of activity associated to this step, the washing step following ultracentrifugation was by-passed. After centrifugation, the supernatant was collected and the pellet resuspended in a small volume of PBS (60 - 200 µL) PBS. Both the supernatant and resuspended pellet were analyzed *via* ITLC to confirm labeling. ITLC was also completed on the samples prior to centrifugation, directly after incubation and following centrifugation to assess labeling. ITLC

analysis was completed with a mobile phase of 9/1 (MeCN/AF (0.1M). Furthermore, the radioactivity in the tubes after each step or transfer was measured.

3.3.2.3Hydrogel Preparation

Raw chitosan (CH) was first purified by dissolution in 0.1M hydrochloric acid and stirring overnight at 40˚C. The solution was then filtered under vacuum and the CH was precipitated with 0.5 M NaOH under continuous stirring. Sodium dodecyl sulfate (SDS) 10% (w/v) was added to the slurry and heated at 95˚C for 5 min. After cooling down to room temperature, the pH was adjusted to 10 with 0.5 m NaOH. The slurry was filtered under vacuum and hydrated CH was washed with Milli-Q water at 40˚C. The CH was then freeze-dried, ground and sieved to obtain a dried and purified CH powder.[39].

A CH solution of 3.33% (w/v) was prepared by dissolving purified CH powder in 0.12 M hydrochloric acid at room temperature, and the solution was sterilized by autoclave at 121˚C for 20 min and stored at 4˚C. Each hydrogel was prepared at room temperature by mixing sterilized CH solution with a gelling agent (GA) solution (containing BGP and SHC to get final concentration of 0.1 M and 0.075 M in the gel, respectively) by using two syringes and a female-to-female Luer-lock syringe connector. This was previously shown to form a hydrogel which remains liquid at room temperature but rapidly gels at body temperature.

3.3.3.3Effect of DMSO on Chitosan Hydrogels

Since the final formulation of [^{18}F]HFB contains 10% v/v DMSO in saline, primary tests consisted in testing the possible negative effect of DMSO on the gelation kinetics and mechanical properties of the chitosan hydrogels. 10% DMSO/saline solution mixed with the CH-GA solution to label the gel (Approach 1: (CH+GA) + DMSO). Alternatively, 10%

DMSO/saline solution was mixed to the acidic chitosan solution prior to adding GA (Approach 2: (CH+ DMSO + GA). The volume and initial concentration of GA was adjusted each time.

Both mixing approaches described above were tested, using 10% DMSO in water (without HFB). Different volumes of DMSO/saline solution were tested: 0.2 mL, 0.1 mL and 0.05 mL (2%, 1% and 0.5% v/v, respectively), while the volume and initial concentration of GA solution was varied (0.2 mL, 0.3 mL and 0.35 mL of the GA at concentrations of 2x, 1.33x and 1.14x, respectively) to keep the final concentration of each compounds constant within the 1mL gel solution. The rheological properties of the hydrogels during gelation at 37°C were compared, as well as their mechanical properties in compression after 24h gelation.

Rheological properties were investigated using an Anton Paar instrument (Physica MCR 301, Germany) with a coaxial cylinder geometry (CC10/T200) in the linear viscoelastic region (at 5% strain and 1Hz frequency). The evolution of the storage (G') and loss (G") moduli was measured during 1h at 37 °C, immediately after mixing the hydrogel components.

After complete gelation, unconfined compression tests were performed using a Bose ElectroForce 3200 instrument equipped with a 200 N load cell. Hydrogel solution (2mL) was added into cylindrical molds (14 mm diameter) and incubated at 37 °C for 24 h. Samples were gently removed from the container and a compression was applied at a constant rate of 0.5 mm s^{-1} until reaching 50% deformation. The secant Young's moduli were calculated as the slope of a line connecting the point of zero strain to a point at a specified deformation.

Statistical analyses of the DMSO samples as compared to controls were completed using an ordinary one-way ANOVA with multiple comparison test (Bonferroni) using Graphpad prism 7 software.

Radiolabeling Hydrogels with [^{18}F]HFB

[^{18}F]HFB was prepared as previously described (**Section 3.2.2.2**) and dissolved in 0.5 mL of DMSO in 4.5 mL of saline. Radiolabeling of chitosan hydrogels was performed using the two approaches described above, this time with [^{18}F]HFB dissolved in the 10% DMSO solution. Both methods were compared in terms of loss of radioactivity during mixing steps and the efflux of [^{18}F]HFB from the hydrogel when immersed in saline solution at 37˚C.

Two approaches were utilized to measure the efflux of [^{18}F]HFB from the hydrogels. A first set of experiments was conducted using transwells (procedure 1). A volume of 2-3 mL of radiolabeled hydrogel was prepared according to approach 1 or 2 and the radioactivity in the syringes was measured after each mixing step. The hydrogels were then dispensed in 0.5 mL portions into 40 μm transwells. The radioactivity in each portion was measured and the hydrogels were allowed to gel in 5 mL of saline for 5 min at 37˚C in a hot water bath. An additional 10 mL of saline was then added to each hydrogel, to completely cover the gel. The efflux of [^{18}F]HFB from the hydrogels was measured at time points of 5 min, 1h, 2h, 4h, 6h and 8h by removing the gel from the saline and rinsing with an additional 5 mL of saline. The radioactivity was measured in the saline and saline rinses and the labeled hydrogels. All data were decay corrected and compared to the initial amount of radioactivity used in the respective incubation.

The second method involved using gel molds (procedure 2) to measure the efflux of [^{18}F]HFB from the chitosan hydrogels. 1 mL of labeled hydrogel was prepared according to

approach 1 and 2 and the radioactivity in the syringes was measured after each mixing step. The labeled hydrogels were then dispensed into a gel mold (a 10-mL syringe cut into small portions with one side covered in parafilm) and allowed to incubate at 37˚C in a cell incubator for 2-3 hours to gel. The hydrogel was then carefully removed from the mold and placed in a beaker of saline. The efflux of [^{18}F]HFB from the hydrogels was measured at time points of 5 min, 1h, 2h, 4h and 6h by removing the gel from the saline and rinsing with an additional 5 mL of saline. The radioactivity was measured in the saline and saline rinses. The labeled hydrogel molds were placed in a new beaker of saline for the subsequent time point. All data were decay corrected and compared to the initial amount of radioactivity used in the respective incubation.

3.3.3.4 Radiolabeling Hydrogels with [^{18}F]F$^-$

To test the specificity of [^{18}F]HFB to label the chitosan-based hydrogels, a control study using only [^{18}F]F$^-$ to label the hydrogels was also conducted. Only approach 2 was performed for the mixing of the radiolabeled hydrogel replacing [^{18}F]HFB by [^{18}F]F$^-$ (for 1 mL of gel: 0.6 mL of chitosan with 0.35 mL of GA (1.14x BGP) followed by the addition of 0.05 mL of [^{18}F]F$^-$ present in O-18 enriched water (as [^{18}F]HF). The hydrogels were mixed using 3 mL syringes connected by a luer lock and the components were passed back and forth through the syringes to ensure complete mixing. As above, transwells and gel molds were used to measure the efflux of [^{18}F]F from the hydrogels.

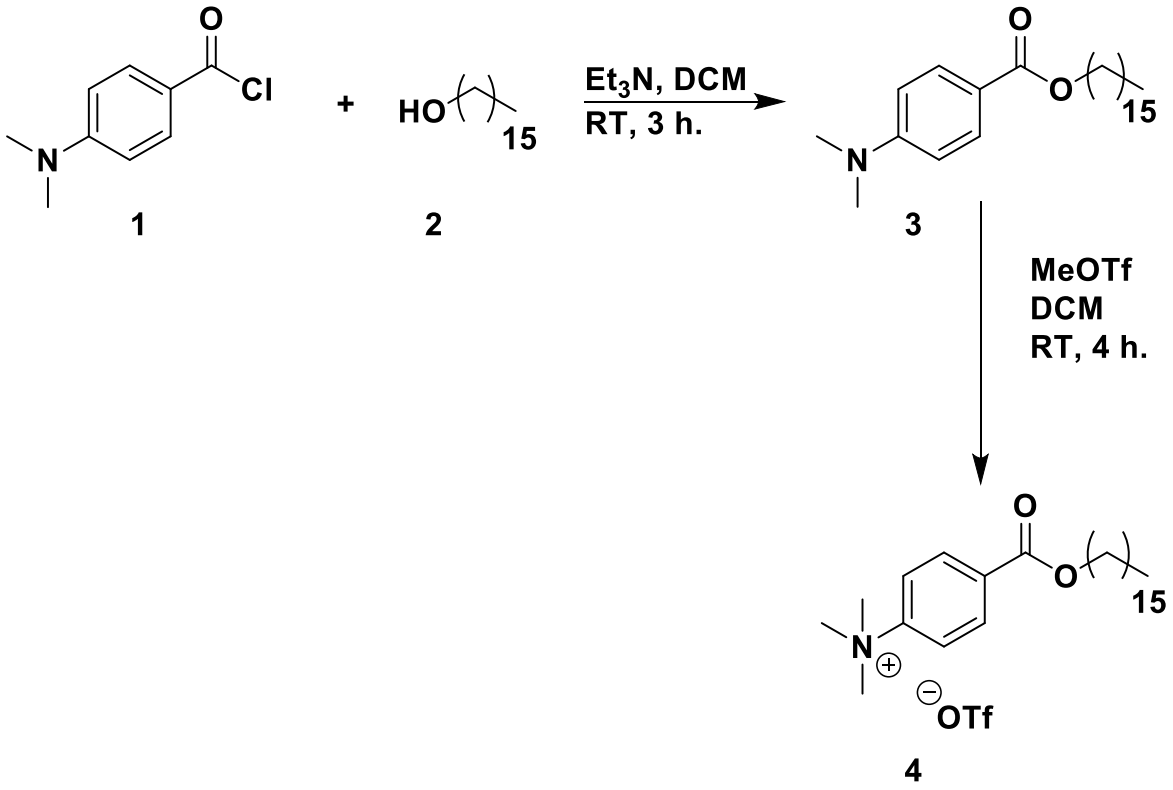

Figure 3.1. Synthetic scheme for the synthesis of the [^{18}F]HFB precursor (4).

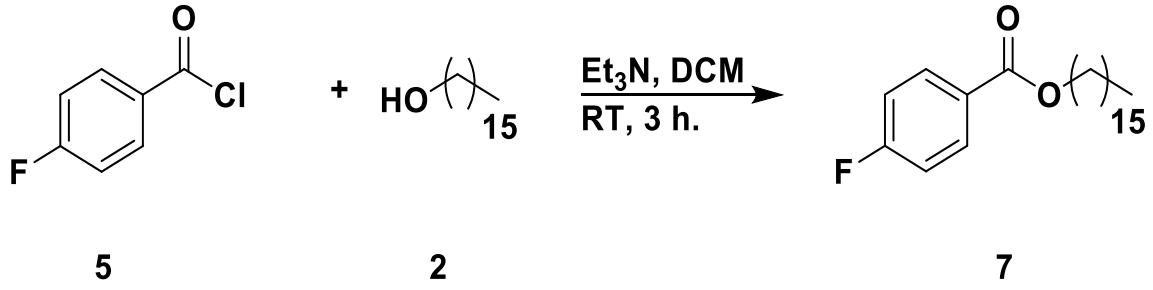

Figure 3.2. Synthetic scheme for the synthesis of cold HFB (7).

Figure 3.3. The IBA Synthera® automated kit based radiochemistry synthesizer.

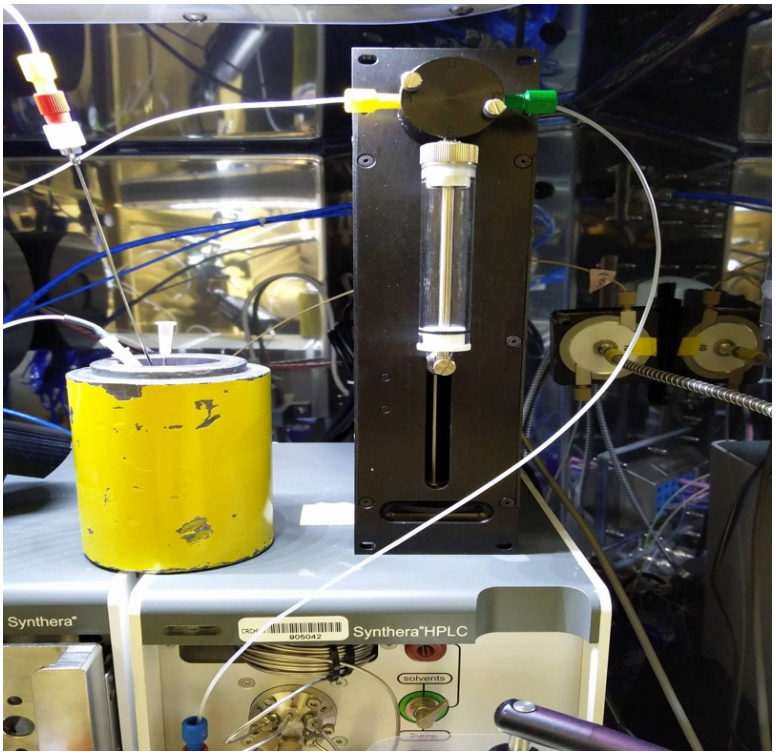

Figure 3.4. Automated syringe driver used to inject into semi-prep HPLC from the intermediate vial.

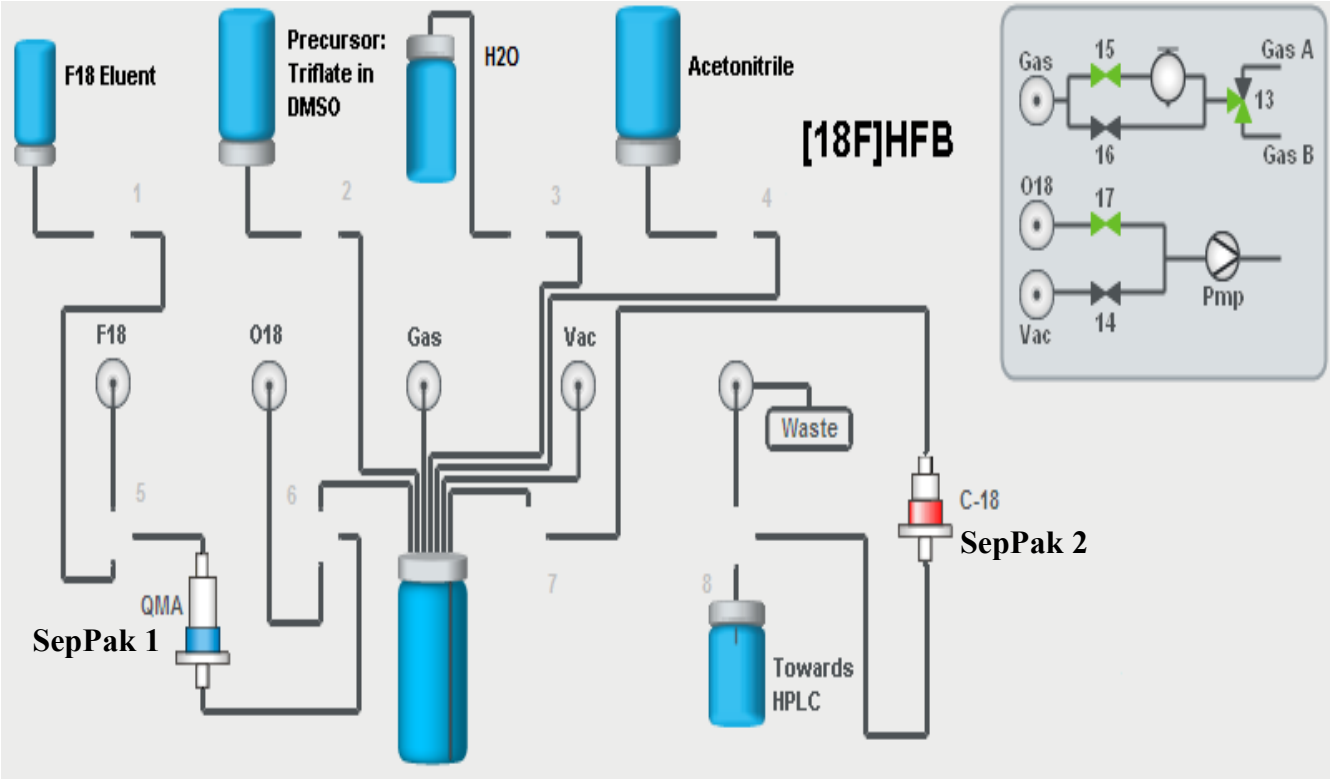

Figure 3.5. Schematic representation of the [^{18}F]HFB IFP used on the Synthera® module.

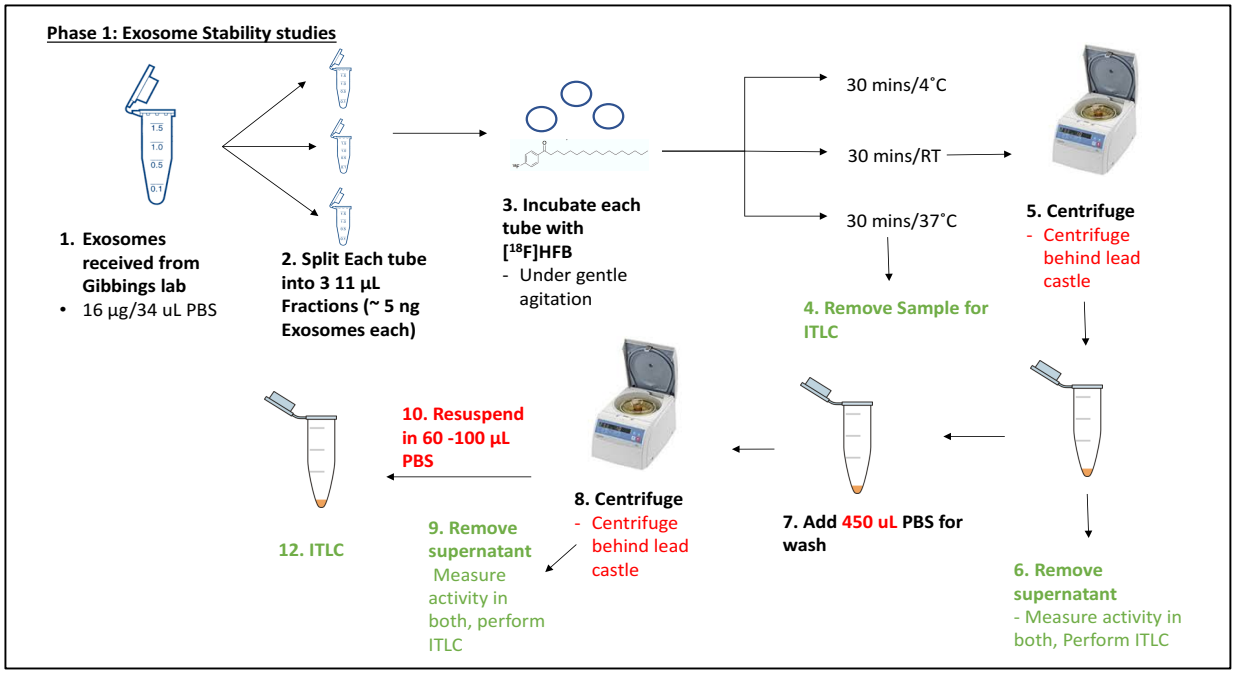

Figure 3.6. First Exosome labeling strategy.

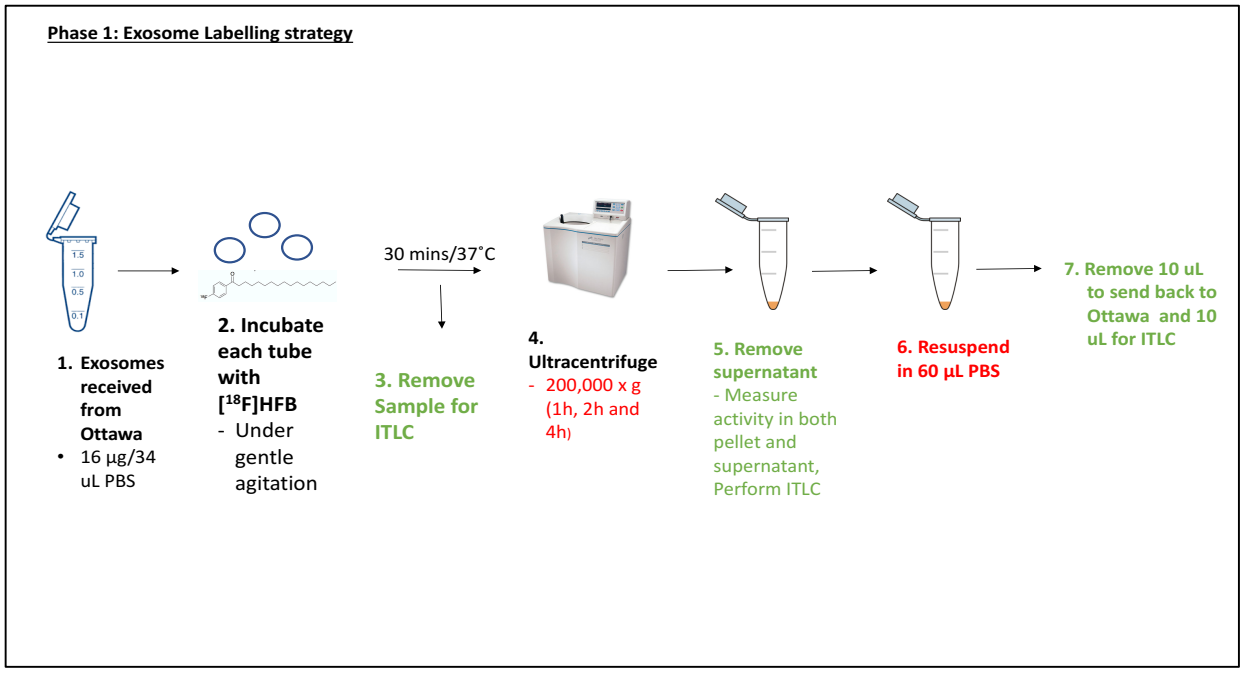

Figure 3.7. Second exosome labeling strategy.

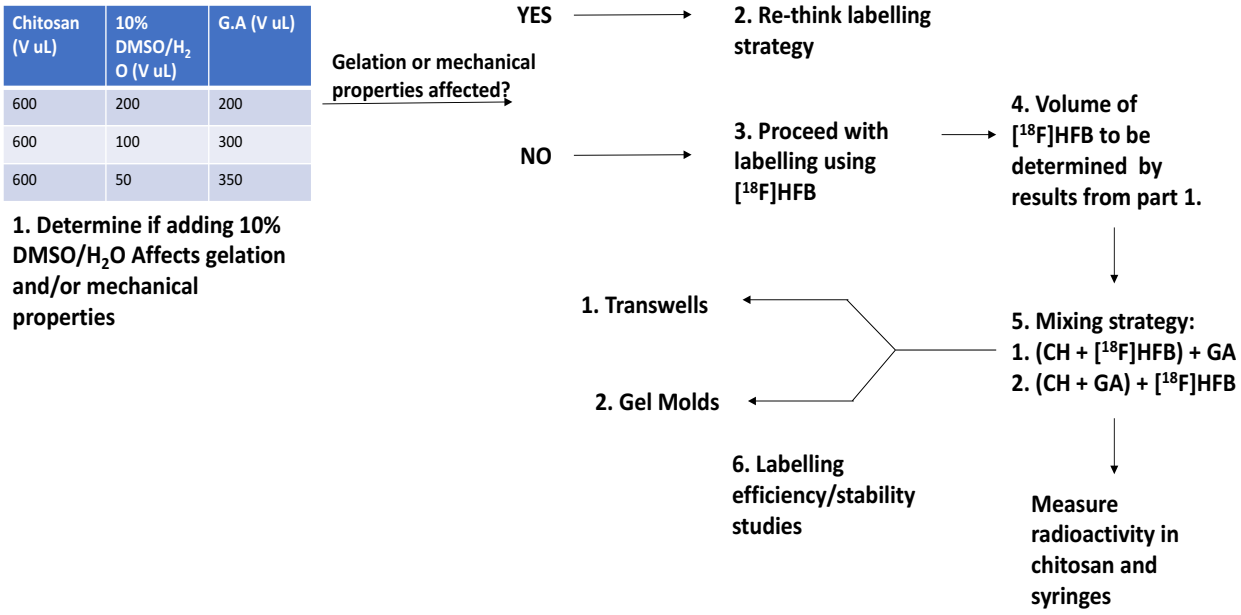

Figure 3.8. Hydrogel labeling strategy including preliminary study on the effect of DMSO on the gelation/mechanical properties of the hydrogels and the two mixing approaches.

Results

4.1 Chemistry

4.1.1 N-hexadecyl-4-(*N,N*-dimethylamino)benzoate

N-hexadecyl-4-(*N,N*-dimethylamino)benzoate was obtained in a 74% yield as a white powder. Melting point: 61-63 ^{o}C. ^{1}H NMR (300 MHz, $CDCl_3$) δ 7.90 (d, *J* = 9.0 Hz 2H), 6.84 (d, *J* = 8.5 Hz, 2H), 4.26 (t, *J* = 6.5 Hz ,2H), 3.06 (s, 6H), 1.80 – 1.68 (m, 2H), 1.50 – 1.12 (m, 26H), 0.88 (t, *J* = 6.4 Hz, 3H). HRMS, calculated for $[C_{25}H_{43}NO_2 + H]^{+}$: 390.3363, measured: 390.3372.

4.1.2 Triflate Precursor: Hexadecyl-4-(*N,N,N*-trimethylamino)benzoate triflate

Hexadecyl-4-(*N,N,N*-timethylamino) benzoate triflate was obtained in a 98% yield as white fluffy powder. HPLC: Luna C8(2) semi-prep column (97:3 MeCN/AF (0.1M), flow: 8 mL/min: 14.7 min. Melting point: 104-106 ^{o}C. ^{1}H NMR (300 MHz, $CDCl_3$) δ 8.25 (d, *J* = 8.6 Hz, 2H), 7.92 (d, *J* = 8.7 Hz, 2H), 4.34 (t, *J* = 6.7 Hz, 2H), 3.79 (s, 9H), 1.87 – 1.68 (m, 2H), 1.49 – 1.13 (m, 26H), 0.87 (t, *J* = 6.4 Hz, 3H). HRMS, calculated for $[C_{26}H_{46}O_2N]^{+}$: 404.3529, measured: 404.3520. Analytical HPLC retention time (Rt) (Shimadzu C18 (50x4.6 mm, 5 μm), 95/5 (MeCN/AF (0.1M), 1.5 mL/min) = 14.7 min (**Figure 4.1)**

4.1.3 HFB Standard: Hexadecyl-4-fluorobenzoate

Hexadecyl-4-fluorobenzoate was obtained in an 86% yield as a white powder. HPLC: Luna C18 analytical column (99:1 MeCN/AF (0.1M), flow: 4 ml/min): 6.01 min. Melting point: 43-44 ^{o}C. ^{1}H NMR (300 MHz, $CDCl_3$) δ 8.06 (m, 2H), 7.10 (m, 2H), 4.30 (t, *J* = 6.7 Hz, 2H), 1.82 – 1.70 (m, 2H), 1.48 – 1.20 (m, 26H), 0.88 (t, *J* = 6.5 Hz, 3H). HRMS, calculated for $[C_{23}H_{38}O_2F]^{+}$: 365.2850, measured: 365.2851. Analytical HPLC retention time

(Rt) (Shimadzu C18 (50x4.6 mm, 5 μm), 95/5 (MeCN/AF (0.1M), 1.5 mL/min) = 6.76 min (**Figure 4.2)**

4.2 Radiochemistry

4.2.1 C18 Seppak Experiments

To remove any unreacted [^{18}F] fluoride, other salts and DMSO prior to going to semi-prep HPLC purification, the reaction mixture was passed through a C18 Seppak light cartridge. The amount of solvent needed to elute HFB (>90%) had to be tested and the following results were obtained:

Table 4.1. Elution experiment 1: 0.5mg HFB and MeCN used as the eluting solvent (collected 0.5 mL fractions).

Vial	Solvent	Volume	HPLC	% of HFB eluted
1	H_2O	1 mL	-------	-------
2	H_2O	0.5 mL	-------	-------
3	H_2O	0.5 mL	-------	-------
4	H_2O	0.5 mL	-------	-------
5	H_2O	0.5 mL	-------	-------
6	MeCN	0.5 mL	HFB	0.5% (0.5%)
7	MeCN	0.5 mL	HFB	27% (27.5%)
8	MeCN	0.5 mL	HFB	61% (88.5%)
9	MeCN	0.5 mL	HFB	10% (98.5%)
10	MeCN	0.5 mL	HFB	1.5% (100%)*

***Percentages represent total amount of HFB eluted from the C18 Seppak light cartridge**

Table 4.2. Elution experiment 2: 0.5mg HFB and MeCN used as the eluting solvent (collected 1 mL fractions).

Vial	Solvent	Volume	HPLC	% of HFB eluted
1	H_2O	5 mL	-------	-------
2	H_2O	5 mL	-------	-------
3	H_2O	5 mL	-------	-------
4	H_2O	5 mL	-------	-------
5	MeCN	1 mL	HFB	9% (9%)
6	MeCN	1 mL	HFB	78% (87%)
7	MeCN	1 mL	HFB	13% (100%)*
8	MeCN	1 mL	HFB	-------

***Percentages represent total amount of HFB eluted from the C18 Seppak light cartridge**

Table 4.3. Elution experiment 2: 0.5mg HFB and MeOH used as the eluting solvent (collected 0.5 mL fractions).

Vial	Solvent	Volume	HPLC	% of HFB eluted
1	H_2O	5 mL	-------	-------
2	H_2O	5 mL	-------	-------
3	H_2O	5 mL	-------	-------
4	H_2O	5 mL	-------	-------
5	MeOH	0.5 mL	HFB	5% (5%)
6	MeOH	0.5 mL	HFB	44% (49%)
7	MeOH	0.5 mL	HFB	31% (80%)
8	MeOH	0.5 mL	HFB	12% (92%)
9	MeOH	0.5 mL	HFB	8% (100%)*
10	MeOH	0.5 mL	HFB	-------

***Percentages represent total amount of HFB eluted from the C18 Seppak light cartridge**

From these experiments, it was concluded that the majority of HFB (>90%) could be eluted from a C18 light cartridge using: 2.0 mL of MeCN or 2.5 mL of MeOH.

4.2.2 Radiochemical Results

For a typical 1hr beam, approximately 1000-1200 mCi was produced and delivered to the dispensing hot cell. Once the activity was measured, this was transferred to the Synthera® ASU by means of suction *via* the modules vacuum pump. For test runs of [^{18}F]HFB, shorter beams or rinses were used to limit the amount of radioactivity, however, for exosome and hydrogel experiments, longer beams with more radioactivity were required. Following delivery of the radioactivity to the Synthera® module, the total synthesis time was approximately 40 min, followed by a 20 min HPLC purification**.** The synthesis of [^{18}F]HFB took place in one reactor with a 20 minute fluorination step at 100˚C, to produce [^{18}F]HFB in a 34% +/- 9%radiochemical yield (RCY, decay-corrected) (~ 330 mCi starting from 1200 mCi). Following semi-prep HPLC (Retention time (Rt) of [^{18}F]HFB = 18-20 min), the solvent was evaporated using a heating block, a vacuum pump and nitrogen gas flow. This step took approximately 10 – 15 minutes to completely evaporate all the solvent. Product reformulation was completed in approximately 5 minutes, to give a total synthesis time from end of beam (EOB) of 1 h 20 minutes, plus another 10 min for quality control by HPLC analysis.

4.2.3 Optimization of fluorination conditions

Four different fluorination conditions were tested with the goal of maximizing the yield of [^{18}F]HFB while minimizing the production of radioactive by-products. The four conditions tested were: 100˚C for 30 min, 140˚C for 30 mins, 80˚C for 30 min and 100˚C for 20 min to give the following results:

Table 4.4 Effect of fluorination conditions on [^{18}F]HFB purity and yield.

Condition	Mass of precursor (mg)	Fluorination Temperature (˚C)/Time (min)	RCY (Decay-Corrected)	Radiochemical Purity (No semi-prep HPLC)	Purity corrected yield
A	3	100/30	43.3%	83%	36%
B	3	140/30	36.7%	50%	18%
C	3	80/30	6.79%	95%	6.45%
D	3	100/20	33%	97%	32%

Through increasing the fluorination temperature to 140˚C, this produced a higher proportion of radioactive by-product (**Figure 4.3 B)** than when fluorination took place at 100˚C (**Figure 4.3 D)**. Dropping the fluorination temperature to 80˚C produced highly pure [^{18}F]HFB, however, in a very low yield (6.45%) (**Figure 4.3 C**). 100˚C produced the optimal ratio of radiochemical purity and yield.

4.2.4 Optimization of semi-prep HPLC conditions

Initial semi-prep HPLC conditions were optimized using a Luna C8(2) column and a mobile phase of 97:3 (MeCN/AF (0.1M) at a flow of 10 mL/min to give a retention time of 8 minutes for [^{18}F]HFB. However, it was noticed that a non-radioactive impurity was co-eluting with the [^{18}F]HFB radioactivity peak. This peak was identified as a non-radioactive impurity and not cold HFB on analytical HPLC using a C18 column, where it was observed that there was a UV peak (254 nm) associated to [^{18}F]HFB, followed by a large UV peak directly after (**Figure 4.4).** This second UV peak was lowering the chemical purity of the final formulation of [^{18}F]HFB. The C8(2) semi-prep column was substituted for a C18

column and the mobile phase switched to 95:5 (MeCN/AF (0.1M) at a flow of 10 mL/min to obtain better resolution between the peaks (**Figure 4.5).** With these conditions, [^{18}F]HFB has a Rt of 18 min, along with higher chemical purity (>95%).

4.2.5 Gas Chromatography of final formulation of [^{18}F]HFB

The results of the GC analysis of the evaporation experiments completed using HPLC solvent and saline to reformulate are summarized as follows:

Table 4.5 Gas chromatography results of first evaporation experiments: 2 min evaporation.

Sample	Volume of solvent (mL) (95/5 MeCN/AF (0.1M)	Evaporation Temperature (˚C)	Evaporation time (dryness + additional time) (min)	PPM of MeCN
1	15	120	8 + 2	1207
2	15	120	9 + 2	850
3	15	120	10 + 2	132
4	15	120	10 + 2	176

Table 4.6. Gas chromatography results of second evaporation experiments: 2.5 min evaporation.

Sample	Volume of solvent (mL) (95/5 MeCN/AF (0.1M)	Evaporation Temperature (˚C)	Evaporation time (dryness + additional time) (min)	PPM of MeCN
1	15	120	8 + 2.5	20
2	15	120	9 + 2.5	0
3	15	120	10 + 2.5	0

The addition of an extra 2.5 minutes after dryness in the second experiments (**Table 4.6)** as compared to 2 minutes of additional evaporation in the first experiments (**Table 4.5)**

drastically reduced the ppm of MeCN in the final formulation from an average of 591.25 ppm to 6.66 ppm.

4.2.6 Quality Control

Figure 4.6 demonstrates a typical analytical HPLC obtained for the final formulation of [^{18}F]HFB**.** The identity of [^{18}F]HFB was confirmed by a co-injection of the final formulation with the cold standard (**Figure 4.7)**. The chemical and radiochemical purity were consistently greater than 98% (after optimization of semi-prep HPLC conditions). Due to the setup of the HPLC, the sample flows first through the radiation detector, followed by the UV detector, resulting in a small delay between the radiation and UV peak times. The molar activity ranged from 46 – 272 mCi/μmol. The amount of residual MeCN in the final formulation was consistently below the accepted limit of 410 ppm.

4.2.7 Exosome Experiments

4.2.7.1 Exosome Exclusive Spin Columns

To remove unbound [^{18}F]HFB from labeled exosomes, the first strategy that was implemented was the use of exosome exclusive spin columns. The results were the following:

Table 4.7. Radioactivity in eluate and remaining on spin column of exosome exclusive spin column tests.

Centrifugation force/time	Activity in eluate (μCi)	Activity remaining on spin column (μCi)
750 x g / 2 min	98 (98%)	2 (2%)
700 x g / 1 min	105 (88%)	15 (12%)
500 x g / 1 min	90 (84%)	17 (16%)

The majority of the radioactivity eluted through the column, while only a small fraction remained on the exosome exclusive spin columns, regardless of the centrifugation conditions. Reducing the force from 700 x g to 500 x g resulted in a small increase of radioactivity remaining on the column.

4.2.7.2 PD-10 Column Experiments

The elution profiles for [^{18}F]HFB in different reformulation conditions are summarized in the following figures: 10% DMSO/PSB **(Figure 4.8.1)**, 5% DMSO/PSB **(Figure 4.8.2)** and 10% DMSO/PBS + 0.1% Tween **(Figure 4.8.3 and 4.8.4).** Briefly, the majority of [^{18}F]HFB was eluted in the solvent front (0.5 mL – 1.0 mL). The elution volume of [^{18}F]HFB through the PD-10 column was slightly increased to 1.0 mL – 2.0 mL with the addition of 0.1% Tween in the final formulation and when it was used as the elution solvent (**Figure 4.8.3-4)**.

4.2.7.3 Exosome Labeling

As shown in **Table 3.1** various radiolabeling conditions were tested for exosomes. The results of these experiments are summarized in **Tables 4.9.1 - 7.** The data is decay corrected and the percentages represented are either a percent of activity remaining from the starting activity, or from the previous step in the experiment. There was a large proportion of [^{18}F]HFB that stuck to the tubes, while this was slightly reduced with the addition of BSA. The effect of [^{18}F]HFB sticking to the incubation and centrifugation tubes was further increased when both of these were completed at 4˚C. Regardless of the incubation temperature or centrifugation conditions, there was no difference in the amount of radioactivity in the resuspended exosome sample and the [^{18}F]HFB controls. In certain experiments (**Table 4.9.5)**, there was more radioactivity in the resuspended pellet from the control samples as compared to the exosome samples. Furthermore, there was no difference

in sticking of [^{18}F]HFB between the regular Eppendorf tubes and the low retention Eppendorf tubes (**Table 4.9.3)**.

4.2.7.4 ITLC Analysis

Figure 4.10 A presents the ITLC analysis of a 34 µL sample of exosomes incubated with 50 µL of [^{18}F]HFB, centrifuged at 200,000 x g for 4 hours and resuspended in 60 µL of PBS and **Figure 4.10 B** is the [^{18}F]HFB control for the same conditions. The retention factor (Rf) of [^{18}F]HFB is approximately 0.83 and there was no difference in retention time, or appearance of a second radioactive peak in the exosome sample as compared to the [^{18}F]HFB control. The same results were obtained for all the labeling conditions.

4.2.8 Hydrogel Experiments

4.2.8.1 Effect of 10% DMSO/Saline on hydrogel rheological and mechanical properties (Work completed by Yasaman Alinejad).

First, to verify that labeling would not strongly impact gel rheological and mechanical properties, the effect of DMSO on these factors was tested. The effect of adding [^{18}F]HFB using approach 1 on the rheological and mechanical properties of hydrogel is summarized in **Figure 4.11.1**. In this method, chitosan was first mixed with DMSO/water (at 0.5%, 1% and 2% v/v) followed by addition of the GA. As seen in **Figure 4.11.1A,** addition of DMSO did not have a great influence on the kinetics of gelation of the hydrogels at 37° C. However, increasing the concentration of DMSO (1% and 2% v/v) had a significant effect on the storage modulus of the hydrogels (G'), as measured after 30 min of gelation (**Figure 4.11.1B**). A similar trend was obtained with approach 2 (chitosan mixed with DMSO/water (0.5%, 1% and 2% v/v), prior to addition of the gelation agent (**Figure 4.11.2**), however, the difference was not large enough to be significant. For the mechanical properties after 24h gelation at 37˚C, the compression tests showed a slight decrease in the secant modulus with

increasing concentration of DMSO for approach 2 (**Figure 4.11.3),** whereas there was a minimal change in the secant modulus for approach 1 (**Figure 4.11.4**) although no significant differences were observed for either approach.

From these experiments, it was concluded that regardless of the method of mixing, DMSO did not present a considerable effect on the rheological properties of the hydrogels during gelation at 37˚C, however, a significant difference in the storage modulus was observed for increasing concentrations of DMSO (1% and 2%). Therefore, it was recommended to formulate the hydrogels with the lowest concentration of DMSO possible (0.5% v/v) as to limit the changes in the mechanical properties of the final hydrogel and for future studies involving cells that do not tolerate higher concentrations of DMSO.

4.2.8.2 Hydrogel radiolabeling using [^{18}F]HFB

During the preparation of the labeled hydrogels, approach 1 resulted in an average loss of radioactivity during mixing of 41.2%, whereas approach 2 had an average loss of radioactivity during mixing of 16.2% (**Figure 4.12.1).** As seen in **Figures 4.12.2-5**, a similar trend is observed in terms of labeling stability, regardless of the approach used to prepare the radiolabeled hydrogels for both the transwell experiments and gel molds. After 8 hours, over 90% of the radioactivity remained in the hydrogel, with a slight efflux of [^{18}F]HFB observed, corresponding to a maximum loss of 9%. Due to the higher losses of radioactivity during mixing seen with approach 1, approach 2 was solely used going forward. Approach 2 was repeated with a larger sample size (n =3) for the transwell experiments and gel molds. The transwell experiments involving the same gel for all time points and gel molds displayed an identical trend as the previous experiments with over 90% labeling stability after 8 hours submerged in saline (**Figure 4.12.6-7).**

4.2.8.3 Hydrogel radiolabeling using F-18

Only approach 2 was utilized to prepare the radiolabeled hydrogels using [^{18}F]F^{-}. As observed in **Figure 4.13.1**, the losses during mixing were very minimal with a 5.5% and 5.1% for the transwell gels and molds, respectively. In terms of radiolabeling stability, **Figure 4.13.2** demonstrates that after 5 mins, only 26% of the initial F-18 remains in the gel with the rest in the saline rinse. After 1 hour, less than 10% of the F-18 was found in the gel and finally, after 6 hours, only 3% of the starting F-18 remained in the hydrogel. A similar trend was observed for the gel mold experiments, where after 5 mins 39% of the starting F-18 remained in the gel, only 3% of starting F-18 remained in the gel after 1 hour, while 1% of the radioactivity remained in the hydrogel after 4 hours (**Figure 4.13.3**).

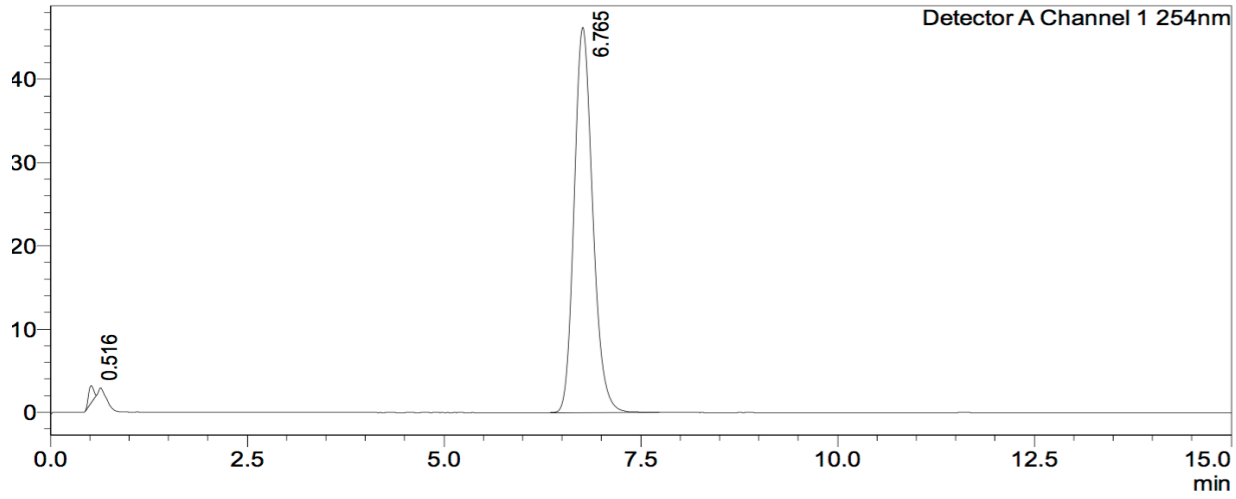

Figure 4.1. Analytical HPLC of the HFB standard ((Shimadzu C18 (50x4.6 mm, 5 µm), 95/5 (MeCN/AF (0.1M), 1.5 mL/min).

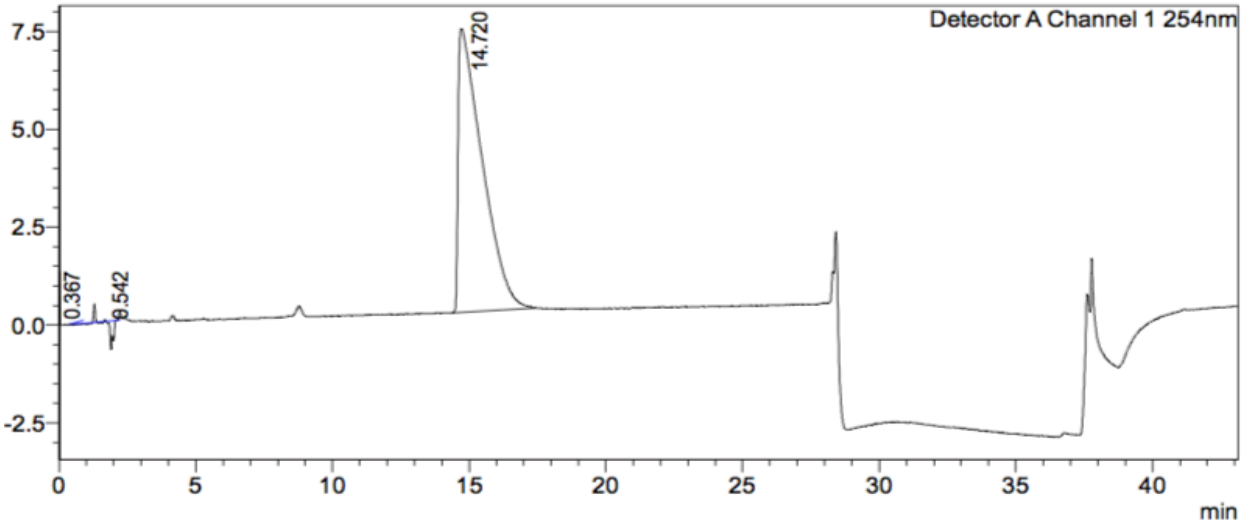

Figure 4.2. Analytical HPLC of the precursor ((Shimadzu C18 (50x4.6 mm, 5 µm), 95/5 (MeCN/AF (0.1M), 1.5 mL/min) with solvent switch to 100% MeCN at 28 min.

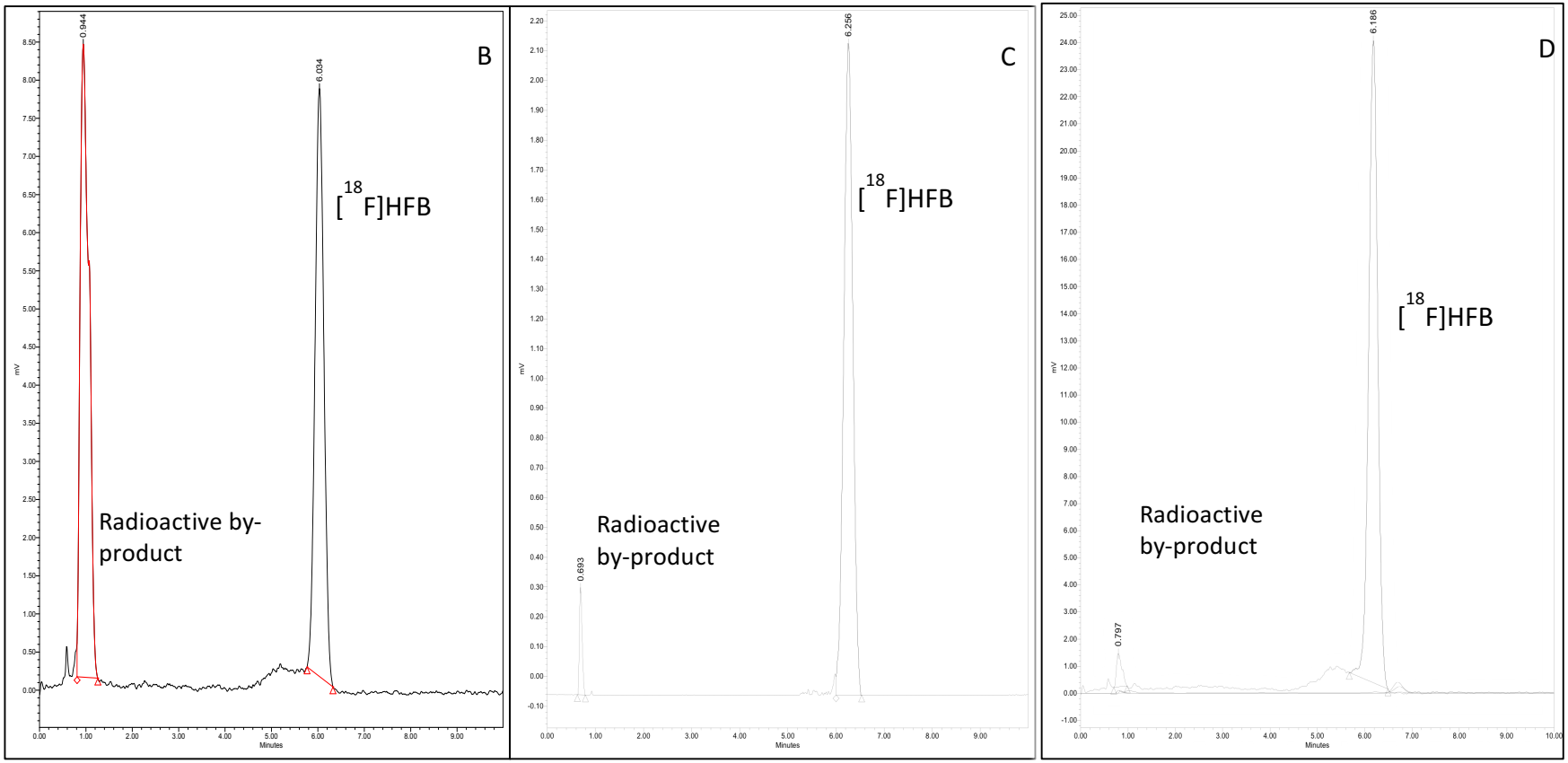

Figure 4.3. Analytical Rad HPLC of the reaction mixtures (Luna C18, 99:1 (MeCN/AF (0.1M) 4 mL/min): **B)** 140˚C/30 min, **C)** 80˚C/30min and **D)** 100˚C/20 min.

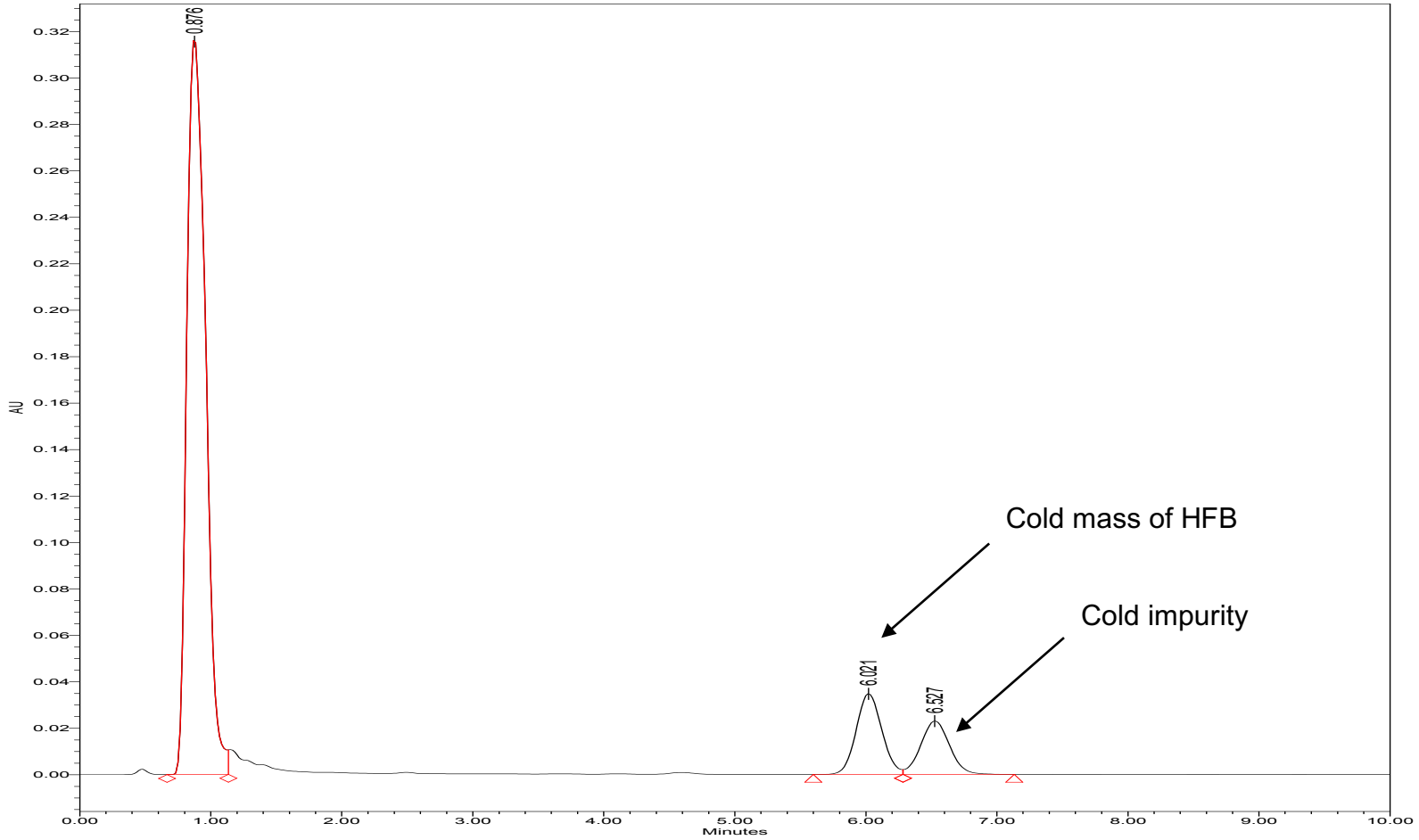

Figure 4.4. Analytical HPLC at 254 nm (Luna C18 99/1 (MeCN/AF (0.1M), 4 mL/min) of the final formulation of [18F]HFB prior to optimizing semi-prep HPLC purification conditions. A non-radioactive impurity was co-eluting with the radioactive peak of [^{18}F]HFB during semi-prep HPLC, while separation of these two peaks was seen on analytical HPLC.

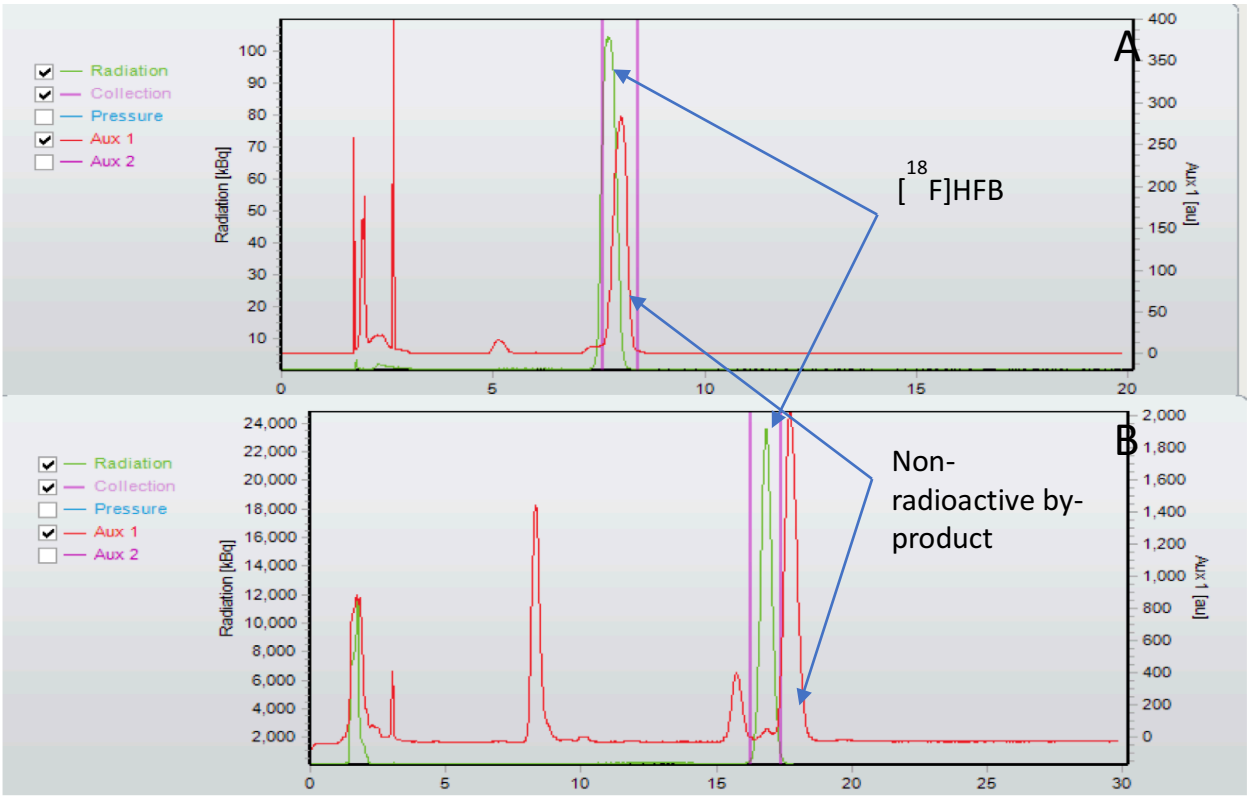

Figure 4.5. Semi-prep HPLC optimization. **A**) C8(2) column (97:3 MeCN/AF (0.1M), 10 mL/min) resulted in co elution of [^{18}F]HFB (Rt = 8 min) with a non-radioactive by-product. **B**) Resolution was improved by switching to a C18 column (95/5 MeCN/AF (0.1M), 10 mL/min) ([^{18}F]HFB Rt = 18 min)

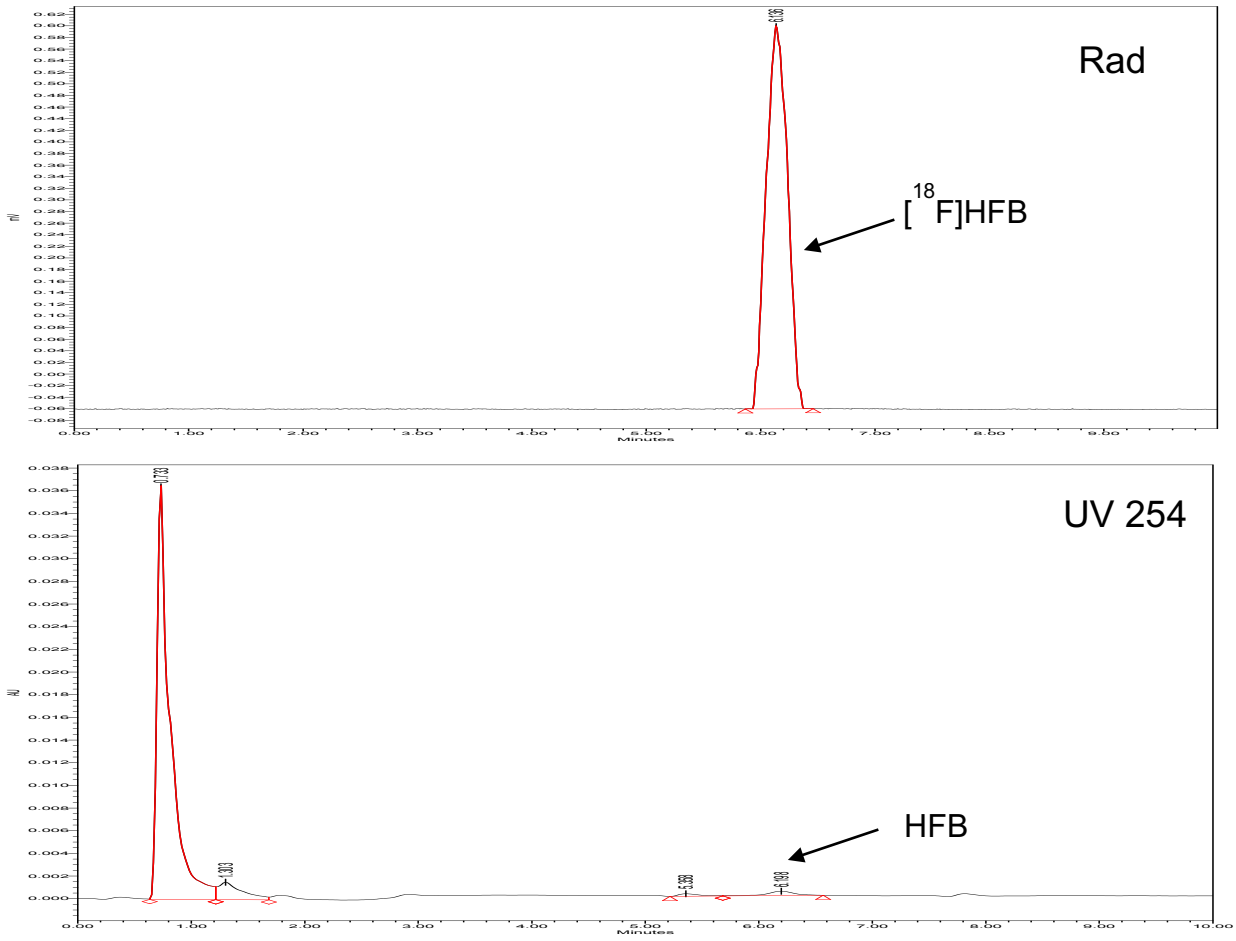

Figure 4.6. Analytical HPLC at 254 nm (Luna C18 99/1 (MeCN/AF (0.1M), 4 mL/min) of the final formulation of [18F]HFB after optimizing semi-prep HPLC purification conditions.

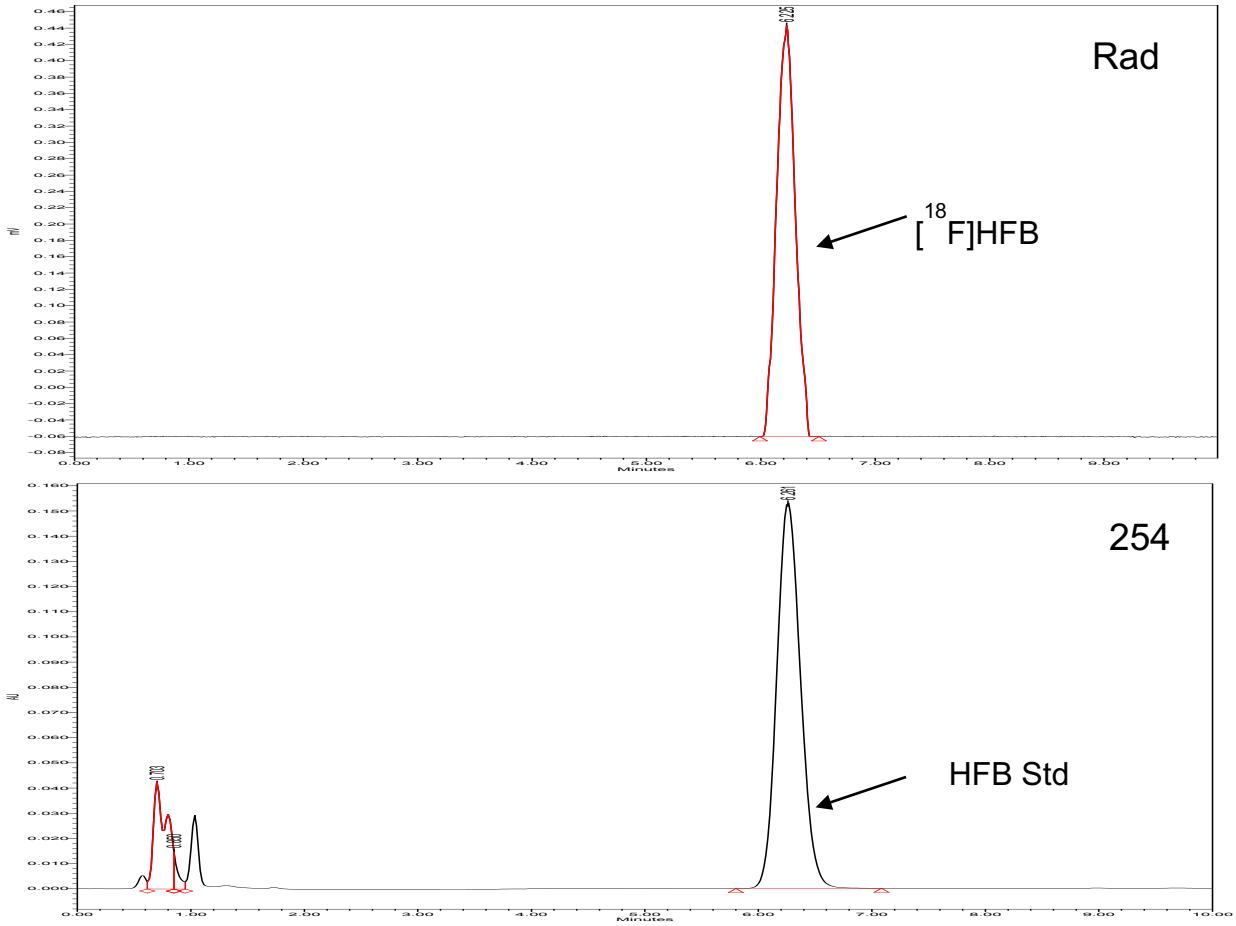

Figure 4.7. Analytical HPLC at 254 nm (Luna C18 99/1 (MeCN/AF (0.1M), 4 mL/min) of the final formulation of [18F]HFB co-injected with HFB standard.

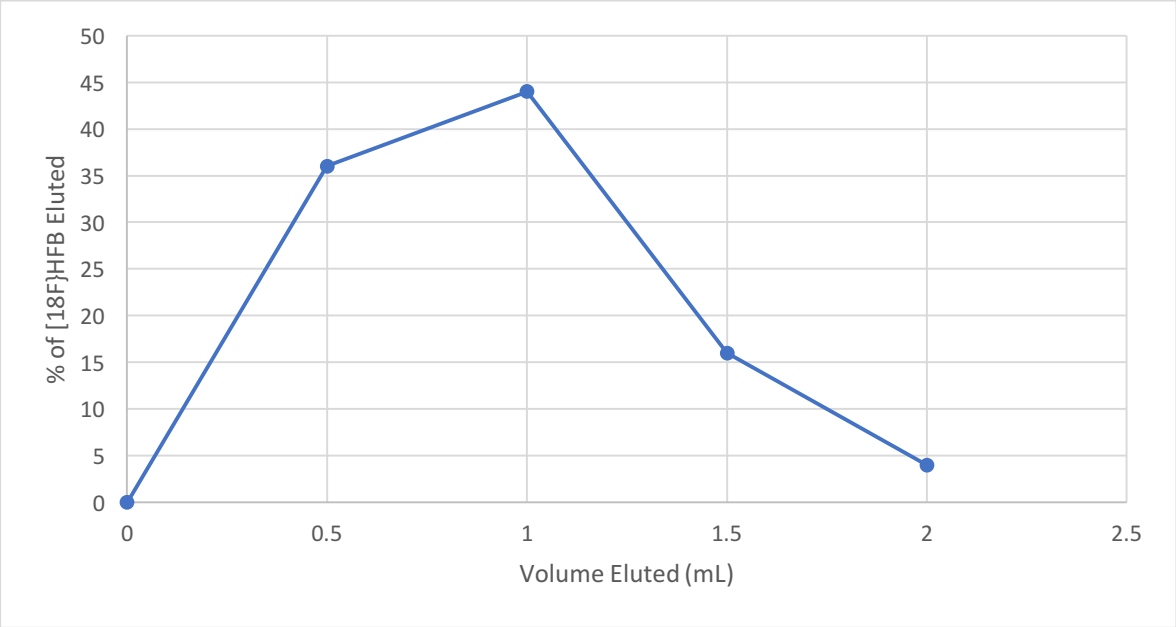

Figure 4.8.1. Elution profile of 1 mL [^{18}F]HFB in 10% DMSO/Saline loaded onto a PD-10 column and eluted using PBS.

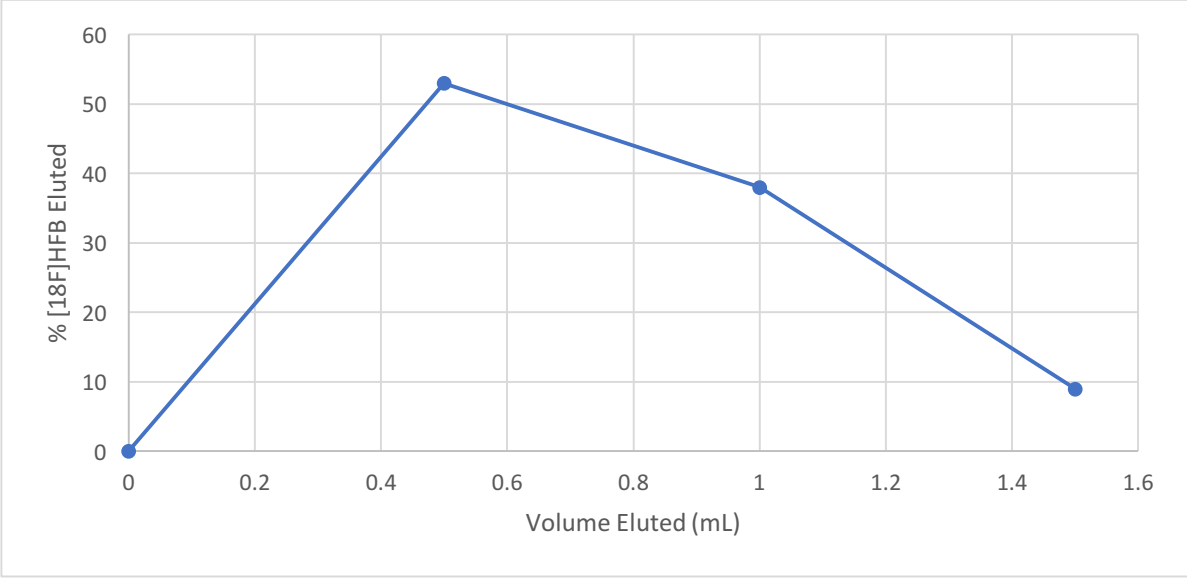

Figure 4.8.2. Elution profile of 1 mL [^{18}F]HFB in 5% DMSO/Saline loaded onto a PD-10 column and eluted using PBS.

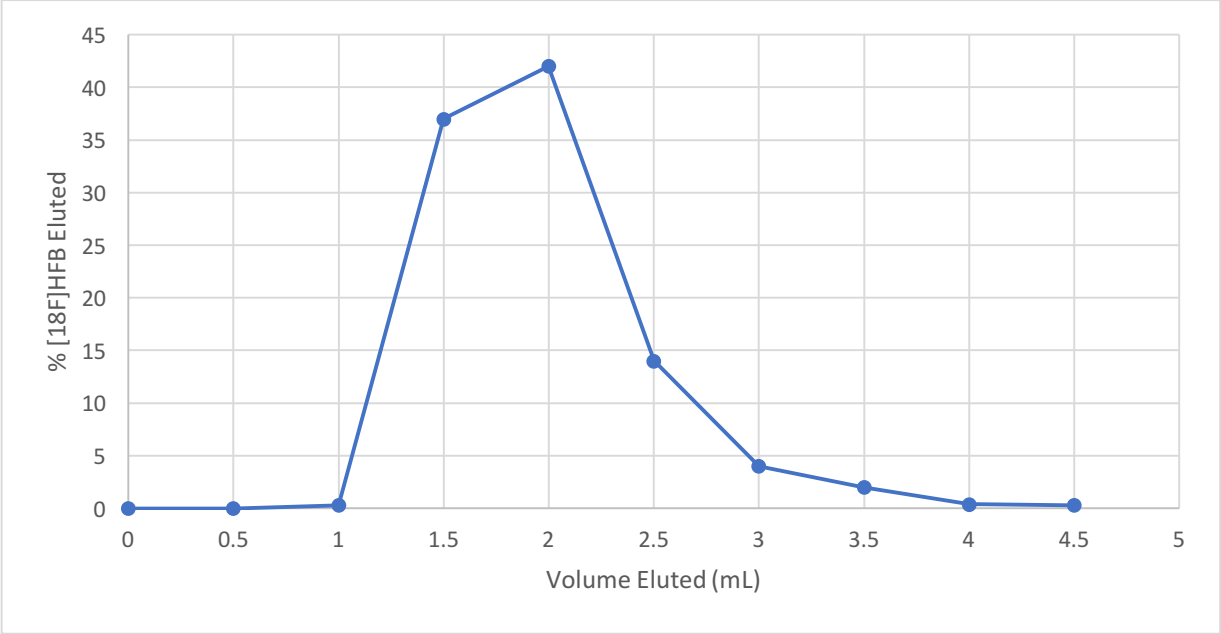

Figure 4.8.3. Elution profile of 1 mL [^{18}F]HFB in 10% DMSO/PBS + 0.1% Tween loaded onto a PD-10 column and eluted using PBS.

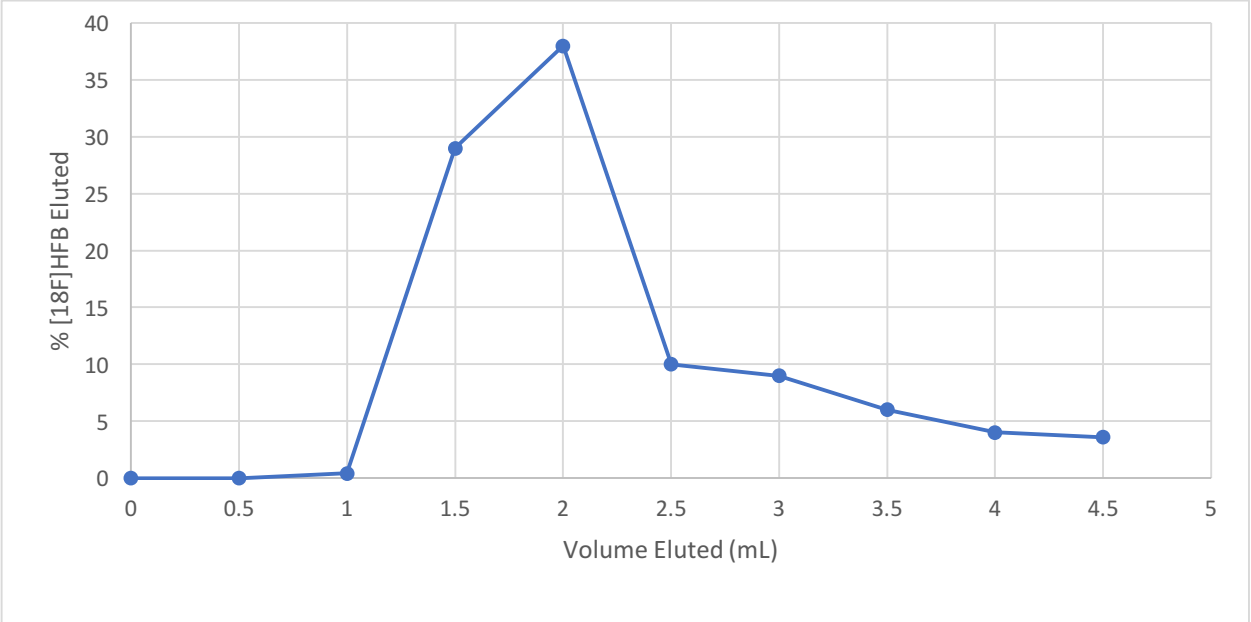

Figure 4.8.4. Elution profile of 1 mL [^{18}F]HFB in 10% DMSO/PBS + 0.1% Tween loaded onto a PD-10 column and eluted using PBS + 0.1% Tween.

Table 4.9.1 Exosome radiolabeling results from 16 Dec 2016 (21,000 x g centrifugation).

			16-Dec-16			21-Dec-16	
			37˚C	RT	4˚C	Control 1 (RT)	Control 3 (RT)
			21,000g/1h/Normal Tube	21,000g/1h/Normal Tube	21,000g/1h/Normal Tube	21,000g/1h/Normal tube	12000rpm/15min/normal
			5.75 mCi start (t = 0)	5.74 mCi start (t = 0)	5.62 mCi start (t = 0)	2.80 mCi Start (t = 0)	2.15 mCi Start (t = 0)
Activity (mCi)	Centrifugation	Supernatant	0.96 (17%)	1.12 (20%)	0.769 (13%)	1.52 (54%)	1.53 (72%)
		Pellet	4.49 (78%)	4.31 (75%)	4.86 (86%)	1.16 (41%)	0.6 (28%)
	Wash	Supernatant	0.1 (2%)	0.076 (1.76%)	0.065 (1.33%)	0.02 (1.7%)	0.03 (5%)
		Pellet	4.29 (95%)	4.16 (96%)	4.64 (95%)	1.13 (97%)	0.54 (90%)
	Resuspension	10 uL (sample)	0.09 (2%)	0.137 (3.29%)	0.125 (2.69%)	0 (0%)	0.002 (0.4%)
		60 uL (tube)	4.29	4.16	4.64	1.02	0.5
			Wash: PBS	Wash: PBS	Wash: PBS	Wash: PBS	Wash: PBS
			Resus: PBS	Resus: PBS	Resus: PBS	Resus: DMSO/PBS	Resus: PBS

Percentages represent either a percentage of the starting activity or pellet from the previous step

Table 4.9.2. Exosome radiolabeling results from 21 Dec 2016 (21,000 x g centrifugation).

			21-Dec-16				
			37˚C	RT	4˚C	Control 1	Control 2
			21,000g/1h/Low RT tube	21,000g/1h/Low RT tube	21,000g/1h/Low RT tube	21,000g/1h/Normal tube	21,000g/1h/Low RT tube
			2.88 mCi Start (t = 0)	2.92 mCi start (t = 0)	2.94 mCi Start (t = 0)	2.80 mCi Start (t = 0)	2.75 mCi Start (t = 0)
			1.74 (60%)	1.61 (55%)	1.45 (49%)	1.52 (54%)	1.28 (46%)
Activity (mCi)	Centrifugation	Supernatant	1.07 (37%)	1.24 (42%)	1.46 (49%)	1.16 (41%)	1.38 (50%)
		Pellet	0.36 (33%)	0.32 (25%)	0.29 (20%)	0.02 (1.7%)	0.167 (12%)
	Wash	Supernatant	0.68 (63%)	0.9 (72%)	1.14 (78%)	1.13 (97%)	1.2 (86%)
		Pellet	0.01 (1.56%)	0.05 (6.25%)	0.015 (1.33%)	0 (0%)	0 (0%)
	Resuspension	10 uL (sample)	0.64	0.8	1.13	1.02	0.98
		60 uL (tube)	Wash: DMSO/PBS	Wash: DMSO/PBS	Wash: DMSO/PBS	Wash: PBS	Wash: DMSO/PBS
			Resus: DMSO/PBS	Resus: DMSO/PBS	Resus: DMSO/PBS	Resus: DMSO/PBS	Resus: DMSO/PBS

Percentages represent either a percentage of the starting activity or pellet from the previous step

Table 4.9.3. Exosome radiolabeling results from 21 Dec 2016 (12,000 rpm centrifugation).

			21-Dec-16			
			37˚C	RT	Control 3	Control 4
			12000rpm/15min/Low RT	12000rpm/15min/Low RT	12000rpm/15min/normal	12000rpm/15min/Low RT
			2.05 mCi start (t = 0)	2.87 mCi Start (t = 0)	2.15 mCi Start (t = 0)	2.20 mCi Start (t = 0)
Activity (mCi)	Centrifugation	Supernatant	1.52 (74%)	2.19 (76%)	1.53 (72%)	1.39 (63%)
		Pellet	0.5 (24%)	0.544 (19%)	0.6 (28%)	0.73 (33%)
	Wash	Supernatant	0.12 (24%)	0.12 (22%)	0.03 (5%)	0.04 (5.4%)
		Pellet	0.32 (64%)	0.479 (88%)	0.54 (90%)	0.68 (93%)
	Resuspension	10 uL (sample)	0 (0%)	0 (0%)	0.002 (0.04%)	0.005 (0.74%)
		60 uL (tube)	0.31	0.4	0.5	0.67
			Wash: DMSO/PBS	Wash: DMSO/PBS	Wash: PBS	Wash: DMSO/PBS
			Resus: PBS	Resus: PBS	Resus: PBS	Resus: DMSO/PBS

Percentages represent either a percentage of the starting activity or pellet from the previous step

Table 4.9.4. Exosome radiolabeling results from 22 Dec 2016 (21,000 x g centrifugation).

			22-Dec-16	
			37-Bone	Control-Bone
			21,000g/2h/Low RT tube	21,000g/2h/Low RT tube
			0.520 mCi Start (t = 0)	0.616 mCi Start (t = 0)
Activity (mCi)	Centrifugation	Supernatant	0.155 (29%)	0.02 (3.24%)
		Pellet	0.343 (66%)	0.53 (86%)
	Wash	Supernatant	0.19 (55%)	0.018 (3.39%)
		Pellet	0.114 (33%)	0.49 (92%)
	Resuspension	10 uL (sample)	0 (0%)	0 (0%)
		60 uL (tube)	0.1	0.46
			Wash: DMSO/PBS	Wash: DMSO/PBS
			Resus: PBS	Resus: PBS

Percentages represent either a percentage of the starting activity or pellet from the previous step

Table 4.9.5. Exosome radiolabeling results from 2 Feb 2017 using ultracentrifugation (200,000 x g).

			02-Feb-17					
			37-200g-1h	37-200g-1h-control	37-200g-2h	37-200g-2h-control	37-200g-4h	37-200g-4h-control
			200,000/1h/Low RT tube	200,000/1h/Low RT tube	200,000/2h/Low RT tube	200,000/2h/Low RT tube	200,000/4h/Low RT tube	200,000/4h/Low RT tube
			666 uCi Start (t = 0)	627 uCi Start (t = 0)	913 uCi Start (t = 0)	722 uCi Start (t = 0)	1825 uCi Start (t = 0)	676 uCi Start (t = 0)
Activity (mCi)	Transfer to Ultracentrifuge tube		0.57 (86.4%)	0.49 (78.6%)	0.78 (85%)	0.55 (76.7 %)	1.43 (78%)	0.51 (76.2%)
	Centrifugation	Supernatant	0.013 (2.4%)	0.016 (3.24%)	0.005 (0.63%)	0.07 (1.27 %)	0.06 (0.43%)	0.002 (0.46%)
		UltraTube	0.43 (73.9 %)	0.35 (69.9%)	0.56 (72.3%)	0.38 (69.1%)	0.99 (69%)	0.35 (67.7%)
	Resuspension	60 uL (tube)	0.001 (0.33 %)	0.001 (0.55%)	0.001 (0.33%)	0.002 (0.68%)	0.01 (1.01%)	0.001 (0.51%)

Percentages represent either a percentage of the starting activity or pellet from the previous step

Table 4.9.6. Exosome radiolabeling results from 10 Feb 2017 using ultracentrifugation (200,000 x g).

			10-Feb-17	
			37-200g-4h	37-200g-4h-control
			200,000/4h/Low RT tube	200,000/4h/Low RT tube
			561 uCi Start (t = 0)	585 uCi Start (t = 0)
Activity (mCi)	Transfer to Ultracentrifuge tube	[redacted]	0.5 (89%)	0.45 (76%)
	Centrifugation	Supernatant	0.025 (5%)	0.025 (6%)
		UltraTube	0.39 (77%)	0.4 (90%)
	Resuspension	60 uL (tube)	0.025 (6.45)	0.025 (6%)

Percentages represent either a percentage of the starting activity or pellet from the previous step

Table 4.9.7 Exosome radiolabeling results from 17 Feb 2017 using ultracentrifugation (200,000 x g).

			17-Feb-17	
			37-200g-4h + BSA	37-200g-4h-control + BSA
			200,000/4h/Low RT tube	200,000/4h/Low RT tube
			1074 uCi Start (t = 0)	1094 uCi Start (t = 0)
Activity (mCi)	Transfer to Ultracentrifuge tube	[redacted]	0.8 (74%)	0.83 (76%)
	Centrifugation	Supernatant	0.25 (30%)	0.27 (33%)
		UltraTube	0.16 (19%)	0.16 (19%)
	Resuspension	60 uL (tube)	0.022 (14%)	0.015 (10%)

Percentages represent either a percentage of the starting activity or pellet from the previous step

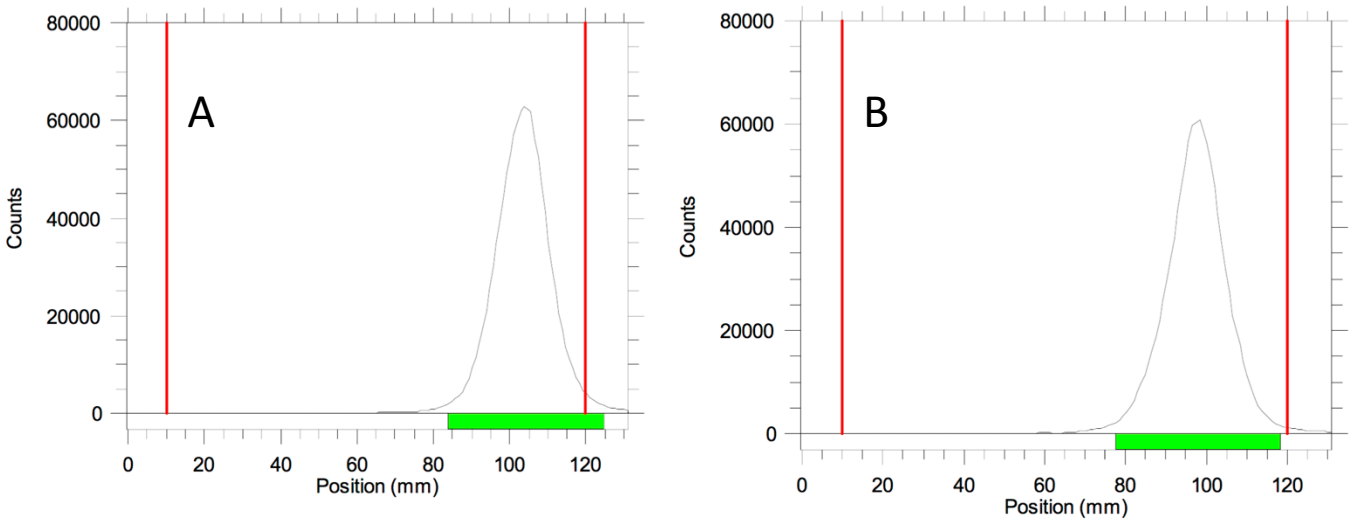

Figure 4.10. ITLC analysis of: A) 34 µl exosomes incubated with 50 µl of [^{18}F]HFB and centrifuged at 200,000 x g for 4 hours and resuspended in 60 µl of PBS. B) [^{18}F]HFB.

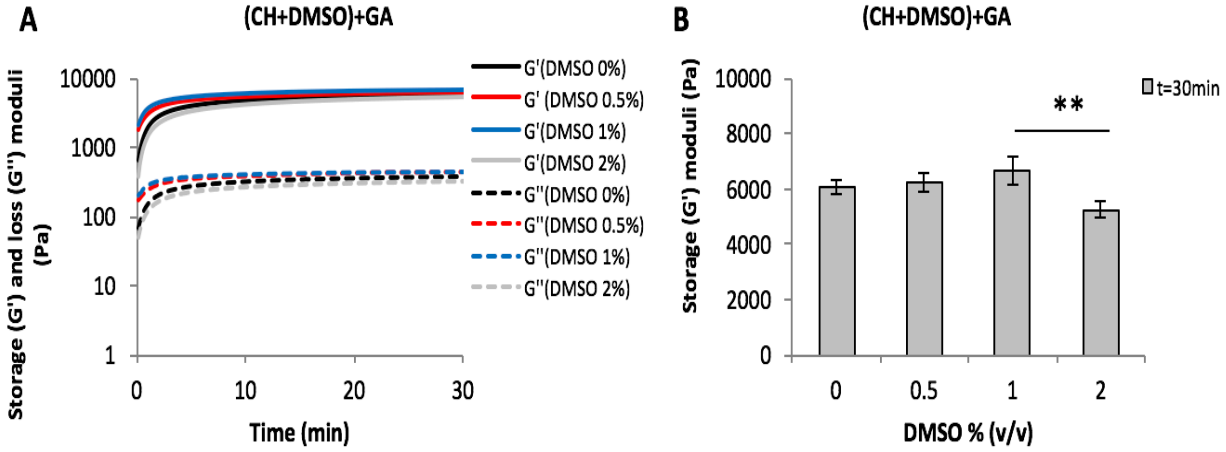

Figure 4.11.1. Effect of 0.5%, 1% and 2% DMSO added first to chitosan followed by addition of the gelation agent (approach 1) on the (A) evolution of storage (G') and loss (G'') moduli of hydrogels during gelation at 37°C *(mean, n=3) and (B) on G' value after 30 min at 37* °C (mean±SD, n=3).

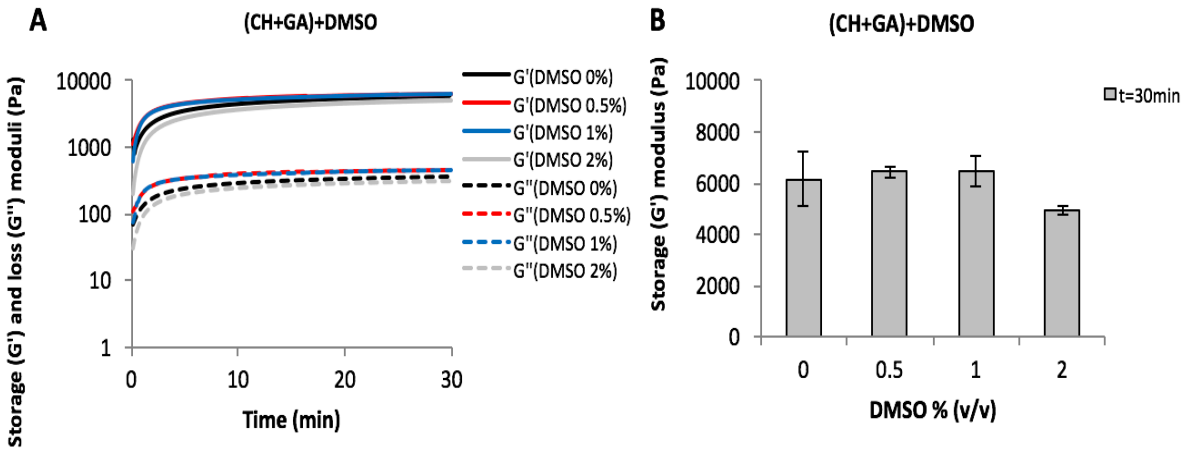

Figure 4.11.2. Effect of 0.5%, 1% and 2% DMSO added following mixing of chitosan and the gelation agent (approach 2) on the (A) evolution of storage (G') and loss (G'') moduli of hydrogels during gelation at 37°C *(mean, n=3) and (B) on G' value after 30 min at 37 °C* (mean±SD, n=3).

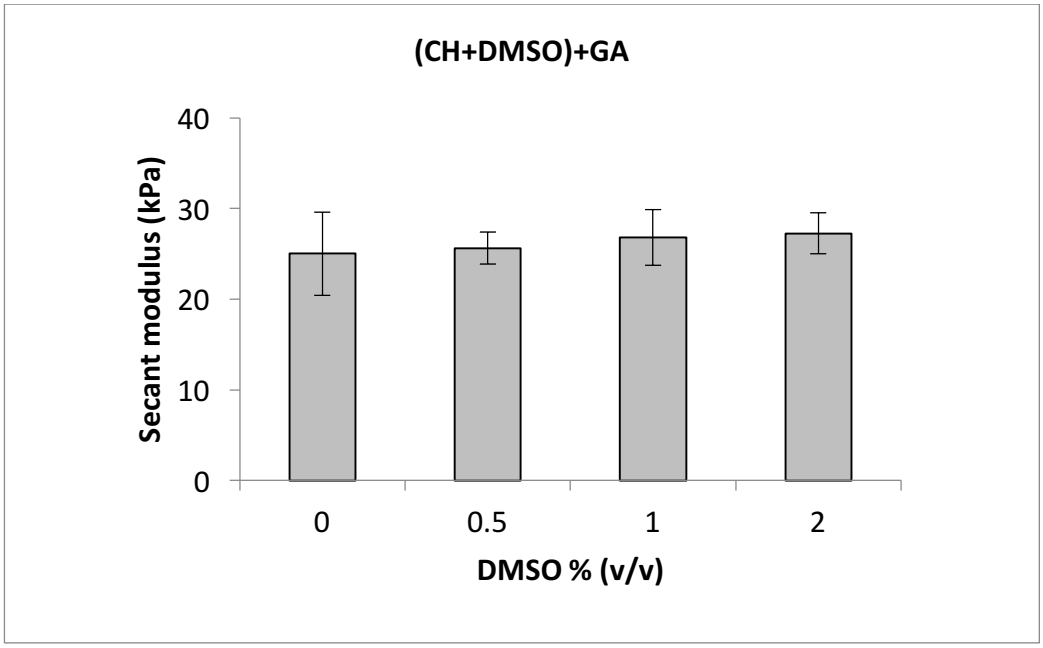

Figure 4.11.3. Effect of 0.5%, 1% and 2% DMSO added first to chitosan followed by addition of the gelation agent (approach 1) on the secant modulus of hydrogels at 50% deformation (mean±SD, n=3).

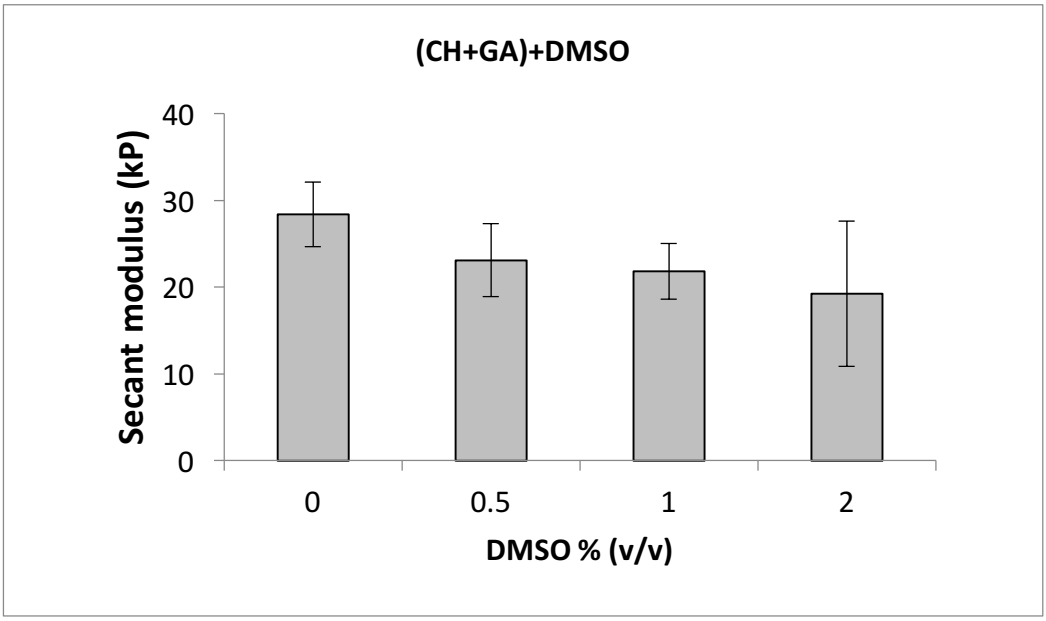

Figure 4.11.4. Effect of 0.5%, 1% and 2% DMSO added following mixing of chitosan and the gelation agent (approach 2) on the on the secant modulus of hydrogels at 50% deformation (mean±SD, n=3).

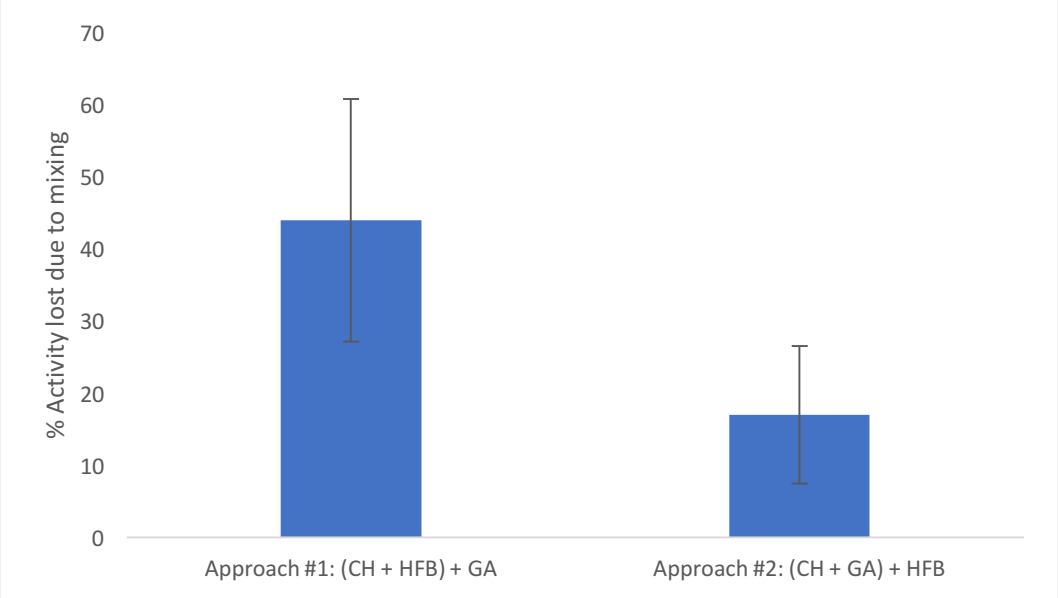

Figure 4.12.1 Percentage of [^{18}F]HFB lost during the preparation of the radiolabeled hydrogels *via* approach 1 (CH +[^{18}F]HFB) + GA and approach 2 (CH + GA) + [^{18}F]HFB (mean±SD, n=5).

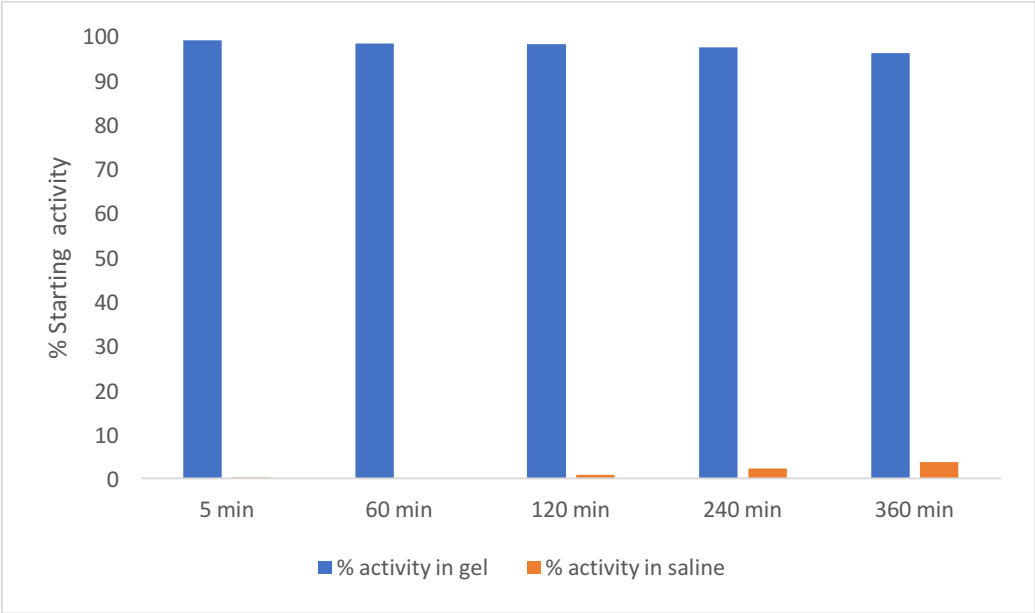

Figure 4.12.2. Percentage of [^{18}F]HFB remaining in labeled hydrogels and saline rinses for approach 1: (CH + [^{18}F]HFB) + GA: transwell experiments (procedure 1) (n = 2).

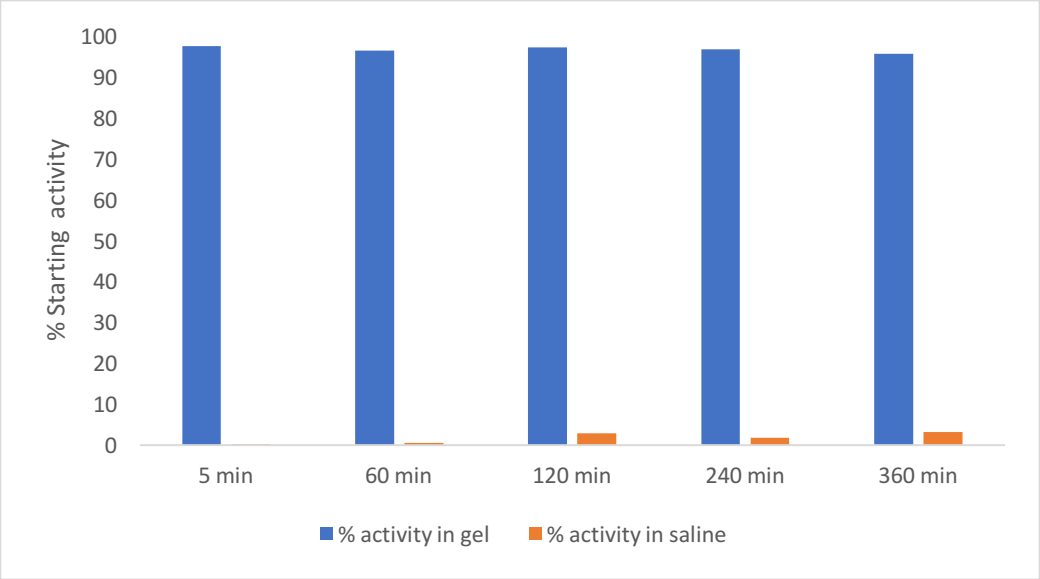

Figure 4.12.3. Percentage of [^{18}F]HFB remaining in labeled hydrogels and saline rinses for approach 2: (CH + GA) + [^{18}F]HFB: transwell experiments (procedure 1) (n = 2).

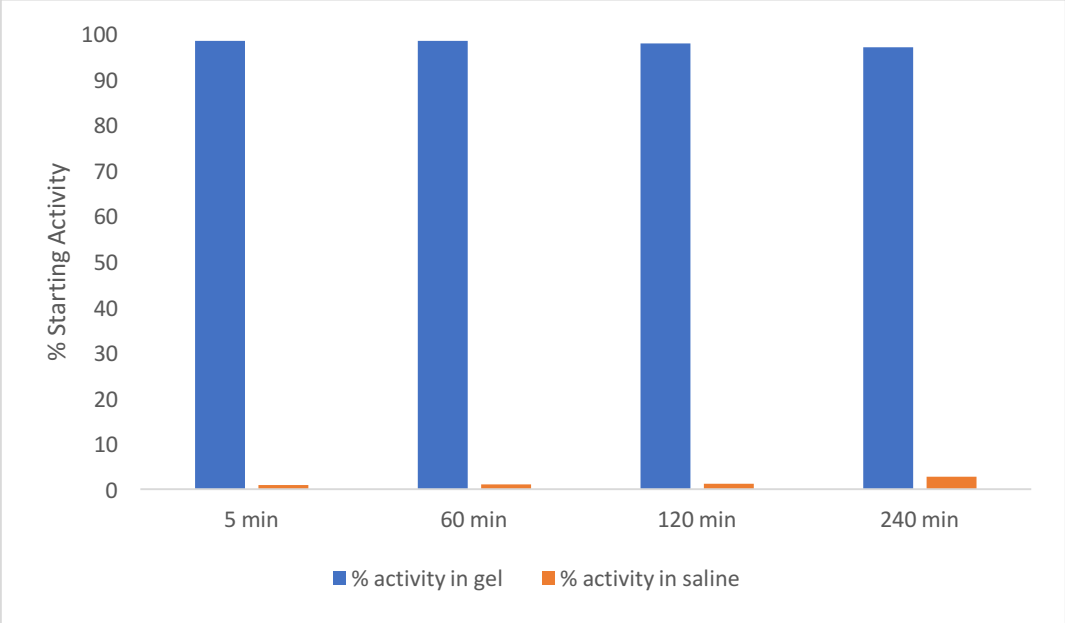

Figure 4.12.4. Percentage of [^{18}F]HFB remaining in labeled hydrogels and saline rinses for approach 1: (CH + [^{18}F]HFB) + GA: gel mold experiments (procedure 2) (n = 2).

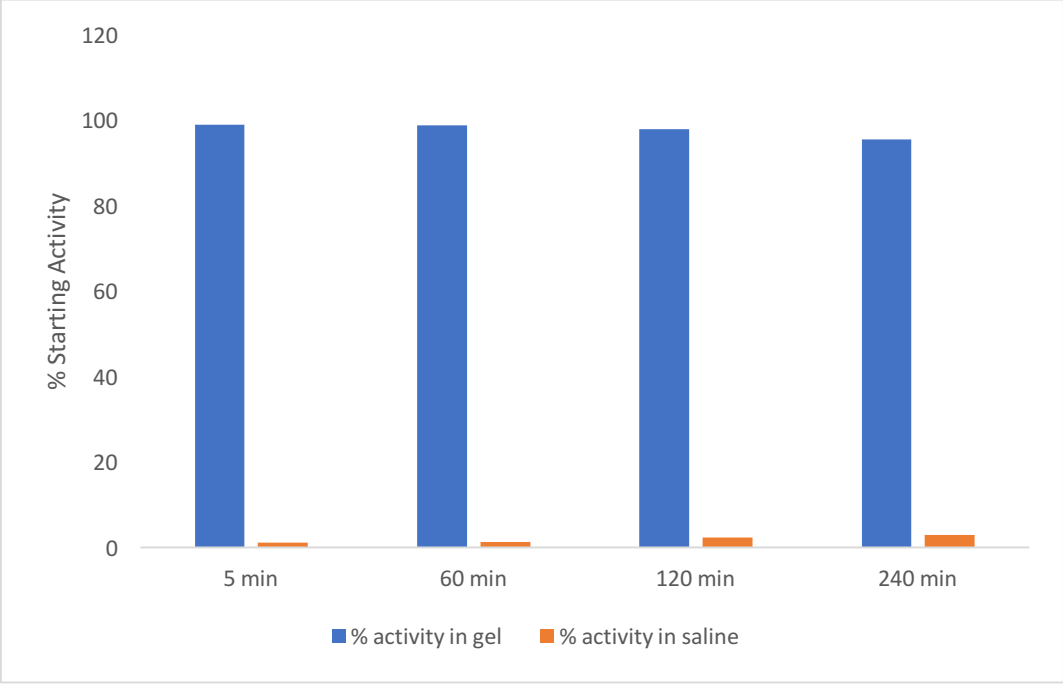

Figure 4.12.5. Percentage of [^{18}F]HFB remaining in labeled hydrogels and saline rinses for approach 2: (CH + GA) + [^{18}F]HFB: gel mold experiments (procedure 2) (n = 2).

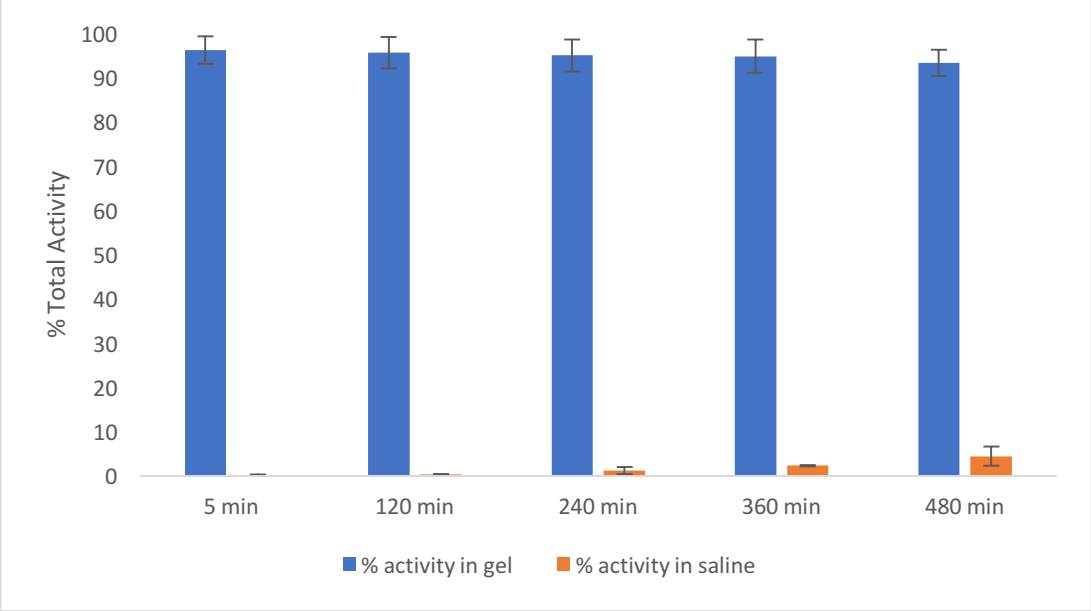

Figure 4.12.6. Percentage of [^{18}F]HFB remaining in labeled hydrogels and saline rinses for approach 2: (CH + GA) + [^{18}F]HFB: transwell experiments (procedure 1), using the same sample for each time point (mean±SD, n=3).

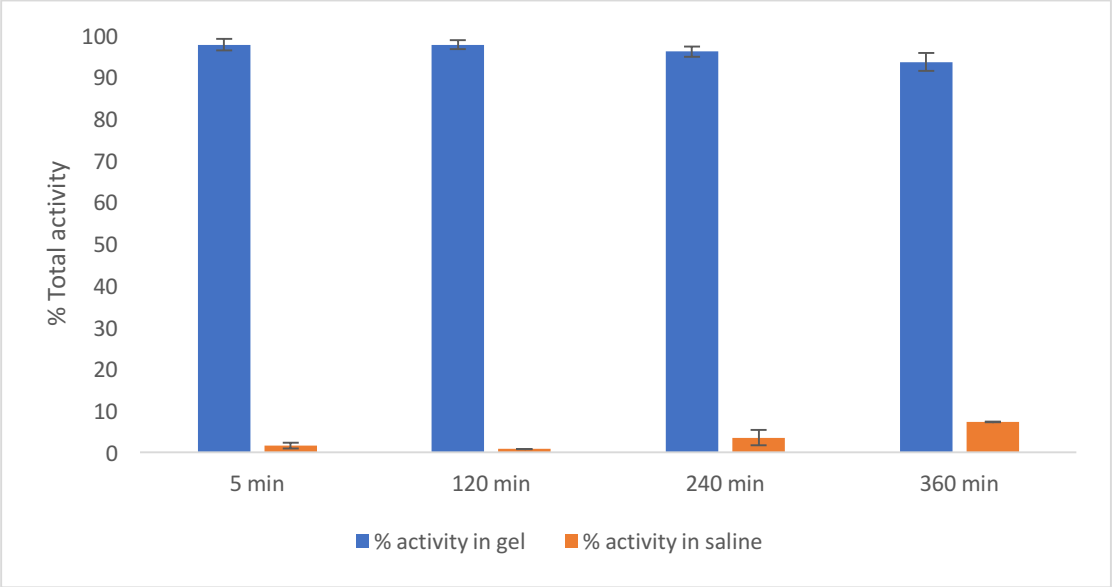

Figure 4.12.7. Percentage of [^{18}F]HFB remaining in labeled hydrogels and saline rinses for approach 2: (CH + GA) + [^{18}F]HFB: gel mold experiments (procedure 2) (mean±SD, n=3).

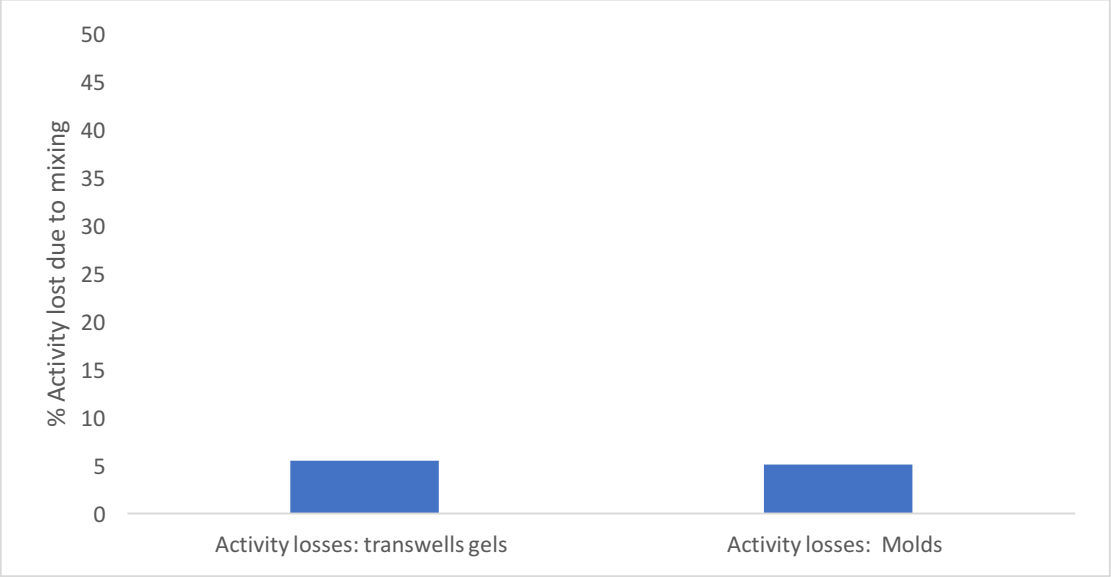

Figure 4.13.1. Percentage of F-18 lost due to mixing (approach 2) for the transwell and mold experiments.

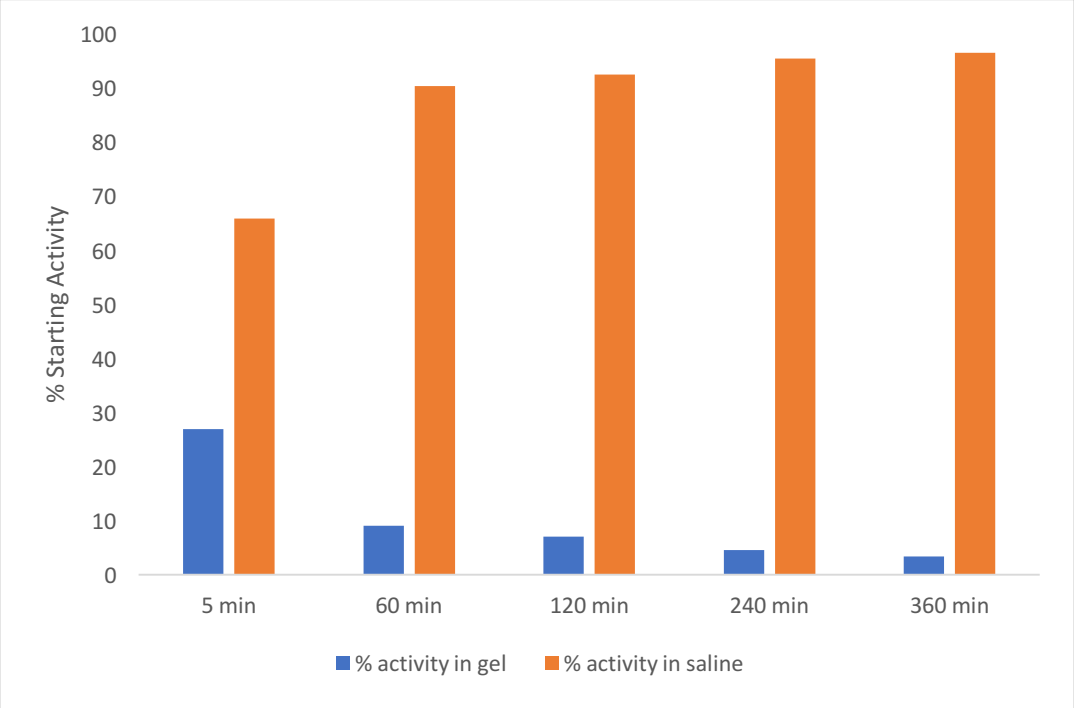

Figure 4.13.2. Percentage of F-18 remaining in labeled hydrogels and saline rinses for approach 2: (CH + GA) + F-18: transwell experiments (procedure 1) (n = 2).

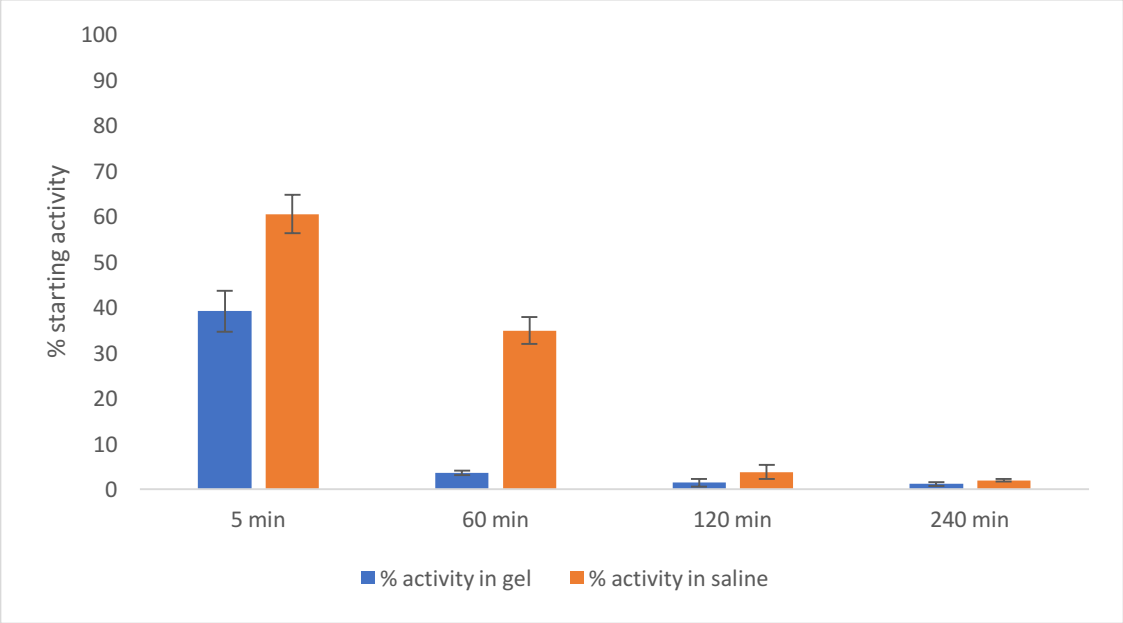

Figure 4.13.3. Percentage of F-18 remaining in labeled hydrogels and saline rinses for approach 2: (CH + GA) + F-18: gel mold experiments (procedure 2) (mean±SD, n=3).

Discussion

5.1 Chemistry

Before proceeding with the radiochemistry work, it was necessary to synthesize both the [^{18}F]HFB precursor as well as the cold HFB as a standard to confirm the identity of the "hot" [^{18}F]HFB product. The synthesis of these compounds was already described in the literature [1]. However, modifications were made to the radiosynthesis and purification to adapt the synthesis to the Synthera platform. The trimethyl ammonium triflate precursor of [^{18}F]HFB (hexadecyl-4-(*N,N,N*-trimethylamino)benzoate triflate) was prepared in two steps; the first step involved the formation of an ester *via* S_N2 substition of a chlorine atom on 4-(*N,N*-dimethylamino)benzoyl chloride by the alcohol group of 1-hexadecanol. The reaction mixture was purified by column chromatography. The final product was re-crystallized using a minimum of hot ethyl acetate for dissolution followed by removal of leftover impurities in the solution at room temperature. The second step was the formation of the trimethyl ammonium substituted triflate salt using methyl triflate. The addition of the methyl group resulted in a quaternary amine which created an ionic bond with the resultant triflate group, turning this into a counter for the leaving group, ideal for [^{18}F]F^- displacement. The cold HFB standard was prepared in a one-step reaction through an S_N2 substitution of a chlorine on 4-fluorobenzoyl chloride by the alcohol group of 1-hexadecanol, and the reaction mixture was purified by flash chromatography. All the compounds were characterized by mass spectrometry and ^{1}H-NMR. They all contained a characteristic multiplet that integrated for 26 protons, belonging to the long lipophilic chain. The purity of the standard was analyzed by analytical HPLC and it was >99% (**Figure 4.1**). The presence of the added methyl group was confirmed by the addition of 3 protons to the singlet at 3.79 ppm, which integrated for a

total of 9 protons. The overall yields for these reactions were all close to 80% and the triflate reaction yield was above 98%.

HPLC conditions were developed for both the cold HFB standard and the precursor to purify the crude reaction mixture and to confirm the identify of hot [^{18}F]HFB. The retention time of cold HFB was 6.0 minutes while the precursor had a longer retention time of 14.7 mins. The large separation time between these two compounds ensure easy purification of the precursor from final labeled compound.

5.2 Radiochemistry

5.2.1 C18 SepPak experiments

When planning the automated radiosynthesis of [^{18}F]HFB using the Synthera® ASU, we wanted to ensure the highest purity of the final product and at the same time increase the lifespan of the semi-prep HPLC column. Since the fluorination reaction was carried out in DMSO - a solvent that can damage HPLC columns overtime and drastically shifts the retention time of compounds – removal of DMSO prior to semi-prep HPLC purification was done *via* C18 SepPak elution. The IFP of the Synthera® contains two ports for cartridges (**Figure 3.5** SepPak positions 1 & 2); the first port is designated for a QMA cartridge for [^{18}F]F$^-$ trapping, and a second is vacant. C18 SepPaks contain long carbon chains that can interact with the long lipophilic chain on [^{18}F]HFB, while unreacted [^{18}F]F$^-$ is eluted through the cartridge. To implement this purification step into the radiosynthesis of [^{18}F]HFB, it was necessary to conduct elution experiments to determine how much volume of solvent will be needed to elute [^{18}F]HFB from the cartridge, following water rinses. The C18 SepPak was initially conditioned and then loaded with HFB dissolved in DMSO and washed with water to remove DMSO and then eluted with either MeCN or MeOH, and the fractions were then

analyzed *via* analytical HPLC. From these experiments, it was determined that over 90% of HFB could be eluted with a smaller volume of MeCN as compared to MeOH. Considering the semi-prep HPLC solvent system consisted of 95% MeCN and AF (0.1M), it was decided that MeCN would be more ideal since this would not change the composition/polarity of the HPLC solvent system. This system was implemented into the automated synthesis of [^{18}F]HFB. However, after the first test run using 2.0 mL of MeCN to elute [^{18}F]HFB, it was noticed that a significant amount of radioactivity remained on the C18 cartridge. The volume of MeCN was then increased to 4 mL, which was sufficient to remove all the radioactivity from the C18 cartridge.

5.2.2 Optimization of the fluorination conditions

Considering the synthesis of [^{18}F]HFB had never been completed using the Synthera® platform, we were interested in optimizing the fluorination conditions to maximize the RCY of [^{18}F]HFB, while minimizing the production of radioactive by-products. The reported fluorination conditions were 95˚C for 20 mins, therefore, we decided to test 4 different conditions: 100˚C/30 mins, 140˚C/30 mins, 80˚C/30 mins and 100˚C for 20 mins. The crude reaction mixture was passed through an activated C18 SepPak and eluted with MeCN, followed by analytical HPLC to determine the radiochemical purity. The fluorination temperature had a drastic impact on the production of a radiochemical by-products that were eluted with the solvent front on analytical HPLC. At 140˚C, the radiochemical purity of [^{18}F]HFB was only 50%, giving a RCY of approximately 36%. When the reaction temperature was reduced to 80˚C, the radiochemical purity was 95%, however, the reaction yield was only 6.45%. The radiochemical purity for 100˚C/30 mins and 100˚C/20 mins differed, with the 20-min reaction time having 97% radiochemical purity as compared to

83% with 30 mins. The RCY for the 30-min reactions was only 4% higher than the 20-min reaction. Since the radiochemical purity was higher for the 20-min reaction, we decided to choose 100˚/20 min for the fluorination conditions. Additionally, the ten-minute difference in the radiosynthesis can make a significant impact for the total synthesis time, which should be kept to a minimum. In the original manual (not automated) radiosynthesis of [^{18}F]HFB by [1], they reached RCYs of 52%, while the highest yield obtained with our automated process (Synthera® ASU) was 45% (decay corrected).

5.2.3 Optimization of semi-prep HPLC conditions

After the first test runs of [^{18}F]HFB, it was noticed that there was a large UV peak that was co-eluting with the radioactive peak of [^{18}F]HFB on semi-prep HPLC **(Figure 4.5)**. At first, we believed that this was a large mass of unlabeled product, however, when the final formulation was analyzed *via* analytical HPLC, the radioactivity peak of [^{18}F]HFB was followed by a large UV peak that did not in fact correspond to the cold mass. The retention times of these two peaks were different enough that they could not be associated to one compound (**Figure 4.4)**. The difference between the semi-prep and analytical HPLC systems was the use of a Luna C8(2) column for semi-prep and a Luna C18 column for analytical HPLC. We then substituted the C8(2) semi-prep column for a C18 semi-prep column as this would likely provide better resolution between the [^{18}F]HFB radioactive peak and the unwanted UV peak. With a solvent system of 95/5 MeCN/AF (0.1M), it was possible to obtain enough separation between the [^{18}F]HFB radioactive peak and UV bi-product peak to greatly increase the chemical purity of [^{18}F]HFB to > 99%.

The original Synthera® ASU set-up to go from the IFP module to to HPLC purification module involved a direct line from the end of the IFP connected to the inlet of the loop. This

means that the mixture to inject must be pushed into the loop by means of compressed nitrogen and a best guess as to how long it takes for the volume of liquid to reach the loop, without under or over-shooting the loop. We were not comfortable with this approach and quickly realized this could lead to substantial losses of radioactivity. Consequentially, we decided to add an automated syringe driver system to this process. We programmed the syringe to suck the eluted C18 SepPak purified reaction mixture and inject this into the loop in a two-step process. The loop size was a 5 mL loop, therefore, we had some room for error in case a bit of air was pushed into the loop. This proved to be a very effective and reproducible loading system for the semi-prep purification.

5.2.4 Gas Chromatography Analysis

Due to its inherent toxicity, the most recent guidelines for residual solvents set the maximum amount of MeCN that should be tolerated in pharmaceutical products at 410 ppm. Considering our semi-prep HPLC solvent is composed of 95% MeCN, we had to develop an effective protocol to remove MeCN and to ensure that it is present in less than 410 ppm in the final formulation of [^{18}F]HFB. The radioactive [^{18}F]HFB peak was collected (**Figure 4.5** – green radioactivity peak) in the dispensing hot cell in our radiochemistry lab, and the solvent was evaporated at 120˚C under N_2 flow combined with vacuum exhaust. The time of evaporation depends on the volume of the peak collected and the typical collected peak volumes were approximately 15 mL (10 mL/min flow for 1.5 min). When the solvent was evaporated to dryness (+ addition of 2 more min), there was still a significant amount of MeCN in the samples, up to three times the allowed limit (**Table 4.5)**. However, when the solvent was evaporated to dryness and an additional 2.5 min was added, this reduced the

amount of MeCN to well below the accepted limits (**Table 4.6)**. Therefore, this procedure was adopted to remove MeCN from the final formulation of [^{18}F]HFB.

During the evaporation step, there would sometimes be a significant loss of product, amounting to 20-30% of the total activity. [^{18}F]HFB has a very long chain and is thus non-volatile, therefore the loss of product cannot be attributed to evaporation of the product. The most likely explanation for the loss of product during evaporation is that some of the product is aspirated through the needle that is connected to the vacuum. This needle was always placed above the liquid; however, the constant flow of nitrogen could have resulted in some of the solvent/product aspired into the needle. To counteract this, the needle was placed just below the septum of the [^{18}F]HFB vial and the N_2 flow was kept to a minimum.

5.2.5 Reformulation and Quality control

During the reformulation step of [^{18}F]HFB, it was imperative to work quickly and to keep the [^{18}F]HFB/DMSO as warm as possible and to minimize the time spent in syringes during transfers. Given that [^{18}F]HFB is a very liphophilic molecule, it sticks to most plastics which can result in significant losses of radioactivity and when it cools down to room temperature, the solubility of [^{18}F]HFB in DMSO is also decreased due to high concentration of saline solution (90%) compared to DMSO. Furthermore, when [^{18}F]HFB was filtered through a 0.22 μm Acrodisc® filter, this also resulted in significant losses of radioactivity due to sticking of the product on the filter. As a result, when very concentrated [^{18}F]HFB was needed for exosome and hydrogel labeling, the filtering step was bypassed in order to minimize losses of activity in the filter.

The SA calculated for [^{18}F]HFB was in the range of 46 – 272 mCi/μmol, which is quite low for [^{18}F]-labeled compounds, with the theoretical maximum molar activity being 1710

Ci/μmol [2]. Since we were not targeting a specific receptor that could easily be saturated by cold mass, we were not concerned with SA. The low SA can be attributed to the presence of cold HFB in the final formulation of [^{18}F]HFB due to reactivity with F-19 in the various tubing. High SA activity was not a goal with this work, changing lines to Tefzel, a fluoropolymer that is resilient to radiolysis, and IFP components [3], or beaming for longer times to produce more F-18 was not completed for this work.

5.3 Exosome radiolabeling

When completing a literature review of exosome biodistribution, there are no robust studies completed using either fluorescence and optical imaging or PET/SPECT imaging. Only one paper can be found on the radiolabeling of exosome mimetic nanovesicles using ^{99m}Tc-HMPAO for SPECT imaging [4]. Our approach for radiolabeling exosomes with [^{18}F]HFB was based off this paper, the previous work with [^{18}F]HFB to label CPCs and non-published reports by the Gibbings lab using fluorescent hydrophobic dyes such as DiR.

In the paper by Choi *et al* [4], the use of ^{99m}Tc with a half-life of 6 hours allowed for a 1 hour incubation at room temperature. Working with ^{18}F (half-life of 110 min) limits the time available to complete manipulations, therefore, it was determined that a 30-min incubation would be tested at three different temperatures: 4˚C, room temperature and 37˚C, as completed by Zhang *et al* [5]to label CPCs. In terms of differences due to temperature in our preliminary experiments, it was noticed that there was more radioactivity in the pellet following centrifugation in the 4˚C incubation as compared to room temperature and 37˚C (**Table 4.9.5)**. At first, we believed this was due to [^{18}F]HFB labeling of exosomes, however, after attempting to resuspend the pellet and measure the activity, all of the radioactivity remained in the tube and none was in the PBS used for resuspension. This could have meant

that the colder temperatures was reducing the solubility of [^{18}F]HFB to the point where it would crash out of solution and end up sticking to the walls of the tubes. We therefore opted to incubate the exosomes with [^{18}F]HFB at 37˚C for the subsequent experiments.

The next challenge was to determine how the radiolabeled exosomes were going to be separated from free [^{18}F]HFB. If a purification step is not completed post-incubation in order to remove leftover [^{18}F]HFB, it would be impossible to differentiate the signal of the radiolabeled exosomes from that of [^{18}F]HFB. This would interfere with the accuracy of the biodistribution studies, therefore it was imperative to remove as much free [^{18}F]HFB as possible (>95% removal). Choi *et al* [4] utilised two approaches for removing free ^{99m}Tc-HMPAO from their labeled exosome mimetic vesicles. The first approach was with exosome exclusive spin columns (EESC) and the second utilized PD-10 size exclusion columns. Both techniques work on the same principle of size exclusion chromatography where larger molecules will pass through the column whereas smaller molecules will interact with the matrix of the column, leading to a longer elution time (and retention) for these free molecules. The EESCs have a molecular weight cutoff of 3000, meaning that molecules below this cutoff will interact with the matrix and be retained, whereas molecules above this weight will bypass the matrix and be eluted. The EESCs have the disadvantage of having a maximum sample loading volume of 100 μL, however, the purification step is very short; purified exosomes can be obtained after 2 minutes of centrifugation at 750 x g. The EESCs were tested with a 100 μL sample of [^{18}F]HFB spun at 750 x g, 700 x g and 500 x g. The eluate was collected and the radioactivity in both the column and eluate was measured. Surprisingly, [^{18}F]HFB with a molecular weight of 364 g/mol was collected in the eluate,

instead of being retained in the spin column (**Table 4.7**). This meant that the EESCs would not be an effective way to remove free [^{18}F]HFB from labeled exosomes.

The PD-10 columns have a higher molecular weight cutoff of 5000 and can tolerate larger sample volumes from 1- 2.5 mL. However, they require more time to complete the purification step as separation is done *via* gravity instead of centrifugation for the elution. Different formulations of [^{18}F]HFB were tested: 10% DMSO/PBS, 5% DMSO/PBS and 10% DMSO/PBS + 0.1% Tween as well as different elution solvents: PBS and PBS + 0.1% Tween. As seen in **Figures 4.8.1 – 4**, the elution profiles of [^{18}F]HFB through the PD-10 columns were similar for all the conditions. [^{18}F]HFB eluted through the column with the solvent front, with the majority of the radioactivity coming out within 0.5 – 1.0 mL. The elution volume of [^{18}F]HFB was slightly increased to 1.5 – 2.0 mL with the addition of 0.1% Tween. This means that [^{18}F]HFB did not interact with the matrix of the PD-10 columns at all and passed directly through the columns, the possible reason for this will be discussed in **section 5.3.1**. In the paper by Choi *et al* [4], PD-10 columns were utilized to separate free ^{99m}Tc-HMPAO from their labeled exosome mimetic vesicles. The labeled vesicles eluted first, while the free ^{99m}Tc-HMPAO was retained in the column due to its smaller size. The collected fractions were analyzed *via* ITLC and similar fractions were combined. With this approach, a 99.6% radiochemical purity was obtained in approximately 30 min [4]**.** Like the EESCs, the PD-10 columns were not effective at separating free [^{18}F]HFB from labeled exosomes because [^{18}F]HFB was eluting with the solvent front which would have given no resolution between labeled exosomes and free [^{18}F]HFB. We then decided to centrifuge to pellet the labeled exosomes while leaving free [^{18}F]HFB in the supernatant.

Considering the small size of exosomes (30 – 150 nm), it takes an enormous amount of force to pellet them. For their purification from cells, a series of sequential centrifugations are completed with the longest step consisting of 100,000 x g centrifugation for 2 hours. We were limited to using a small bench top centrifuge in the radiochemistry laboratory that had a maximum force of 21,000 x g and therefore used this as a starting point. We were also limited in time due to the half-life of ^{18}F, therefore we decided to choose a 1 hour centrifugation at 21,000 x g. The activity in the supernatant and pellet was measured after centrifugation and up to 86% of the initial radioactivity was found in the pellet, however after resuspension, all the activity remained stuck to the tube and none was found in the resuspension. We believed that at this force of centrifugation, exosomes were not being pelleted. After consulting with Dr Mélanie Dieudé (Researcher with expertise in exosomes/vesicles) at the CRCHUM, we were told that to fully pellet exosomes requires 18 hours of centrifugation at 200,000 x g. Based off this, we decided to change our strategy and ultracentrifuge at 200,000 x g for up to 4 hours, testing 1h and 2h centrifugations as well. With this strategy, the same results were obtained as before: the radioactivity was sticking to the tubes and no activity was found in the resuspended pellets. Furthermore, a washing step was sometimes completed following centrifugation and a minimum of activity was removed with the wash as [^{18}F]HFB was stuck to the tubes. Consequentially, we decided to test low retention Eppendorf tubes which have been shown to reduce the sticking of proteins and peptides and improve sample recovery. There was no difference in results between normal Eppendorf tubes and the low retention tubes. Finally, there was no difference between the control samples of [^{18}F]HFB without exosomes in terms of re-suspended radioactivity (**Table 4.9.1-7**). In certain instances, there was even more radioactivity in the re-suspended pellet of

the controls than in the exosome samples (**Table 4.9.3**). This confirmed that the radioactivity values come from free [^{18}F]HFB and not labeled exosomes and that no labeling of exosomes occurred.

As part of our protocol, we also decided to test different incubation volumes, with the lowest volume being 84 µL (34 µL of exosomes + 50 µL of [^{18}F]HFB) and highest volume 1000 µL (10 µL of exosomes + 990 µL of [^{18}F]HFB). In the paper by Zhang *et al* [5], it was demonstrated that the highest labeling efficiency for CPCs was obtained when the volume of [^{18}F]HFB was kept small (1 mL) and the concentration of cells was high (2 x 10^6 cells/mL). Even with 50 µL of [^{18}F]HFB, we were able to reach activities of 1 mCi in the incubation which allowed for measurements of activity several hours later. Varying the concentration of [^{18}F]HFB and exosomes did not impact the success of radiolabeling. Considering the small size of the exosomes, it is quite plausible that the tracer and exosomes did not "interact" with each other in solution, this not being the case for CPCs and [^{18}F]HFB. Furthermore, BSA was also tested during the incubation of [^{18}F]HFB with exosomes. Firstly, BSA has been demonstrated to be a fatty acid transporter across cell membranes [6] and given that [^{18}F]HFB resembles a lipid, we hypothesized that BSA may help with uptake of [^{18}F]HFB into exosomes. Secondly, BSA has also been shown to reduce the adhesion of proteins to reaction tubes, which was a major problem with [^{18}F]HFB. The addition of BSA slightly reduced the amount of radioactivity that was stuck to the tubes, however, did not help with the radiolabeling of exosomes, as confirmed *via* ITLC.

ITLC analysis was completed to verify if the exosomes were labeled or not and this approach was inspired by Choi *et al [4]*. In their paper, they could see a significant difference in migration distance for labeled exosomes as compared to free tracer. Radiolabeled

exosomes migrated a short distance on their ITLCs while their free tracer migrated the majority of the ITLC plate (**Figure 5.1)**. ITLC conditions were developed for [^{18}F]HFB which resulted in an Rf for [^{18}F]HFB of 0.83. Under these conditions, it is expected that labeled exosomes would remain at the base line on the ITLC. **Figure 4.10** demonstrates that there was no difference in the ITLCs obtained for the exosome samples as compared to the [^{18}F]HFB controls. The migration distance of [^{18}F]HFB was slightly changed with the addition of BSA, however, only one peak was observed when labeled exosomes would have created a second radioactive peak with a much different Rf.

5.3.1 Limitations with [^{18}F]HFB for exosome labeling

The original developers of [^{18}F]HFB, Ma et al [1], claimed that [^{18}F]HFB was absorbed into the membranes of cells, like hydrophobic fluorescent dyes. I hypothesize that that there may be a different underlying mechanism by which [^{18}F]HFB labels cells, based off the results obtained with the EESCs and PD-10 size exclusion columns. I hypothesize that when placed in solution, [^{18}F]HFB forms micelles/liposomes due to its inherent structure. The hydrophobic long-chain tail and the slightly more polar head groups align to form a micelle, much like a phospholipid bilayer. Consequentially, this "micelle" would greatly increase the molecular weight of the [^{18}F]HFB "complex" and possibly explain why were unable to use EESCs and PD-10 columns to separate free [^{18}F]HFB from labeled exosomes. The [^{18}F]HFB "complex" could be approximately the same size as exosomes explaining their direct elution through these columns. As for the cell labeling, I believe the [^{18}F]HFB micelles were taken up by cells through an endocytosis process, rather than being incorporated into membranes, therefore cell labeling was still effected. In terms of exosome radiolabeling, considering

exosomes are much smaller than cells and the [^{18}F]HFB micelles could be similar in size to exosomes, the same endocytosis process did not take place.

To overcome the potential production of micelles, we tried adding 0.1% Tween to the formulation of [^{18}F]HFB for the PD-10 column tests. Tween is a detergent used to prepare stable oil-in-water emulsions and is also used to increase membrane permeability. A similar detergent (saponin) was used to render exosome more permeable for loading of catalase for treatment of Parkinson's Disease (PD) in mice [7]. The addition of Tween to the final formulation slightly increased the elution volume needed for [^{18}F]HFB to pass through the PD-10 columns. Dr. Gibbings was against the idea of using Tween in our exosome incubations as it creates large holes in membranes which can greatly affect the biodistribution of the exosomes through drastically modifying their surface and can also cause exosomes to burst. Whereas in the PD study, the authors were not concerned with completing a robust biodistribution study of their exosomes, they simply wanted to demonstrate that exosomes could cross the BBB and deliver a large drug which is why saponin was used.

5.3.2 Future directions for radiolabeling exosomes

Although radiolabeling exosomes with [^{18}F]HFB did not prove to be successful, I believe it is still a possibility to determine their biodistribution *via* PET through different strategies. Going forward, it would be interesting to try another F-18 based radiotracer that is currently being used in the clinic: 14(R,S)-[^{18}F]Fluoro-6-this-heptadecanoic acid ([^{18}F]FTHA). [^{18}F]FTHA is an analogue of a long chain fatty acid utilised to measure free-fatty acid uptake and oxidation [8]**.** The same strategy could be applied for [^{18}F]FTHA as for [^{18}F]HFB to determine if [^{18}F]FTHA can be incorporated into the membrane of exosomes. [^{18}F]FTHA

precursor is commercially available and kits can be ordered from ABX to develop the radiosynthesis of [^{18}F]FTHA with our Synthera® ASU which could also be applied in the clinic. If this strategy does not work, another strategy could be to label an antibody specific to CD63. CD63 is a protein that is found in most exosomes and is used a biomarker to identify exosomes [9]. Antibody radiolabeling is an emerging field with many possibilities available, and F-18 could either be directly substituted onto the antibody or can be incorporated into a chelator for indirect labeling. Finally, another strategy could be to use a longer-lived PET radioisotope such as I-124 that has a half-life of 4.18 days. It would be possible to develop an I-124 based radiotracer that can be incubated with cells and therefore incorporated into exosomes as they are formed. The longer half-life of I-124 would allow for this sort of approach (longer incubation and ultracentrifuge time) and the labeled exosomes could be easily purified from the cell media using sequential centrifugation.

5.4 Radiolabeling chitosan-based hydrogels

Before proceeding with the radiolabeling of the chitosan hydrogels, it was first necessary to determine the effect of adding DMSO on the gelation kinetics and mechanical properties of the gels. This work was completed by an expert in biomaterials, Dr. Yasaman Alinejad (postdoctoral fellow in Dr Lerouge's lab) and her study set the starting point for our hydrogel radiolabeling experiments. From these results, it was concluded that if we maintained the final concentration of 10% DMSO/saline to 0.5% v/v, the hydrogels would be minimally affected (**Figures 4.11.1-4)**. Concentrations above 0.5% v/v of 10% DMSO/saline had a significant impact on the storage modulus (approach 1) of the hydrogels, although the secant modulus remained unchanged. Another important factor was the sequence of mixing of the components of the hydrogels as there are two options: Approach 1(Chitosan + [^{18}F]HFB) +

Gelation agent; or Approach 2 (Chitosan + Gelation agent) + [^{18}F]HFB. The order of mixing did not seem to have a large difference in the rheological or mechanical properties of the hydrogels, however, after completing some radiolabeling experiments, the order of mixing had a large impact on the yield of labeling the hydrogel and on losses of radioactivity. As seen with the exosome experiments, [^{18}F]HFB sticks to any plastics and tubes, therefore, it is crucial to minimize the amount of transfers involved as to minimize losses of radioactivity. When [^{18}F]HFB is mixed with chitosan as a first step as in approach 1, the additional mixing step required to add the gelation agent results in losses of radioactivity averaging 42.1%. Comparing this to addition of [^{18}F]HFB as a final step, after mixing of chitosan and the gelation agent as in approach 2, an average of 16.2 % of activity is lost due to mixing. Consequentially, after validating these losses through repeated experiments, we decided to forgo approach 1 and solely use approach 2 going forward where [^{18}F]HFB was added in the second step.

With regards to labeling efficiency, Ahmadi *et al* had observed an 82% efficiency when using [^{18}F]HFB to non-covalently label a collagen matrix [10]. With our chitosan radiolabeling, > 90% labeling efficiency was observed up until eight hours, where we started to see a slight efflux of [^{18}F]HFB thereafter, corresponding to a maximum loss of radioactivity of 9%. High labeling efficiency was found, regardless of the order of mixing (approach 1 vs. 2) and a similar trend was obtained whether the hydrogels were placed in transwells or in molds (**Figures 4.12.1-6)**. We wanted to test the labeling efficiency in both the transwells and molds as neither approach represents *in vivo* conditions perfectly. For the transwell experiments, the hydrogel was allowed to gel only for a short period of time before being submerged in saline. This resulted in a more liquid gel, whereas the gel molds were

allowed to fully gel and form a rigid gel before being submerged in saline. We were worried that in a more liquid gel, there may have been a higher efflux of [^{18}F]HFB as compared to the mold due to the radiotracer not being as embedded in the gel. This was not the case as there was similar labeling stability for the transwell and mold experiments. These experiments allowed us to conclude that there was uniform mixing of [^{18}F]HFB throughout the hydrogel and that even if the hydrogel is not fully in a "gel state", the interactions between [^{18}F]HFB and the chitosan are strong enough to prevent [^{18}F]HFB from being washed out of the gel. We hypothesized that similar results can be expected *in vivo*.

To validate the specificity of [^{18}F]HFB for radiolabeling the chitosan-based hydrogels, a control was completed with free F-18. The same procedure was followed with F-18, directly from the cyclotron, instead of [^{18}F]HFB. As compared to [^{18}F]HFB, there was less F-18 lost during the mixing of the hydrogels due to the fact that F-18 does not have the same lipophilic properties as [^{18}F]HFB. Considering the hydrogels are largely composed of water and free F-18 is in the form of a fluoride ion, one would predict that the F-18 would be retained in the hydrogel. But this was not the case and a large part of the F-18 was found in the saline rinses after just 5 minutes of incubation. After 1 hour of incubation less than 10% of the radioactivity remained in the hydrogel for both the transwell experiments and gel molds and almost no activity remained after 4 hours. This control validated our strategy to use [^{18}F]HFB as a radiolabeling agent for chitosan-based hydrogel and demonstrates that [^{18}F]HFB is an excellent radiotracer to be retained within the hydrogel.

The only other study completed on radiolabeling chitosan-based hydrogels utilized Na^{131}I and they obtained 95% labeling yields with high stability over 6 days [11]. Working with ^{131}I's long half-life of 8 days allows for this type of work to be completed, however in

this study, we are mainly concerned with short term follow up of the localization of our chitosan hydrogels after injection *in vivo*, thus ^{18}F is suitable for our purposes. Moving forward, we would like to assess the radiolabeled hydrogel in small animal models. When working with the animal models, it will be important to complete a control scan in parallel with free [^{18}F]HFB in order to assess its retention in comparison to the labeled biomaterial with [^{18}F]HFB. With this, we should be able to account for the approximatively 9% loss of [^{18}F]HFB that is observed from the gels after 8 hours.

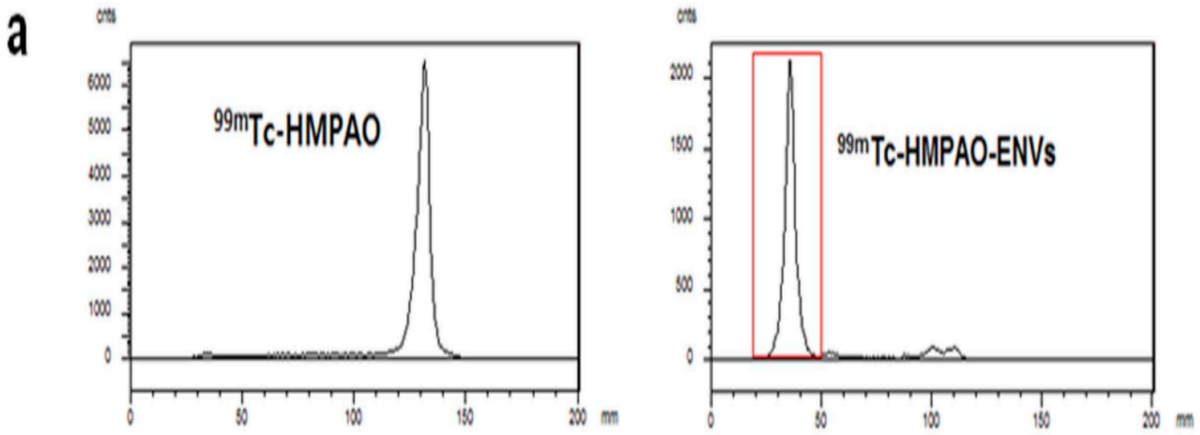

Figure 5.1. ITLC analysis for radiolabeling of ENVs using [99mTc]-HMPAO and Radiolabeled ENVs (0.9% saline) [4].

Conclusion

The automated synthesis of [^{18}F]HFB was completed using the Synthera® ASU platform. Both the fluorination and semi-prep HPLC conditions were optimized to maximize the yield and chemical/radiochemical purity of [^{18}F]HFB. [^{18}F]HFB was obtained in 34% +/- 9% RCY with > 95% chemical/radiochemical purity within a total synthesis time of 60 minutes. The molar activity in the range of 46-190 mCi/μmol at EOS was low, however, we were not concerned with this as our target was not a saturable receptor. Various strategies were effected for radiolabeling exosomes, including different incubation temperatures, volumes of [^{18}F]HFB/exosomes, different centrifugation forces/times and the addition of BSA. However, there was no difference between the exosome samples and controls (free [^{18}F]HFB) in regards to radioactivity and ITLC analysis. Chitosan-based hydrogels were successfully labeled using [^{18}F]HFB with a labeling stability of over 90% even after 8 hours incubated in saline, while a control study using free F-18 exhibited less than 10% of the radioactivity remaining in the hydrogel after 60 mins. The order of mixing was optimized to add [^{18}F]HFB as a final step to minimize losses of radioactivity in the labeling process. [^{18}F]HFB of exosomes and biomaterials presents a novel approach to determining their *in vivo* distribution. Work is underway to continue the hydrogel radiolabeling experiments and to determine the *in vivo* safety and efficacy of the hydrogels in animal models. This translational work will eventually lead to implementing the use of hydrogels in humans for various applications such as regenerative therapies and drug delivery.

References

1. Ruiz, G.A.M. and H.F.Z. Corrales, *Chitosan, Chitosan Derivatives and their Biomedical Applications*, in *Biological Activities and Application of Marine Polysaccharides*. 2017, InTech.
2. Jacobson, O., D.O. Kiesewetter, and X. Chen, *Fluorine-18 radiochemistry, labeling strategies and synthetic routes.* Bioconjugate chemistry, 2014. **26**(1): p. 1-18.
3. Colombo, M., G. Raposo, and C. Théry, *Biogenesis, secretion, and intercellular interactions of exosomes and other extracellular vesicles.* Annual review of cell and developmental biology, 2014. **30**: p. 255-289.
4. Le Bars, D., *Fluorine-18 and medical imaging: Radiopharmaceuticals for positron emission tomography.* Journal of fluorine chemistry, 2006. **127**(11): p. 1488-1493.
5. Choi, H., et al., *Noninvasive imaging of radiolabeled exosome-mimetic nanovesicle using 99mTc-HMPAO.* Scientific reports, 2015. **5**: p. 15636.
6. Saha, G.B. and E. de Kerviller, *Basics of PET imaging.* J Radiol, 2006. **87**: p. n719.
7. Gad, S.C., *Pharmaceutical manufacturing handbook: production and processes*. Vol. 5. 2008: John Wiley & Sons.
8. Cherry, S.R., *Fundamentals of positron emission tomography and applications in preclinical drug development.* The Journal of Clinical Pharmacology, 2001. **41**(5): p. 482-491.
9. Massoud, T.F. and S.S. Gambhir, *Molecular imaging in living subjects: seeing fundamental biological processes in a new light.* Genes & development, 2003. **17**(5): p. 545-580.
10. Brix, G., et al., *Radiation exposure of patients undergoing whole-body dual-modality 18F-FDG PET/CT examinations.* Journal of Nuclear Medicine, 2005. **46**(4): p. 608-613.
11. Schlyer, D.J., *PET tracers and radiochemistry.* ANNALS-ACADEMY OF MEDICINE SINGAPORE, 2004. **33**(2): p. 146-154.
12. Hutchins, G.D., et al., *Small animal PET imaging.* ILAR journal, 2008. **49**(1): p. 54-65.
13. Ollinger, J.M. and J.A. Fessler, *Positron-emission tomography.* IEEE Signal Processing Magazine, 1997. **14**(1): p. 43-55.
14. Lewellen, T.K., *Recent developments in PET detector technology.* Physics in medicine and biology, 2008. **53**(17): p. R287.
15. Lecomte, R., *Novel detector technology for clinical PET.* European journal of nuclear medicine and molecular imaging, 2009. **36**(1): p. 69-85.
16. Meyer, J.H., et al., *Prefrontal cortex 5-HT2 receptors in depression: an [18F] setoperone PET imaging study.* American Journal of Psychiatry, 1999. **156**(7): p. 1029-1034.
17. Jacobson, O., et al., *Rapid and simple one-step F-18 labeling of peptides.* Bioconjugate chemistry, 2011. **22**(3): p. 422-428.

17A. Stephenson, Nickeisha A., et al. "Iodonium Ylide–Mediated Radiofluorination of 18F-FPEB and Validation for Human Use." *Journal of Nuclear Medicine*56.3 (2015): 489-492.

17B. Tredwell, Matthew, et al. "A General Copper-Mediated Nucleophilic 18F Fluorination of Arenes." *Angewandte Chemie International Edition* 53.30 (2014): 7751-7755.

18. Löser, R., et al., *Use of 3-[18F] fluoropropanesulfonyl chloride as a prosthetic agent for the radiolabelling of amines: Investigation of precursor molecules, labelling conditions and enzymatic stability of the corresponding sulfonamides.* Beilstein journal of organic chemistry, 2013. **9**(1): p. 1002-1011.
19. Ma, B., et al., *A simple method for stem cell labeling with fluorine 18.* Nuclear medicine and biology, 2005. **32**(7): p. 701-705.
20. Zhang, Y., et al., *18F-FDG cell labeling may underestimate transplanted cell homing: more accurate, efficient, and stable cell labeling with hexadecyl-4-[18F] fluorobenzoate for in vivo tracking of transplanted human progenitor cells by positron emission tomography.* Cell transplantation, 2012. **21**(9): p. 1821-1835.
21. Ahmadi, A., et al., *PET imaging of a collagen matrix reveals its effective injection and targeted retention in a mouse model of myocardial infarction.* Biomaterials, 2015. **49**: p. 18-26.
22. Sun, D., et al., *Exosomes are endogenous nanoparticles that can deliver biological information between cells.* Advanced drug delivery reviews, 2013. **65**(3): p. 342-347.
23. De Rosa, G., et al., *Nanotechnologies: a strategy to overcome blood-brain barrier.* Current drug metabolism, 2012. **13**(1): p. 61-69.
24. Papakostas, D., et al., *Nanoparticles in dermatology.* Archives of dermatological research, 2011. **303**(8): p. 533-550.
25. Almeida, J.P.M., et al., *In vivo biodistribution of nanoparticles.* Nanomedicine, 2011. **6**(5): p. 815-835.
26. Javeed, N. and D. Mukhopadhyay, *Exosomes and their role in the micro-/macro-environment: a comprehensive review.* Journal of biomedical research, 2016. **30**.
27. Savina, A., M. Vidal, and M.I. Colombo, *The exosome pathway in K562 cells is regulated by Rab11.* Journal of cell science, 2002. **115**(12): p. 2505-2515.
28. Mathivanan, S., H. Ji, and R.J. Simpson, *Exosomes: extracellular organelles important in intercellular communication.* Journal of proteomics, 2010. **73**(10): p. 1907-1920.
29. Bobrie, A., et al., *Rab27a supports exosome-dependent and-independent mechanisms that modify the tumor microenvironment and can promote tumor progression.* Cancer research, 2012. **72**(19): p. 4920-4930.
30. Zhang, Y., et al., *Exosomes derived from IL-12-anchored renal cancer cells increase induction of specific antitumor response in vitro: a novel vaccine for renal cell carcinoma.* International journal of oncology, 2010. **36**(1): p. 133.
31. Haney, M.J., et al., *Exosomes as drug delivery vehicles for Parkinson's disease therapy.* Journal of Controlled Release, 2015. **207**: p. 18-30.
32. Tokatlian, T. and T. Segura, *siRNA applications in nanomedicine.* Wiley Interdisciplinary Reviews: Nanomedicine and Nanobiotechnology, 2010. **2**(3): p. 305-315.
33. Akhtar, S. and I.F. Benter, *Nonviral delivery of synthetic siRNAs in vivo.* The Journal of clinical investigation, 2007. **117**(12): p. 3623-3632.
34. Peer, D., et al., *Systemic leukocyte-directed siRNA delivery revealing cyclin D1 as an anti-inflammatory target.* Science, 2008. **319**(5863): p. 627-630.
35. Rozema, D.B., et al., *Dynamic PolyConjugates for targeted in vivo delivery of siRNA to hepatocytes.* Proceedings of the National Academy of Sciences, 2007. **104**(32): p. 12982-12987.

36. Alvarez-Erviti, L., et al., *Delivery of siRNA to the mouse brain by systemic injection of targeted exosomes.* Nature biotechnology, 2011. **29**(4): p. 341-345.
37. Johnson, I., *Review: Fluorescent probes for living cells.* The Histochemical Journal, 1998. **30**(3): p. 123-140.
38. Fatimi, A., et al., *A new injectable radiopaque chitosan-based sclerosing embolizing hydrogel for endovascular therapies.* Acta biomaterialia, 2012. **8**(7): p. 2712-2721.
39. Assaad, E., M. Maire, and S. Lerouge, *Injectable thermosensitive chitosan hydrogels with controlled gelation kinetics and enhanced mechanical resistance.* Carbohydrate polymers, 2015. **130**: p. 87-96.
39A. Ceccaldi, Caroline, et al. "Optimization of injectable thermosensitive scaffolds with enhanced mechanical properties for cell therapy." *Macromolecular bioscience* (2017).
40. Fatimi, A., F. Zehtabi, and S. Lerouge, *Optimization and characterization of injectable chitosan-iodixanol-based hydrogels for the embolization of blood vessels.* Journal of Biomedical Materials Research Part B: Applied Biomaterials, 2015.
41. Kim, D.-W., et al., *Radiolabeled chitosan hydrogel containing VEGF enhances angiogenesis in a rodent model of acute myocardial infarction.* Macromolecular Research, 2014. **22**(3): p. 272-278.
42. Lapi, S.E. and M.J. Welch, *A historical perspective on the specific activity of radiopharmaceuticals: What have we learned in the 35years of the ISRC?* Nuclear medicine and biology, 2013. **40**(3): p. 314-320.
43. Studenov, A.R., et al., *Studies of the mechanism of the in-loop synthesis of radiopharmaceuticals.* Applied radiation and isotopes, 2004. **61**(6): p. 1195-1201.
44. van der Vusse, G.J., *Albumin as fatty acid transporter.* Drug metabolism and pharmacokinetics, 2009. **24**(4): p. 300-307.
45. Takala, T., et al., *14 (R, S)-[18 F] Fluoro-6-thia-heptadecanoic acid as a tracer of free fatty acid uptake and oxidation in myocardium and skeletal muscle.* European journal of nuclear medicine and molecular imaging, 2002. **29**(12): p. 1617-1622.